Impact of N-terminally truncated $A\beta_{4-42}$ on memory and synaptic plasticity – Tg4-42 a new mouse model of Alzheimer's disease

Doctoral Thesis

In partial fulfillment of the requirements for the degree
“Doctor rerum naturalium (Dr. rer. nat.)”
in the Molecular Medicine Study Program
at the Georg-August University Göttingen

Submitted by
Katharina Dietrich

Born in
Cottbus, Germany

Göttingen, 2014

Members of the thesis committee

Supervisor

Prof. Dr. Thomas A. Bayer
Department for Psychiatry
Division of Molecular Psychiatry
University Medical Center, Georg-August University Göttingen

Second member of the thesis committee

Prof. Dr. Dr. Hannelore Ehrenreich
Division of Clinical Neurosciences
Max Planck Institute of Experimental Medicine, Göttingen

Third member of the thesis committee

Prof. Dr. Uwe-Karsten Hanisch
Department of Neuropathology
University Medical Center, Georg-August University Göttingen

Date of Disputation: 17.12.2014

Affidavit

Here I declare that my doctoral thesis entitled "**Impact of N-terminally truncated Aβ$_{4-42}$ on memory and synaptic plasticity – Tg4-42 a new mouse model of Alzheimer's disease**" has been written independently with no other sources and aids than quoted.

Katharina Dietrich

Göttingen, November 2014

Related Publications

Parts of the present thesis have been published and are listed below.

Original Articles:

Bouter, Y.*, Dietrich, K.*, Wittnam, J.L.*, Rezaei-Ghaleh, N.*, and Pillot, T., et al. (2013a). **N-truncated amyloid β (Aβ) 4-42 forms stable aggregates and induces acute and long-lasting behavioral deficits.** Acta Neuropathol *126*, 189-205.

Bouter, Y.*, Kacprowski, T.*, Weissmann, R., Dietrich, K., and Borgers, H., et al. (2014). **Deciphering the Molecular Profile of Plaques, Memory Decline and Neuron Loss in Two Mouse Models for Alzheimer's Disease by Deep Sequencing.** Front. Aging Neurosci. *6*, 75.

(* equal contributions)

Poster:

Dietrich, K., Bouter, Y., Wittnam, J., Pillot, T., and Papot-Couturier, S., et al. (2013). **Tg4-42: A new mouse model of Alzheimer's disease—N-truncated beta-amyloid 4-42 affects memory decline and synaptic plasticity.** Alzheimers Dement *9*, P498.

Bouter, Y., Dietrich, K., Wittnam, J., Pillot, T., and Papot-Couturier, S., et al. (2013b). **Tg4-42: A new mouse model of Alzheimer's disease—N-truncated amyloid β (Aβ) 4-42 induces severe neuron loss and behavioral deficits.** Alzheimers Dement *9*, P498.

Contents

Acknowledgements

I gratefully acknowledge the continuous support and guidance of Prof. Dr. Thomas A. Bayer who gave me the chance to work under his supervision. I truly appreciate his patience and enthusiasm for my project during the past three years. I want to thank for insightful scientific discussions and the possibility to travel and participate in an international scientific environment. Also, I would like to express my gratitude towards PD Dr. Oliver Wirths for his support, help and inspiring comments.

I wish to thank Prof. Dr. Dr. Hannelore Ehrenreich and Prof. Dr. Uwe-Karsten Hanisch for agreeing to serve as members of my PhD committee and for their support and insightful comments on my project.

I gratefully acknowledge the *Moleculare Medicine* study program which gave me the opportunity to do my PhD thesis in Göttingen and provided a variety of supportive courses. My thanks also go to Dr. Erik Meskauskas for his continuous support and dedication.

My sincere thanks go to Prof. Dr. Michael Müller for our cooperation that enables me to perform the electrophysiological experiments. I am deeply grateful for his guidance and sustained support. He has always been able to offer assistance, despite working on his own projects.

My thanks also go to the Department of Neuropathology for the cooperation that enables me to accomplish the qRT-PCR experiments. I owe special thanks to Nasrin Saiepour and Franziska Paap for their sophisticated support and scientific help.

I am deeply grateful to the *Alzheimer Stiftung Göttingen* for the *Inge und Fritz-Kleekamm-Forschungspreis* that appreciated our research and supported financially the present study.

I truly appreciate the never-ending support and patience of Nina Karbe, Nadine Ilse, Axel Zigan and the other members of the animal facility. Without their help, this work would not have been possible. I want to express my gratitude to the Department of Medical Statistics for the educational guidance and fruitful discussions.

Many thanks go to all the former and current lab members of Prof. Bayer's lab. Beyond that, special thanks are dedicated to Sadim Jawhar, PhD, Jessica L. Wittnam, PhD, Dr. Antje Hillmann and Dr. Anika Saul for teaching and letting me into the secrets of research. Thanks for all the support and patience. I am deeply grateful to Petra Tucholla and Yvette Heise for always providing support, help and a friendly ear.

I owe special thanks to the lab members of Prof. Müller's lab: Oliwia A. Janc, Dr. Christiane Menzfeld, Belinda Kempkes and Karolina Can. Thanks for the endless emotional support and continuous help in overcoming technical and scientific obstacles. Being able to work with them was a peerless adventure.

I want to express my gratitude to all rotation students of the Bayer lab. Special thanks go to Frederik Sprenger, Anna Greda and Anne Marieke Eveleens. I appreciate the possibility to teach and learn at the same time.

I am deeply indebted to Yvonne Bouter for sharing all the ups and downs of the past three years. My PhD would not have been the same without her. I truly appreciate her scientific support and lifesaving tips for the experimental work. Thanks for opposing my fear of flying and having such a great time in Boston and New York. Thanks for endless conversations on science and life in general.

Additional thanks go to Dr. Antje Hillmann, Sadim Jawhar, PhD, Dr. Christiane Menzfeld, Oliwia A. Janc and Yvonne Bouter for proofreading my thesis and providing insightful and invaluable comments.

Beyond, I owe special thanks to my parents and loved ones. The past years would not have been possible without their love and unconditional belief in me.

More and above, my heartfelt gratitude is dedicated to Michael Krusche for being who he is and never letting me down at the worst of times. Thanks for all indispensable advices and technical supports. Thanks for always being there.

Abstract

A heterogeneous mixture of amyloid beta (Aβ) variants exists in Alzheimer's disease (AD) brains. So far, little is known how individual Aβ species contribute to development and progression of this neurodegenerative disorder.

Several studies revealed an important role of N-terminally truncated Aβ species in AD etiology. Besides other Aβ isoforms, N-truncated $Aβ_{4-42}$ is highly abundant in AD brains and is one of two dominant isoforms in the hippocampus and cortex of sporadic and familial AD subjects. In a recent work it was demonstrated that $Aβ_{4-42}$ exhibits one of the highest aggregation propensities to form stable aggregates. Moreover, it demonstrates strong toxic effects when studied in primary cortical neurons and is able to induce working memory deficits after intracerebroventricular injection into wildtype mouse brains. Despite these findings a possible role of $Aβ_{4-42}$ in AD etiology has not been analyzed in detail so far.

The aim of the present work was to investigate the potential neurotoxic effects of $Aβ_{4-42}$ in *in vivo* and *in vitro* model systems. Recently, the first transgenic mouse model expressing exclusively N-terminal truncated $Aβ_{4-42}$ (Tg4-42 mouse line) was generated in our lab. This mouse model was used to study the effects of $Aβ_{4-42}$ expression on neuropathology such as Aβ accumulation, inflammation and neuron loss. Furthermore, hemizygous Tg4-42 mice at three and 12 months of age underwent several behavioral tests to assess motor abilities and cognitive function. Acute hippocampal tissue slices of Tg4-42 mice at three, 12 and 24 months of age were used to examine the impact of $Aβ_{4-42}$ on synaptic function and plasticity. Relative gene expression levels of synaptic markers were additionally analyzed in hippocampal tissue of young Tg4-42 mice.

Using immunohistochemistry, it was shown that Tg4-42 mice develop region-specific intraneuronal Aβ accumulation most notably in the hippocampus starting at two to three months of age. This is accompanied by a marked astro- and microgliosis in the same brain region. DAPI-staining revealed a distinct loss of neuronal cells in hippocampal CA1 area that deteriorates while aging. Additionally, Tg4-42 mice demonstrated age-dependent deficits in spatial learning, spatial reference memory and forms of associative memory when performing Morris water maze and fear conditioning tasks. Neurophysiological analyses in acute hippocampal tissue slices revealed an increased basal synaptic transmission at Schaffer collateral/CA1 synapses. In contrast, short-term and long-term plasticity were not affected. Commencing analysis of gene expression levels demonstrated a down-regulation of synaptoporin and neuroligin 1 levels in

hippocampal tissue of three-month-old transgenic mice that might be linked to the detected hyperexcitability. These findings indicate a pathological role for N-truncated $A\beta_{4-42}$ in AD etiology as these impairments are comparable to AD typical dysfunctions.

List of figures

List of tables

List of abbreviations

Abbreviations	Description
aa	amino acid
ABC	avidin-biotin complex
ACSF	chilled artificial cerebrospinal fluid
Actb	gene encoding for β-Actin
AD	Alzheimer's disease
ADAM	a disintegrin and metalloproteinases
AICD	amyloid precursor protein intracellular domain
AMPA	α-amino-3-hydroxy-5-methyl-4-isoxazolepropionic acid
AMPAR	α-amino-3-hydroxy-5-methyl-4-isoxazolepropionic acid receptor
ANOVA	analysis of variance
Aph-1	anterior pharynx-defective 1
APLP	amyloid precursor-like protein
APOE	apolipoprotein E
APP	amyloid precursor protein
AT	acquisition training of Morris water maze
Aβ	amyloid beta
BACE	β-site APP cleaving enzyme
CA1	*Cornu Ammonis* 1 - subdivision of hippocampal formation
CA3	*Cornu Ammonis* 3 - subdivision of hippocampal formation
CAA	cerebral amyloid angiopathy
CaMKII	α-calcium/calmodulin-dependent protein kinase II
cAMP	cyclic adenosine 3',5'-monophosphate
cDNA	complementary DNA
CI	confidence interval
CNS	central nervous system
CS	conditioned stimulus
CSF	cerebrospinal fluid
CT	cued training of Morris water maze
CT	threshold cycle
CTFα/β	C-terminal fragment α/β
DAB	3, 3'-diaminobenzidine
DAPI	4',6-diamidino-2-phenylindol
ddH_2O	distilled, deionized water
DG	dentate gyrus

Abbreviations	Description
Dlgh4	gene encoding for PSD95
DNA	desoxyribonucleic acid
DNase	desoxyribonuclease
dNTP	desoxynucleoside triphosphate
EC	entorhinal cortex
EDTA	ethylenediaminetetraacetic acid
EOAD	early-onset Alzheimer's disease
EtOH	ethanol
FAD	familial Alzheimer's disease
FCS	fetal calf serum
fEPSP	field excitatory postsynaptic potential
GABA	gamma-aminobutyric acid
GFAP	glial fibrillary acidic protein
IO curve	input-output curve
kDa	kilo-Dalton
LOAD	late-onset Alzheimer's disease
LTD	long-term depression
LTP	long-term potentiation
M	molar
MCI	mild cognitive impairment
mGluR	metabotropic glutamate receptors
mo.	month
MWM	Morris water maze
Nct	nicastrin
NEP	neprilysin
NFT	neurofibrillary tangles
Nlgn	neuroligin 1
NMDA	N-methyl-D-aspartate
NMDAR	N-methyl-D-aspartate receptor
NR2A	subunit of NMDAR
NR2B	subunit of NMDAR
PBS	phosphate buffered saline
PCR	polymerase chain reaction
PEN-2	presenilin enhancer 2
PFA	paraformaldeyhde
PHF	paired helical filaments
ppf	paired-pulse facilitation

Abbreviations	Description
PS1/PS2	presenilin 1/2
PSD95	postsynaptic density protein 95
PT	probe trial of Morris water maze
PTP	post-tetanic potentiation
qRT-PCR	quantitative real-time polymerase chain reaction
RM-ANOVA	repeated measures analysis of variance
RNA	ribonucleic acid
Rnase	ribonuclease
RNAsin	ribonuclease inhibitor
ROX	6-Carboxyl-X-Rhodamine
rpm	revolutions per minute
RT	room temperature
SAD	sporadic Alzheimer's disease
sAPPα/β	soluble α/β amyloid precursor protein fragment
SD	standard deviation
SDS	sodium dodecyl sulfate
SEM	standard error of the mean
SNAP25	synaptosome-associated protein of 25 kDa
SNARE	soluble N-ethylmaleimide-sensitive fusion protein attachment protein receptor
STP	short-term potentiation
Synpr	gene encoding for synaptoporin
TGN	trans-Golgi network
TRH	thyrotropin-releasing hormone
t-SNARE	target-associated SNARE
US	unconditioned stimulus
VAMP	vesicle-associated membrane protein, also called synaptobrevin
VGCC	voltage-dependent Ca^{2+} channel
v-SNARE	vesicle-associated SNARE
WT	wildtype

1 Introduction

1.1 Alzheimer's disease

1.1.1 Initial description

In 1906, the German psychiatrist and neuropathologist Dr. Alois Alzheimer gave a lecture in which he described for the first time a form of dementia that is meanwhile known as Alzheimer's disease (Maurer et al., 1997). This description of "a characteristic serious disease of the cerebral cortex" (Maurer et al., 1997) based on determination of clinical symptoms of his patient Auguste D that was later corroborated by histopathological findings. The broad range of symptoms "included reduced comprehension and memory, as well as aphasia, disorientation, unpredictable behavior, paranoia, auditory hallucinations and pronounced psychosocial impairment" (Maurer et al., 1997). When later analyzing her brain he described plaques, neurofibrillary tangles and arteriosclerotic changes as characteristics of this form of dementia (Maurer et al., 1997).

1.1.2 Epidemiology

Alzheimer's disease (AD) is a progressive neurodegenerative disorder and the most common type of dementia accounting for an estimated 60 – 80 % of cases (Alzheimer's Association, 2014). In 2013, *World Health Organization* (WHO) and *Alzheimer's Disease International* estimated that 44.4 million people suffered from dementia worldwide (Bickel, 2014). Currently, approximately 1.5 million people with dementia are living in Germany of which two-thirds suffer from Alzheimer's disease. It was calculated that this number will increase up to 3.0 million affected people by 2050 (Bickel, 2014). *Alzheimer's Association* reported that an estimated 5.2 million Americans of all ages have AD in 2014 and there could be as many as 7 million by 2050 (Alzheimer's Association, 2014). It is assumed that the number of affected individuals will grow dramatically due to an increase in global population and human lifespan based on "advances in medicine and medical technology as well as social and environmental conditions" (Alzheimer's Association, 2014, Platt et al., 2013). Thus, AD is becoming an even greater burden in both social and economic terms.

1.1.3 Risk factors

Except for genetic mutations that cause (familial) AD, several other factors are known as risk factors of this disorder. The primary risk factor for AD is aging although advanced age alone is not sufficient to cause it. Most people develop AD at the age of 65 or older (Alzheimer's Association, 2014). Additionally, environmental factors and inherited alleles

of AD associated genes account as risk factors for AD (Platt et al., 2013). The latter comprise the apolipoprotein E (APOE) gene that exists in three allele isoforms (ε2, ε3 or ε4) and is known to increase the risk to develop AD (see section 1.4). The environmental risk factors comprise social and cognitive engagement as well as education. Moreover, cardiovascular disease risk factors including smoking, obesity, diabetes, high cholesterol and hypertension as well as traumatic brain injury were assumed to elevate the probability to develop AD (Alzheimer's Association, 2014).

1.1.4 Symptoms and disease progression

In general, dementia is defined as an “acquired syndrome” (Holtzman et al., 2011) characterized by a gradual neurodegeneration that first affects the short-term memory and later on the long-term memory (Zolezzi et al., 2014) as well as other cognitive abilities (Holtzman et al., 2011). Although affecting people differently some neuropsychological/neuropsychiatric and neurologic alterations are common symptoms of AD. The neuropsychological symptoms include progressive loss in remembering new items (anterograde amnesia), deficits in language (aphasia), object use (apraxia), form recognition of faces or objects (agnosia) as well as step-by-step planning and solving problems (Lalonde et al., 2012, Alzheimer's Association, 2014). Moreover, affected people may suffer from apathy, dysphoria, social withdrawal and depression (Lalonde et al., 2012). Neurologic symptoms comprise e.g. hallucinations, deficient postural control, myoclonus as well as epileptic seizures and usually occur late in disease progression (Lalonde et al., 2012). As the disease progresses the individual’s cognitive and functional abilities decline and often culminate in becoming “bed-bound and reliant on around-the-clock care” (Alzheimer's Association, 2014).

By now, it is accepted that AD is a slowly progressive disease that may begin 20 or more years before clinical symptoms emerge (Alzheimer's Association, 2014). Three stages of disease progression were proposed: preclinical, mild cognitive impairment (MCI) and dementia (Hall and Roberson, 2012). At it, the “continuum” of AD describes the time between the first neuropathological alterations in the brain and the symptoms of advanced AD (Alzheimer's Association, 2014). The first stage, preclinical AD, includes the “spectrum of presymptomatic autosomal dominant mutation carriers, asymptomatic biomarker-positive older individuals at risk for progression to MCI due to AD and AD dementia, as well as biomarker-positive individuals who have demonstrated subtle decline from their own baseline that exceeds that expected in typical aging, but would not yet meet criteria for MCI” (Sperling et al., 2011). Mild cognitive impairment is supposed to be an intermediate stage between asymptotic phase and dementia onset. This term often refers to the symptomatic predementia phase of AD and is characterized by a “cognitive

impairment in elderly persons not of sufficient severity to qualify for a diagnosis of dementia" (Lyketsos et al., 2002, Albert et al., 2011). MCI patients demonstrate impairments in memory or other cognitive abilities that are not normal for their age and education while "their day-to-day functioning is generally preserved" (Lyketsos et al., 2002). MCI is a chronic condition and might be a precursor to AD albeit it "does not always lead to dementia" (Alzheimer's Association, 2014, Lyketsos et al., 2002). Finally, the dementia stage is applied when cognitive or behavioral symptoms have progressed to the inability "to function at work or in usual daily activities" (McKhann et al., 2011) as described above.

1.1.5 Diagnosis

In general, diagnosis of AD is complicated as many AD patients demonstrate evidence of pathologic changes related to other dementias and 'pure' AD is uncommon. Neuropathological alterations, like amyloid plaques and neurofibrillary tangles, "coexist with other pathologies in 1/3 – 1/2 of patients with clinically diagnosed AD" (Ashe and Zahs, 2010). AD is often combined with either vascular dementia, dementia with Lewy bodies (DLB) or with both (Ashe and Zahs, 2010, Alzheimer's Association, 2014). Additionally, other factors that can cause dementia must be ruled out, e.g. brain tumor, subdural hematoma, thyroid disease or chronic infections (Holtzman et al., 2011). Nonetheless, it is possible to distinguish AD from other forms of dementia. Based on the medical and family history (psychiatric history, cognitive and behavioral changes) and an examination of the individual a staging system for dementia severity, i.e. Clinical Dementia Rating (CDR) is applied. Thus, the presence or absence of dementia as well as the severity is determined (Holtzman et al., 2011, Alzheimer's Association, 2014). In order to clinically evaluate an individual's cognitive abilities several neuropsychological tests are applied. These tests include mental status exams like Mini-Mental State Examination (MMSE) or Alzheimer's Disease Assessment Scale (ADAS) as well as memory tests like Benton Visual Retention Test (BRVT) (Webster et al., 2014). Using those neuropsychological assessments, deficits in "cognitive domains such as episodic memory, semantic memory, working memory, and attention, as well as dysfunction in language, praxis, and executive functioning" (Webster et al., 2014) can be analyzed. In 2011, revised guidelines for AD diagnosis were published that take the aforementioned stages of AD progression into account. In the preclinical stage of AD measurable changes of several biomarkers in the brain, cerebrospinal fluid and/or blood can indicate first signs of AD though the individuals are not cognitively affected yet. However, these proposed criteria are not established diagnostic tools so far and further studies are required (Sperling et al., 2011). MCI and dementia stage are diagnosed using the aforementioned

tools as well as brain imaging (positron emission tomography (PET) or magnetic resonance imaging (MRI)). Additionally, efforts are on the way to establish the incorporation of various biomarkers for diagnosing these disease stages (Albert et al., 2011, McKhann et al., 2011). So far, a definite AD diagnosis can solely be made after death when performing neuropathological evaluations after brain autopsy. Based on new guidelines from 2012, a neuropathologic change is now confirmed when an 'ABC' score was obtained. This score is ranked on three parameters: "histopathologic assessments of beta-amyloid (Aβ-)-containing amyloid plaques (A), Braak staging of neurofibrillary tangles (B), and scoring of neuritic amyloid plaques (C)" (Webster et al., 2014). Moreover, the novel guidelines take into account that AD neuropathological changes can even occur in the absence of cognitive impairments and thus emphasize the 'continuum' of AD mentioned before.

1.1.6 Treatment

To date, AD is still an incurable disorder and none of the available drugs can slow or ultimately stop the dysfunction and death of neurons in the brain. The developed drugs can merely improve symptoms or temporarily decelerate disease progression. However, those drugs were only effective in some patients (Alzheimer's Association, 2014, Alzheimer's Society, 2014). The *U.S. Food and Drug Administration* (FDA) had approved five prescription drugs of which only four are currently available: donepezil, rivastigmine, galantamine, memantine. Three of them, rivastigmine, galantamine and donepezil are cholinesterase inhibitors which prevents the breakdown of acetylcholine by acetylcholinesterase. Additionally, galantamine stimulates nicotinic receptors to release more acetylcholine. Rivastigmine further prevents the breakdown of butyrylcholine. Memantine act as N-methyl D-aspartate (NMDA) receptor antagonist regulating glutamate activation (Alzheimer's Society, 2014). Whereas donepezil, rivastigmine and galantamine are available for people with mild to moderate AD, memantine is prescribed for the treatment of moderate to severe AD (Alzheimer's Society, 2014). Besides pharmacologic treatments, non-pharmacologic therapies are applied to maintain cognitive function, improve quality of life or reduce behavioral symptoms like depression or apathy. Although these therapies are naturally not capable of stopping AD, cognitive training, cognitive stimulation and training in daily-living activities were often successful (Alzheimer's Association, 2014).

Since the pharmacologic treatments are limited to treating symptoms, efforts are on the way to target the underlying causes of AD. In the course of this, immunotherapy among other therapeutic approaches was considered as a promising tool. Several active and passive immunotherapies are currently investigated and look promising. However, since

several immunotherapies are still in clinical phase testing it remains to be seen if clinical efficacy can be achieved (Spencer and Masliah, 2014).

1.2 Neuropathological hallmarks

1.2.1 Amyloid deposits

Extracellular deposits of amyloid beta (Aβ) are characteristic hallmarks of AD. The main component of these so-called amyloid plaques is the Aβ peptide, a 38- to 43-amino acid peptide that derives from the amyloid precursor protein (APP) (Holtzman et al., 2011). In general, two different forms of amyloid plaques exist: neuritic and diffuse plaques (Bayer et al., 2013). Neuritic plaques (Figure 1A) are “microscopic foci of extracellular amyloid deposition and associated axonal and dendritic injury” (Selkoe, 2001). They are often found in limbic and association cortices and contain Aβ in fibrillar forms with a β-sheet conformation (Selkoe, 2001, Holtzman et al., 2011). Within as well as around those plaques swollen, degenerating neurites, i.e. dystrophic neurites, appear that can contain enlarged lysosomes, mitochondria and paired helical filaments (Holtzman et al., 2011, Selkoe, 2001). Furthermore, these plaques are often associated with microglia and/or reactive astrocytes that are either within or adjacent to the central core of the plaque or surround the plaque, respectively (Selkoe, 2001). Diffuse plaques (Figure 1B) are “usually large” (Duyckaerts et al., 2009) and lack the compacted appearance of neuritic plaques (Selkoe, 2001). In these plaques the Aβ has a non-β sheet (nonfibrillar) conformation (Holtzman et al., 2011). Although, Aβ deposition is highly dependent on the disease stage Thal *et al.* described five phases of Aβ pathology expansion. Deposition of Aβ starts in the neocortex and later spreads to i. a. striatum, hippocampus and brainstem (Thal et al., 2002). In many AD cases Aβ aggregates are also found in blood vessels. These aggregates are then called cerebrovascular plaques or cerebral amyloid angiopathy (CAA, Figure 1B) and can contribute to ischemic damage or cause lobar hemorrhage and rarely inflammatory vasculitis (Holtzman et al., 2011). However, amyloid plaques are not specific to AD as they can also occur in healthy people or in other diseases (Bayer et al., 2013).

1.2.2 Neurofibrillary tangles

The second prominent feature of AD that was already described by Alois Alzheimer is the formation of neurofibrillary tangles (NFTs). NFTs (Figure 1C) are “intracellular structures composed predominantly of a hyperphosphorylated, aggregated form of the microtubule-binding protein, tau” (Holtzman et al., 2011). Physiological, the phosphoprotein tau binds to “microtubules through its microtubule-binding domains” and

promotes “microtubule assembly and stability” (Blennow et al., 2006) and is present in all neurons (Holtzman et al., 2011). In AD, tau is hyperphosphorylated, dissociates from microtubules and aggregates in cell bodies and dystrophic neurites. Impaired axonal transport and thus altered neuronal and synaptic function are the consequences (Blennow et al., 2006). These aggregates appear as paired helical filaments (PHFs) and have high β sheet content (Selkoe, 2001, Duyckaerts et al., 2009). Expansion of tau pathology starts in the transentorhinal region and spreads to hippocampus, amygdala and neocortical association areas (Blennow et al., 2006). As with the amyloid plaques, NFTs are not specific to AD since they are also present in other neurodegenerative diseases (Bayer et al., 2013). To date, it is controversially discussed whether NFTs are a cause or a consequence of AD (Blennow et al., 2006). However, it was shown that they contribute to neuronal dysfunction and correlate with disease progression (Holtzman et al., 2011).

1.2.3 Brain atrophy and neuron loss

On the macroscopic level, brain atrophy is an additional characteristic feature of AD (Figure 1D). However, as with the aforementioned hallmarks, atrophy of hippocampal and cortical regions also appear in other types of dementia, like frontotemporal dementia and vascular dementia (Blennow et al., 2006). In AD, the first neurodegenerative changes “occur in the medial temporal lobe, including the hippocampus and entorhinal cortex” (Blennow et al., 2006) as well as the amygdala (Duyckaerts et al., 2009). Whereas the inferior temporal and the superior and middle frontal gyri show distinct atrophy, the inferior frontal and the orbitofrontal gyri are not affected (Halliday, 2003). Among others Kril *et al.* found a strong correlation between neuron number and hippocampal volume and brain volume. Thus, they were able to proof that atrophy occurs as a result of neuron loss (Kril et al., 2004).

Since neuron loss is difficult to assess it still remained unclear whether or not “neuronal death is the essence of Alzheimer pathology” (Duyckaerts et al., 2007). Controversial opinions were expressed concerning the course and severity of neuron loss in AD. However, neuron loss was confirmed in several brain regions including layer II of entorhinal cortex, CA1 region, superior temporal gyrus, supramarginal gyrus, amygdala, substantia nigra and parts of the locus coeruleus (Duyckaerts et al., 2009). The cause of neuronal loss is still controversially debated. While some groups found a correlation between neurofibrillary tangles and neuron loss (e.g. Gómez-Isla et al., 1997) other groups suggested that intraneuronal and/or oligomeric Aβ play a key role in causing neurotoxicity and neuronal death (e.g. Bayer and Wirths, 2010, Haass and Selkoe, 2007).

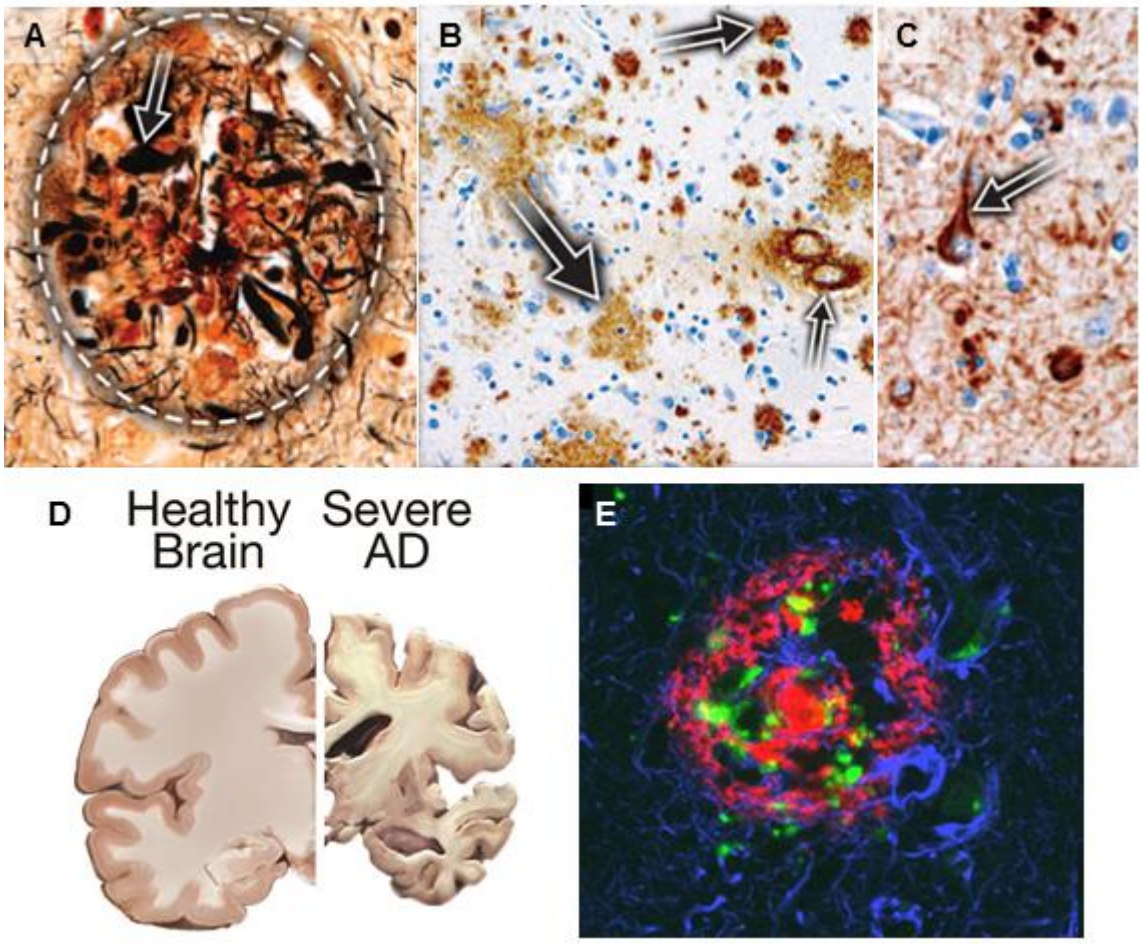

Figure 1 | Neuropathological hallmarks of AD.
(A) High-power photomicrograph of a silver-stained neuritic amyloid plaque (encircled by dashed lines) with dystrophic neurites (arrow). **(B)** Anti-Aβ antibody immunohistochemical staining of an AD brain shows diffuse plaques (large arrow), compact plaques (medium-size arrow) and cerebral amyloid angiopathy (CAA; small arrow). **(C)** Anti-phospho-tau antibody immunohistochemical staining demonstrates hyperphosphorylated tau accumulation in neuronal cell bodies (arrow). Figures (A-C) adapted from (Holtzman et al., 2011). **(D)** Comparison of a cognitively normal individual (left) with a severe AD case (right) reveals distinct brain atrophy in AD. Figure adapted from (http://www.nia.nih.gov/sites/default/files/02_healthybrain_lg.jpg, 12.10.2014). **(E)** Immunohistochemical staining of an AD brain revealed microglia (anti-CD68 antibody, green) and astrocytes (anti-GFAP antibody, blue) in close proximity to Aβ (anti-Aβ antibody, red). Figure adapted from (Venneti et al., 2009).

1.2.4 Synaptic loss and dysfunction

Besides neuron loss, synaptic dysfunction, decrease in markers for certain neurotransmitter as well as synaptic loss are typical hallmarks of AD (Holtzman et al., 2011). Decreased numbers of synapses were observed in different brain regions of AD patients including cortex (lamina III of Brodmann's area) and hippocampal CA1 region (DeKosky and Scheff, 1990, Scheff et al., 2007). Moreover, levels of presynaptic and postsynaptic markers were altered in AD patients, e.g. synaptophysin (Masliah et al., 1994) and PSD95 (Shinohara et al., 2014). However, Shimohama *et al.* described that

only some markers are decreased while others are maintained indicating “differential involvement of synaptic components in AD” (Shimohama et al., 1997). Additionally, it was observed that neurons with certain neurotransmitter systems are particularly vulnerable. This includes glutamatergic, cholinergic and norardrenergic neurons (Holtzman et al., 2011). Although deficits in other neurotransmitters like GABA or serotonin occur during disease progression, early AD symptoms correlate with dysfunction of cholinergic and glutamatergic synapses (Selkoe, 2002). These findings have previously led to the design of several drugs as described before. It is assumed that “synapses play a major physiopathological role in AD” (Duyckaerts et al., 2009) and that synaptic loss and dysfunction are among the strongest correlates of cognitive decline (Querfurth and LaFerla, 2010, Selkoe, 2002). Several studies indicated that synaptic dysfunction occurs prior to “physical deterioration of neuronal structures” (Marcello et al., 2012). Koffie *et al.* postulate that AD starts as a “disease of synaptic dysfunction and synapse loss then progresses to include widespread neuronal loss and neuronal network failure” (Koffie et al., 2011). It is supposed that intraneuronal Aβ rather than extracellular plaques contribute to this synaptic pathology (e.g. Bayer and Wirths, 2010). Recently, studies described that soluble assembly states of Aβ (oligomeric Aβ) cause cognitive impairments by affecting synaptic structure and plasticity (Haass and Selkoe, 2007, Marcello et al., 2012). A variety of targets and mechanisms responsible for Aβ-mediated effects on synapses are currently debated. This includes the interaction of Aβ with various receptors, like acetylcholine or glutamate receptors, as well as with other synaptic proteins, e.g. EphB2 or PrP^C (Marcello et al., 2012).

1.2.5 Inflammation

Ongoing inflammatory processes as seen by e.g. reactive astrocytes, activated microglia, early components of the complement cascade or proinflammatory cytonkines/chemokines feature another hallmark of AD (Selkoe, 2001, Duyckaerts et al., 2009, Akiyama et al., 2000). Activated microglia within neuritic plaques and clustered at sites of aggregated Aβ deposition as well as astrocytes surrounding the amyloid core are well-known characteristics in AD brains (Figure 1E, Duyckaerts et al., 2007, Akiyama et al., 2000). Levels of theses glia cells as well as their expressed biochemical markers are elevated in the brains of AD patients (Querfurth and LaFerla, 2010, Duyckaerts et al., 2009). Several studies showed that exposure to Aβ led to activation of microglia thus implying “a crucial step in the initiation of inflammation” (Akiyama et al., 2000). Activated microglia produce a variety of proinflammatory mediators and potentially neurotoxic substances including complement, cytokines, reactive oxygen intermediates, secreted proteases, excitatory amino acids and NO (Akiyama et al., 2000). Likewise, astrocytes are

capable of expressing several inflammatory mediators, like complement receptors, complement components, cytokines and chemokines (Akiyama et al., 2000). However, microglia also demonstrated a neuroprotective role since they participate in removing compacted amyloid deposits and are also capable of internalize soluble Aβ from the extracellular space (Graeber and Streit, 2010, Mandrekar-Colucci and Landreth, 2010). Similarly, it was shown that reactive astrocytes "can take up and degrade extracellular deposits of Aβ42" (Sofroniew and Vinters, 2010). It still remained an unanswered question "if inflammation is a cause, contributor, or secondary phenomenon in this disorder" (Wyss-Coray and Rogers, 2012). Inflammatory response is assumed to bring along both beneficial as well as detrimental effects (Duyckaerts et al., 2007). It is strongly discussed and poorly understood whether inflammatory mechanisms cause damage in AD or contribute to the removal of primary pathologic processes (Akiyama et al., 2000, Graeber and Streit, 2010). In AD brains damaged neurons and neurites, (insoluble) Aβ deposits and NFTs may provide stimuli for inflammation. Since these stimuli are often present from early preclinical to terminal stages of AD the up-regulation of inflammation is chronic as well. Direct and indirect alterations from inflammatory mechanisms are likely to worsen those pathogenic processes that previously initiate them. Hence it is assumed that those inflammatory processes contribute to AD pathogenesis (Akiyama et al., 2000).

1.3 The amyloid precursor protein (APP)

1.3.1 Isoforms of APP

As previously mentioned, Aβ peptides originate from the larger amyloid precursor protein by several proteolytic cleavage events. The amyloid precursor protein (APP) is a type 1 transmembrane glycoprotein (Puzzo et al., 2014) with a large extracellular domain and a smaller cytoplasmic part (Bayer et al., 2013). APP is highly conserved in evolution and a member of the amyloid precursor-like proteins (APLPs) family that revealed substantial homology within the extracellular and cytoplasmic tail but a large divergence within the Aβ region (Selkoe, 2001). It is found in the peripheral nervous system as well as in skeletal muscle cells and is abundantly expressed in the brain, especially by neurons (Panegyres and Atkins, 2011, Puzzo et al., 2014). There are several isoforms of APP that arise "from alternative splicing" and a "variety of posttranslational modifications", like "addition of N- and O-linked sugars, sulfation and phosphorylation" (Selkoe, 2001). At least four types of mRNA are known that are generated by alternative splicing of exons 7 and 8. These isoforms of APP are named after the number of amino acids: APP 695, APP 714, APP 751 and APP 770 (Panegyres and Atkins, 2011). The 751- and 770-amino acid isoforms contain a region homologous to the Kunitz-type serine protease inhibitor (KPI) motif (encoded by exon 7), are mainly expressed outside the brain and play a role in the

coagulation pathway in the plasma (Selkoe, 1998, Holtzman et al., 2011). APP 714 and APP 695 lack exon 7 and are mainly expressed in the CNS. Differential splicing of exon 15 results in other isoforms that are found in lymphocytes, macrophages and microglial cells (Panegyres and Atkins, 2011).

1.3.2 Non-amyloidogenic and amyloidogenic processing of APP

APP can be processed by two enzymatic pathways: the non-amyloidogenic or the amyloidogenic pathway (Figure 2). This proteolytic cleavage is performed by several membrane bound and site-specific cleaving enzymes known as secretases (Zolezzi et al., 2014).

Within the non-amyloidogenic pathway, α-secretase cleaves the APP within the ectodomain liberating two bigger soluble fragments, the extracellular N-terminal domain soluble APP-α (sAPPα) and the 83-aa-long C-terminal fragment CTFα (C83) (Carrillo-Mora et al., 2014). As α-secretase cleaves APP in the middle of the Aβ domain, i.e. between residue 16 and 17 of Aβ fragment, generation of Aβ is prevented (Haass, 2004). Secondly, the membrane-retained CTFα is further cleaved by γ-secretase releasing the smaller 3 kDa fragment p3 ($Aβ_{17-40/42}$) and the approximately 50-aa-long amyloid intracellular domain (AICD) (Carrillo-Mora et al., 2014, Querfurth and LaFerla, 2010).

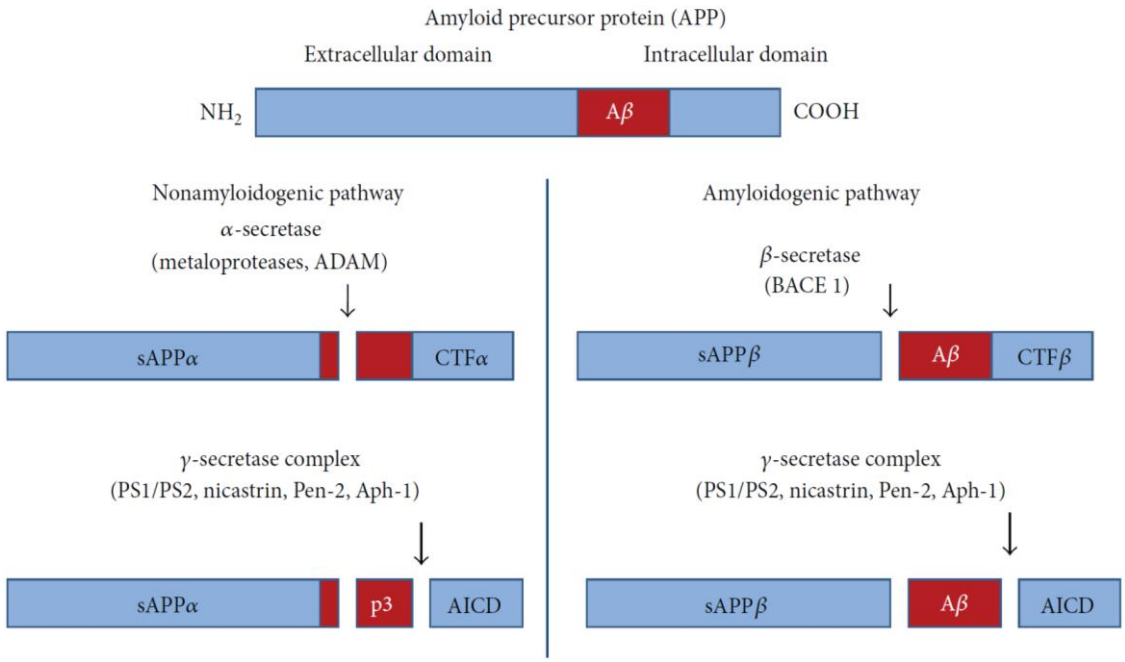

Figure 2 | APP processing and generation of β-amyloid.
The amyloid precursor protein (APP) can be processed by either the non-amyloidogenic or amyloidogenic pathway. This processing is mediated by several secretases and generates different derivatives including the Aβ peptide. Figure adapted from (Carrillo-Mora et al., 2014).

Within the amyloidogenic pathway, APP is proteolyzed by β-secretase liberating the soluble N-terminal fragment soluble APPβ (sAPPβ) and the 99-aa-long C-terminal fragment CTFβ (C99) (Carrillo-Mora et al., 2014). In a next step, the membrane-retained CTFβ is cleaved by γ-secretase generating the 4 kDa Aβ peptide and the AICD domain (Carrillo-Mora et al., 2014). Due to the heterogeneous cleavage of γ-secretase Aβ peptides and AICD fragments of varying length are produced (Marcello et al., 2012).

Since APP undergoes a regulated cleavage first of its ectodomain and second of its transmembrane domains by specific membrane-anchored secretases, generation of Aβ is "one example of a general physiological mechanism […] known as 'regulated intramembrane proteolysis' (RIP)" (Haass and Selkoe, 2007).α-secretase activity was demonstrated by three proteases that belong to the ADAM family (a family of disintegrin and metalloproteinases) (Buxbaum et al., 1998, Lammich et al., 1999, Koike et al., 1999). The β-secretase is considered to be "the Aβ production rate limiting enzyme" (Zolezzi et al., 2014). It was identified as a type 1 transmembrane protein with aspartyl protease activity termed β-site APP cleaving enzyme 1 (BACE-1) (Vassar et al., 1999, Haass, 2004). BACE is a member of the pepsin family of aspartyl proteases, but is assumed to define a novel subgroup of membrane-associated hydrolases. It is assumed that APP is not the main substrate of BACE-1. Although little is known about the physiological substrate so far, some candidates were suggested including APPSwe, P-selectin glycoprotein ligand-1, sialyl-transferase ST6Gal I, interleukin-1 type II receptor, APLP1 and APLP2, neuregulin-1 and neuregulin-3 (Haass, 2004, Kandalepas and Vassar, 2012). The γ-secretase is an intramembranous complex that consists of four proteins: nicastrin (Nct), presenilin enhancer 2 (PEN-2), anterior pharynx-defective 1 (Aph-1), presenilin 1 or 2 (PS1/PS2). Thereby, the presenilins represent the catalytic core even though they are not sufficient for γ-secretase activity alone (Carrillo-Mora et al., 2014, Blennow et al., 2006, Haass, 2004). A variety of presenilin substrates were identified including APP, Notch, "APP homologs APLP-1/-2, ErbB-4, E-cadherin, N-cadherin, LRP, Nectin-1-α, the Notch ligands Delta and Jagged, and CD44" (Haass, 2004).

Although APP and the mentioned secretases are all integral transmembrane proteins and share similar trafficking routes, the amyloidogenic and non-amyloidogenic pathways may occur at different places within the cell (cf. Thinakaran and Koo, 2008). After maturation processes, APP and the secretases can traffic to the cell surface. However, BACE-1 and γ-secretase can also be transported directly to the sorting endosomes where BACE-1 is recycled to the trans-Golgi network and γ-secretase is sorted to late endosomes/lysosomes (De Strooper and Annaert, 2010). α-secretase activity is mainly localized in the secretory route (trans-Golgi network) or at the plasma-membrane

(Lammich et al., 1999, De Strooper and Annaert, 2010). APP molecules that were not cleaved by α-secretase at the surface membrane can be internalized into endocytic compartments and are cleaved by β- and γ-secretase to generate Aβ (Marcello et al., 2012). Similar, after its synthesis β-secretase is targeted to the plasma membrane where it is enriched in lipid rafts but can be also reinternalized to early endosomes. Thus, BACE-1 and APP have “similar trafficking routes and meet within endosomes” (Haass, 2004). Although, BACE-1 can cleave APP at the cell surface or in early endosomes, the preferential site of β-secretase activity is mainly restricted to the endoplasmic reticulum and the endosomal/lysosomal system due to its acidic pH optimum (Kinoshita et al., 2003, Haass, 2004, De Strooper and Annaert, 2010). It was suggested that γ-secretase activity is widely distributed between trans-Golgi network, surface and endosomes. However, several studies underlined that it takes place in endosomal sorting compartments, i.e. late endosomes, multivesicular bodies and lysosomes (De Strooper and Annaert, 2010).

Moreover it was found that intracellular organelles generate Aβ peptides of different lengths. $Aβ_{1-40}$/$Aβ_{x-40}$ is exclusively produced in the trans-Golgi network (TGN) and packed into post-TGN secretory vesicles. Insoluble $Aβ_{x-42}$ is generated and maintained within the endoplasmic reticulum. Additionally, $Aβ_{1-42}$ and $Aβ_{x-42}$ are made in the TGN and packed into secretory vesicles. Peptides produced in the TGN consist of soluble and insoluble populations (Greenfield et al., 1999).

It was shown that 90 % of APP processing occurred within the non-amyloidogenic pathway and 10 % within the amyloidogenic pathway under normal conditions. The cause for the shift to an increased APP processing by the amyloidogenic pathway remained unclear. It might be due to an increase in cholesterol levels resulting in lipid raft formation, increased β-secretase levels, mutations in AD-related proteins or a decrease in Aβ clearance resulting in gradual accumulation (Platt et al., 2013).

A complex machinery in the brain contributes to clearance of Aβ from the brain as well as to degradation of Aβ peptides and accumulations. This includes physiological parameters such as blood and CSF as well as a variety of clearance receptors like LRP1 and VLDLR. Moreover, a broad range of Aβ degrading proteases like neprilysin and neprilysin-2 (NEP, NEP2), angiotensin converting enzyme (ACE), endothelin converting enzyme (ECE1, -2), matrix metalloproteinases, plasmin, insulin-degrading enzyme (IDE) and cathepsin B/D are involved (De Strooper, 2010, Marr and Hafez, 2014, Leissring, 2014).

1.3.3 Physiological functions of APP and its derivatives

Although its actual functions remained unclear so far, a variety of physiological functions were attributed to full-length APP, several domains of APP or its fragments. This also includes a receptor or growth factor function (Marcello et al., 2012). It was suggested that a domain of APP stimulates neurite outgrowth and promotes synaptogenesis (Rossjohn et al., 1999). Full-length APP "may play important roles in maintaining nerve cell structure and signal transduction" and "may have a range of physiological functions associated with developing and adult neurons" (Marcello et al., 2012). The APP-derived sAPPα was shown to promote neuronal survival (Li et al., 1997), stimulates proliferation of neural stem cells (Caillé et al., 2004) and can facilitate LTP and spatial memory (Taylor et al., 2008). Similarly, a physiological role was attributed to Aβ since this peptide is also produced during normal metabolism (Haass et al., 1992). Kamenetz *et al.* showed that activity-dependent Aβ production participates in a negative feedback that regulates neuronal hyperactivity indicating a role of Aβ in homeostatic plasticity (Kamenetz et al., 2003). It was also demonstrated that Aβ can act as a positive regulator at presynaptic level (Abramov et al., 2009) and increase synaptic transmission (Puzzo et al., 2008). Different Aβ species may act via various receptors and thus produce several synaptic effects (Ondrejcak et al., 2010). Furthermore, dose-dependent neuroprotective, trophic as well as antioxidative physiologic effects were described for Aβ (Thinakaran and Koo, 2008, Carrillo-Mora et al., 2014).

1.4 Genetic background of AD

AD is a heterogeneous disorder (Blennow et al., 2006) which can be divided into subcategories due to two criteria: heritability, i.e. familial and sporadic cases (FAD and SAD, respectively) as well as the age of onset, i.e. early-onset AD (EOAD) and late-onset AD (LOAD). Familial AD is inherited in an autosomal dominant fashion with an early onset before the age of 65 years. In contrast, sporadic AD is not inherited and usually starts when patients are 65 years or older, i.e. late-onset AD (Holtzman et al., 2011). Both forms are phenotypically very similar and often indistinguishable (Selkoe, 2001). While the familial form of AD is very rare (prevalence below 1 %) the sporadic form accounts for the vast majority of all cases (up to 99 %, Holtzman et al., 2011). In familial forms of AD, mutations are assumed to cause an increase of Aβ production or aggregation whereas in sporadic AD failure of clearance mechanisms might play a role (cf. Marcello et al., 2012, Blennow et al., 2006).

Within the familial form of AD (FAD), mutations are known in the APP gene on chromosome 21q21, the PS1 gene on chromosome 14q24.3 as well as in the PS2 gene

on chromosome 1q31-q42 (Blennow et al., 2006, Karch et al., 2014). Approximately 180 mutations in PS1, 20 mutations in PS2 and 36 mutations in APP have been reported leading to an increase in total Aβ levels, Aβ42/Aβ40 ratio or the aggregation (Marr and Hafez, 2014). Missense mutations in APP (Figure 3) are located at or near the APP cleavage sites of β- and γ-secretases. Mutations near the C-terminus of the Aβ region elevate the Aβ42 level increasing the Aβ42/Aβ40 ratio. Mutations that occur near the β-secretase cleavage site result in an overproduction of all Aβ species (Holtzman et al., 2011). Moreover, a multiplication of the entire chromosome 21, as seen in trisomy 21 (Down's syndrome) leads to an overproduction of Aβ peptides and can predispose to an early onset of AD (Selkoe, 2001). Mutations in PS1 and PS2 are "distributed throughout the protein, with some clustering occurring in the transmembrane domains" (Karch et al., 2014). PS1 mutations are the most common cause of FAD (Holtzman et al., 2011). AD patients with PS1 mutations revealed "the earliest and most aggressive form of AD" with a clinical onset in their 40s and 50s, but sometimes also in their 30s (Selkoe, 2001). As with the APP mutations total levels of Aβ42 or the Aβ42/Aβ40 ratio are increased in patients with PS mutations (Holtzman et al., 2011).

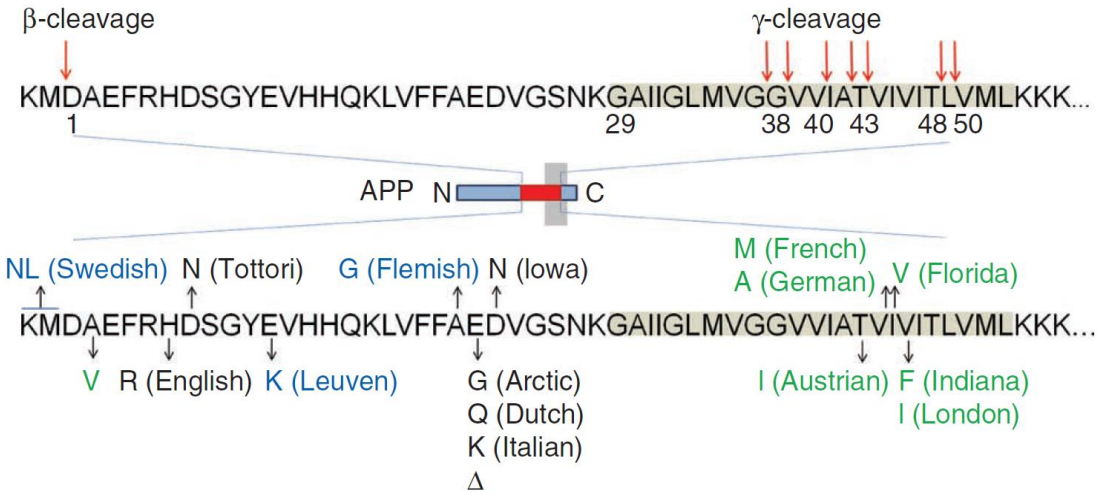

Figure 3 | Mutations in the amyloid precursor protein.
Generation of Aβ from amyloid precursor protein (APP) and sites of β- and γ-secretase cleavage are shown in the upper part of this figure. Additionally, selected mutations in Aβ region of APP are demonstrated below. Mutations lead to increase of total Aβ production (blue), alter Aβ biophysical properties (black) or affect the Aβ spectrum in quantitative and qualitative ways (green). Figure adapted from (Benilova et al., 2012).

Within the sporadic form of AD (SAD) "the most significant effectors of risk occur in genes strongly linked to Aβ" (Marr and Hafez, 2014). The strongest risk factor known so far is the apolipoprotein E (APOE) (Blennow et al., 2006) which can affect aggregation, clearance and catabolism of Aβ (Marr and Hafez, 2014). APOE is a glycoprotein that plays a role "in mobilization and redistribution of cholesterol", neuronal growth, nerve

generation, immune response and activation of lipolytic enzymes (Karch et al., 2014). The APOE gene is located on chromosome 19q13.2 and exists in three allele isoforms: ε2, ε3 or ε4. The ε3 form is the most common isoform but does not alter the risk of AD. The ε2 and ε4 form are less common but are known to modify one's risk of developing AD (Alzheimer's Association, 2014, Selkoe, 2001, Raber et al., 2004). Whereas ε2 is believed to decrease the probability (Corder et al., 1994), the ε4 form increases the risk to develop AD even at a younger age. This risk is even more pronounced when inheriting two copies of the ε4 form (Corder et al., 1993). Several studies like genome-wide association studies, whole-exome and whole-genome sequencing showed that also other genes predispose to AD. These novel genetic risk factors include clusterin (CLU), complement receptor 1 (CR1), ephrin receptor A1 (EPHA1), ATP-binding cassette transporter (ABCA7), triggering receptor expressed on myeloid cells 2 protein (TREM2), phospholipase D3 (PLD3), *etc.* (Karch et al., 2014). In general, these new candidate genes shed light on pathways implicated in AD including lipid (cholesterol) metabolism, endocytosis and inflammatory response (Karch et al., 2014, Medway and Morgan, 2014).

1.5 The Amyloid cascade hypothesis

1.5.1 The "classical" amyloid cascade hypothesis

The "classical" amyloid cascade hypothesis has been the central paradigm of AD research for many years. According to this hypothesis, accumulation of Aβ is the primary cause driving AD pathology. It states that altered APP metabolism leads to amyloid deposition and subsequently to neuritic plaques, neurofibrillary tangles and neuropil threads and finally causes neuronal damage and dementia (Hardy and Allsop, 1991). Several arguments support this hypothesis. Duplication and different mutations in the APP and PS1/PS2 genes were identified that directly caused Aβ deposition and led to early-onset forms of AD (Rovelet-Lecrux et al., 2006, Hardy and Selkoe, 2002). Transgenic mice expressing different FAD-related mutations demonstrated pathological features of AD including amyloid plaques and cognitive impairments (cf. Webster et al., 2014). Moreover, mutations in the gene encoding the tau protein led to deposition of tau in NFTs, but not to deposition of amyloid. Overexpression of mutant human APP and tau in transgenic mice led to increased formation of tangles while amyloid plaques are unaltered. Both findings indicate that changes in Aβ metabolism and plaque formation occur prior to tau pathology. Furthermore, APP transgenic mice were crossed with APOE-deficient mice. Their offspring revealed decreased cerebral Aβ deposition pointing to an involvement of APOE in Aβ metabolism (Hardy and Selkoe, 2002). Patients suffering from trisomy 21 (Down's syndrome) possess a multiplication of chromosome 21 on which APP

is located. They develop AD pathology in terms of senile plaques, NFTs and neuron loss already at young ages (cf. Mann, 1988).

In contrast, various arguments challenge this amyloid hypothesis. An important observation was that in humans the number of amyloid plaques does not correlate well with the degree of cognitive deficits (Hardy and Selkoe, 2002, Giannakopoulos et al., 2003). Although having abundant NFTs and senile plaques some humans stayed cognitively normal during their whole life (Snowdon, 1997). Similarly, transgenic mice showed impairments in behavioral tests prior to plaque deposition (e.g. Hsia et al., 1999). Moreover, AD patients were immunized with the anti-Aβ42 active vaccine AN1792. Subsequent analysis revealed a clearance of amyloid plaques but did not stop progressive neurodegeneration (Holmes et al., 2008). Additionally, several studies showed that synaptic loss is "the major structural correlate to cognitive dysfunction" instead of NFTs, senile plaques or neuron loss as these pathological features showed a poorer statistical correlation with dementia (Marcello et al., 2012). Based on these findings 'revised' amyloid hypotheses were proposed.

1.5.2 The soluble amyloid hypothesis

The "classical" amyloid cascade hypothesis focusses solely on insoluble amyloid aggregates. However, the idea of soluble Aβ oligomers as the toxic and disease-causing agent is gaining more and more support (e.g. Klein, 2002, Haass and Selkoe, 2007, Pimplikar, 2009, Benilova et al., 2012). The detection of buffer-soluble bioactive oligomers (e.g. dimers, trimers, tetramers, dodecamers, and higher oligomers) led to the concept that soluble Aβ plays a key role in AD pathology (Mucke and Selkoe, 2012). Such oligomers were isolated from culture medium, brains of AD patients and AD mouse models (Walsh et al., 2005, Shankar et al., 2008, Lesné et al., 2006). Several studies proved that soluble (synthetic or natural) oligomers are neurotoxic and capable of causing synaptic dysfunction as well as cognitive changes (e.g. Walsh et al., 2002, Cleary et al., 2004, Shankar et al., 2007, Shankar et al., 2008, Selkoe, 2008, Tomiyama et al., 2010). Furthermore, it was described that some oligomeric Aβ species "are small and soluble enough to diffuse […] through the brain parenchyma" and into synaptic clefts impairing synaptic structure and function and finally neuron survival (Haass and Selkoe, 2007). In the course of this, it was also suggested that insoluble amyloid aggregates might be relatively inactive but can serve as reservoirs of these smaller, soluble assemblies (Haass and Selkoe, 2007, Mucke and Selkoe, 2012). However, an exact definition of the term 'toxic Aβ oligomer' is still lacking (Benilova et al., 2012). A variety of oligomeric Aβ assemblies including protofibrils, annular assemblies, Aβ-derived diffusible ligands (ADDLs), Aβ*56 as well as dimers and trimers was described (Hardy and Selkoe, 2002,

Haass and Selkoe, 2007). It was proposed that soluble oligomers comprise "Aβ assemblies that are not pelleted from physiological fluids by high-speed centrifugation" (Haass and Selkoe, 2007) but not all aforementioned forms fulfil this definition. Ultimately, the difficulty to ascribe the mentioned neurotoxic effects principally to one certain Aβ species still persists (Hardy and Selkoe, 2002, Haass and Selkoe, 2007).

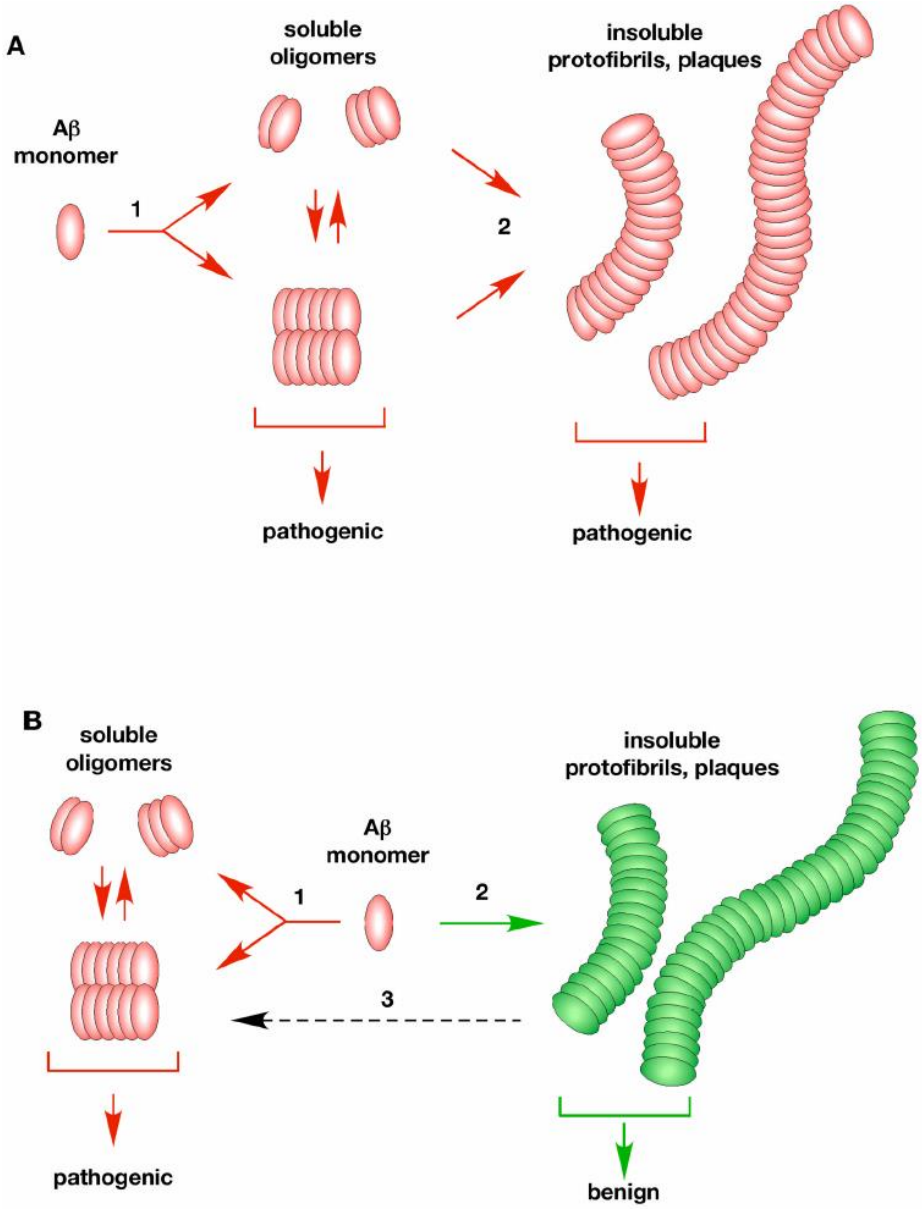

Figure 4 | Potential pathways of Aβ aggregation *in vivo.*
Since only little is known about how Aβ aggregates/oligomerizes two possibilities were suggested. **(A)** In a linear oligomerization pathway Aβ monomers initially form low molecular weight soluble aggregates (1). In a second step, these oligomers further aggregate into insoluble protofibrils, fibrils and plaques (2). Both soluble oligomers and insoluble fibrils are considered to be pathogenic. **(B)** Another possibility claims that there are two distinct pathways: (1) a pathogenic pathway that forms soluble oligomers (dimers/Aβ*56/ADDLs) which cause the disease and (2) a non-pathogenic pathway that leads to the formation of insoluble aggregates and plaques. The insoluble aggregates are thought to be benign. Moreover, it was suggested that the insoluble aggregates may slowly leach forming the pathogenic soluble oligomers (3). Figure adapted from (Pimplikar, 2009).

So far, it remained poorly understood by which molecular pathways Aβ forms soluble oligomers, insoluble fibrils and plaques (Figure 4, Pimplikar, 2009). It was suggested that monomeric Aβ self-aggregates forming dimers, trimers, oligomers and protofibrils which further aggregate to fibrils and finally plaques (Pimplikar, 2009, Glabe, 2008, Duyckaerts et al., 2007). Kumar *et al.* described two kinetic phases of Aβ aggregation. During the 'lag phase' monomeric Aβ slowly accumulates and forms oligomers. In the 'elongation phase' those oligomers promote the formation of protofibrils which ultimately aggregate to mature fibrils (Kumar et al., 2011). Whether or not insoluble amyloid aggregates are pathogenic or benign is still controversially discussed. Benilova *et al.* suggested a "dynamic equilibrium between toxic oligomers and inert fibrils" that "might exist around the plaques, resulting in local 'spillover' of neurotoxic species in surrounding tissue" (Benilova et al., 2012). However, a consensus seems to exist that Aβ oligomers are pathogenic and strongly contribute to AD pathology (Figure 4).

1.5.3 The intraneuronal amyloid hypothesis

Two early findings point to the fact that amyloid-β might not only be an extracellular phenomenon. Masters *et al.* described that amyloid is first deposited in the neuron and afterwards in the extracellular space (Masters et al., 1985b). Despite neurofibrillary tangles, amyloid protein was also detected intracellularly (Grundke-Iqbal et al., 1989). On the one hand, cell biological studies revealed that Aβ peptides can be generated at different subcellular sites including the endoplasmic reticulum, the trans-Golgi network and the endosomal-lysosomal system (see section 1.3.2, Selkoe, 1998, Greenfield et al., 1999, Perez et al., 1999). On the other hand, cellular uptake of Aβ from the environment might also contribute to intracellular accumulation (e.g. Bahr et al., 1998). In 2000, Gouras *et al.* claimed that "intracellular Aβ42 accumulation is an early event in neuronal dysfunction" as they found Aβ42 within neurons of areas that are known to develop AD pathology very early, like hippocampus and entorhinal cortex (Gouras et al., 2000). In contrast, this intraneuronal Aβ42 staining was less evident in brain regions that are less affected by AD, e.g. primary sensory and motor cortices. Additionally, they found that intraneuronal Aβ42 immunoreactivity attenuates with increasing cognitive dysfunction and Aβ plaque deposition (Gouras et al., 2000). Another study demonstrated that in brains of AD patients intraneuronal Aβ deposition occurs prior to the appearance of PHF-immunoreactive structures (Fernández-Vizarra et al., 2004). Moreover, studies using transgenic AD mouse models revealed synaptic dysfunction and/or behavioral changes prior to plaque deposition as well as presence of intraneuronal Aβ that precedes tangle formation (Hsia et al., 1999, Moechars et al., 1999, Oddo et al., 2003). Similarly, two other models showed an intracellular Aβ immunoreactivity which decreased with aging but

preceded the occurrence of amyloid plaques (Wirths et al., 2001, Wirths et al., 2002). Moreover, one of these mouse models, APP/PS-1 double-transgenic mice, developed an age-related neuron loss that did not correlate with extracellular amyloid plaques (Schmitz et al., 2004). Several studies described that mutations in AD-related genes also increase intracellular Aβ levels (e.g. Qi et al., 2003). Based on these and other findings (Wirths et al., 2004, Giménez-Llort et al., 2007) a modified amyloid cascade hypothesis was proposed (Figure 5). It states that intraneuronal levels of Aβ42 increase due to ageing, Down's syndrome and AD-related mutations. Intraneuronal Aβ accumulates and further cause synaptic and neuronal dysfunction, subsequently neurodegeneration and ultimately dementia. Simultaneously, amyloid plaques are produced. Intraneuronal Aβ levels increase as Aβ can be internalized from these plaques again (Wirths et al., 2004).

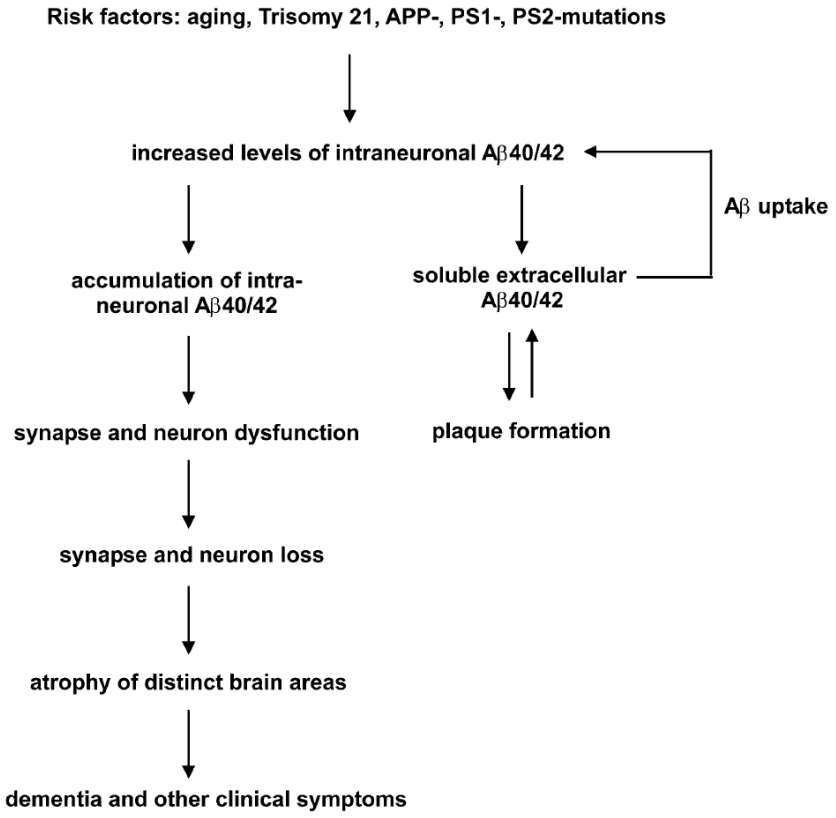

Figure 5 | The modified amyloid cascade hypothesis.
Based on recent findings the "classical" amyloid cascade hypothesis was revised and now incorporates the emerging role of intraneuronal Aβ in AD pathology. Figure adapted from (Wirths et al., 2004).

This hypothesis was further supported by the detection of intraneuronal Aβ in other transgenic mouse models, like 5XFAD (Oakley et al., 2006), TBA2.1 (Alexandru et al., 2011), Tg2576 (Takahashi et al., 2013) and APP^{SL}PS1KI (Casas et al., 2004). More strikingly, intraneuronal accumulation in these and other mouse models was correlated with AD-typical alterations including neuron loss, synaptic deficits, motor and/or cognitive

impairment (e.g. Abramowski et al., 2012, Billings et al., 2005, Breyhan et al., 2009, Christensen et al., 2008a, Alexandru et al., 2011, Jawhar et al., 2010). Additionally, it was suggested that intracellular Aβ can also promote hyperphosphorylation of tau (Giménez-Llort et al., 2007).

1.6 Amyloid-β variants

Early studies revealed that Aβ peptides are present in culture medium (Haass et al., 1992), in human CSF (Seubert et al., 1992) and in the amyloid deposits of AD patients (Prelli et al., 1988, Miller et al., 1993, Iwatsubo et al., 1994, Näslund et al., 1994, Saido et al., 1995). These peptides showed both N- as well as C-terminal heterogeneity (Selkoe, 1998) displaying different solubility, stability and biological as well as toxic properties (Benilova et al., 2012). Aβ numbering is based on the numbers of amino acids that comprise the peptide beginning with aspartyl as first amino acid residue of Aβ sequence (Figure 3). The APP-processing enzyme γ-secretase cleaves at different position and thus generates C-terminal heterogeneity itself. Various C-terminally modified Aβ variants like Aβ43, Aβ42, Aβ40, Aβ38 and Aβ37 were found in cell culture and body fluids as described above (Benilova et al., 2012). Aβ42 and Aβ40 turned out to be the major soluble Aβ peptides. Presenilin mutations increase the ratio of Aβ42 to Aβ40 species ('Aβ42/Aβ40 ratio') (De Strooper, 2010). However, it was also found that level of Aβ43 was increased in some FAD patients while Aβ37 and Aβ38 were decreased indicating an impact of additional Aβ variants. Both normal and AD brains "continuously and abundantly" (Benilova et al., 2012) generate Aβ40. In contrast, other Aβ variants are produced at lower levels (Benilova et al., 2012). Immunohistochemical studies showed that the first Aβ species deposited in AD brains end at residue 42 indicating that the diffuse plaques are almost exclusively composed of Aβ42 (Selkoe, 1998). Since the Aβ42 peptide has two additional hydrophobic residues, it aggregates much faster than Aβ40 (Selkoe, 1998). Thus, both quantitative changes as well as the biophysical and pathobiological attributes of Aβ have to be considered (Benilova et al., 2012).

Heterogeneity of Aβ variants is also generated by different "enzymatic processes mediated by aminopeptidases, glutaminylcyclase or isomerases" (Benilova et al., 2012) and by phosphorylation of Aβ (Kumar et al., 2011). Moreover, Aβ species can be additionally modified by post-translational modifications including oxidation, nitration, glycosylation and racemization (Kummer and Heneka, 2014). The resulting Aβ peptides take part in different Aβ functions in the healthy brain as well as in e.g. oligomerization/fibrillization in the AD brain (Benilova et al., 2012, Kumar et al., 2011).

1.6.1 N-terminally truncated amyloid-β variants

Although their significance for pathogenesis has long been unclear, mounting evidences suggest a role of N-terminally truncated Aβ variants in AD etiology. Besides Aβ variants starting with an Asp at position 1, other diverse N-truncated Aβ peptides were identified "starting with amino residue Ala-2, pyroglutamylated Glu-3, Phe-4, Arg-5, His-6, Asp-7, Ser-8, Gly-9 Tyr-10 and pyroglutamylated Glu-11" (Bayer and Wirths, 2014). Several groups detected a variety of N-truncated Aβ species in brain or CSF samples of AD patients (e.g. Miller et al., 1993, Roher et al., 1993, Saido et al., 1995, Wiltfang et al., 2001, Sergeant et al., 2003, Miravalle et al., 2005, Portelius et al., 2010, Abraham et al., 2013, Guzmán et al., 2014). Gouras *et al.* claimed that plaque-associated as well as intraneuronal Aβ "appears to be N-terminally truncated" (Gouras et al., 2000). However, Thal *et al.* described that N-truncated Aβ "is found either in full-length Aβ-containing plaques or in deposits consisting exclusively of N-terminal-truncated Aβ" (Thal et al., 2000). Several mouse models harboring N-truncated Aβ variants have been generated in the last years. Particularly, the N-terminally modified Aβ species pyroglutamate-amyloid-β (pE3-Aβ) has been extensively analyzed in the TBA2, TBA2.1/TBA2.2, APP^{SL}PS1KI, 5XFAD, TBA42 and FAD42 mouse models (Wirths et al., 2009, Alexandru et al., 2011, Casas et al., 2004, Jawhar et al., 2011b, Jawhar et al., 2011a, Wittnam et al., 2012). However, little is known about other N-truncated Aβ variants and their effects *in vivo*.

So far, the specific enzymes which mediate the generation of N-truncated Aβ are largely unknown or at least not understood in detail. Nevertheless, several candidates were proposed (Bayer and Wirths, 2014). Besides being responsible for cutting APP before position 1 of the Aβ fragment, BACE-1 is also capable of cleaving between Tyr-10 and Glue-11 releasing $Aβ_{11-x}$ (Vassar et al., 1999). Bien *et al.* reported that the metalloproteinase meprin β showed a similar activity like BACE-1 as it cleaved at the aspartate at position 1. Strikingly, they additionally described that this protease could also cleave at the alanine at position 2 releasing an $Aβ_{2-x}$ peptide (Bien et al., 2012). Takeda *et al.* suggested that α-secretase-like proteases are involved in generation of $Aβ_{5-40/42}$ and found that cleavage between Phe-4 and Arg-5 was independent of BACE-1 cleavage (Takeda et al., 2004). Moreover, it was proposed that aminopeptidase A (Sevalle et al., 2009), neprilysin (NEP, Howell et al., 1995, Leissring et al., 2003), insulin-degrading enzyme (Kummer and Heneka, 2014), plasmin (van Nostrand and Porter, 1999), angiotensin-converting enzyme (ACE, Hu et al., 2001) as well as myelin basic protein (MBP, Liao et al., 2009) are involved in N-terminally truncation of Aβ.

Whether or not the occurrence of these N-truncated species accompanies with changes in their assembly characteristics and biophysical properties was studied by

various groups. Using sedimentation analyses, electron microscopy, circular dichroism and cell culture Pike *et al.* showed that “N-terminal deletions enhance aggregation of Aβ into neurotoxic, β-sheet fibrils” (Pike et al., 1995b). Further, the authors suggested that those amino-terminal deletions initiate or at least contribute to Aβ deposition (Pike et al., 1995b). An Aβ isoform with a pyroglutamate at position 3 (AβN3(pE)-40/42) induced an increased cell loss in comparison to full-length Aβ species, aggregated extensively and showed a more pronounced resistance to astrocyte-induced degradation. Hence, Russo *et al.* suggested that N-terminal deletion and cyclization contributes to toxicity of this Aβ species (Russo et al., 2002). Another group found that N-terminal pyroglutamate led to a higher aggregation propensity that was independent of the C terminus (Schilling et al., 2006), increased the hydrophobicity and changed the pH-dependent solubility profile (Schlenzig et al., 2009). Moreover, $Aβ_{3(pE)-42}$ co-oligomerizes with $Aβ_{1-42}$ to form cytotoxic, metastable low-n oligomers that show a prion-like behavior. A correlation between pyroglutamate Aβ and tau-dependent cytotoxicity was also reported (Nussbaum et al., 2012). Youssef *et al.* described “impaired spatial working memory and delayed memory acquisition in Y-maze and Morris water maze” after intracerebroventricular injection of soluble oligomeric Aβ3(pE)-42 in wildtype mice (Youssef et al., 2008). Jang *et al.* demonstrated that N-truncated Aβ variants including $Aβ_{pE3-42}$, $Aβ_{17-42}$ and $Aβ_{9-42}$ are capable of forming ion channels in the lipid bilayers. These ion channels are toxic as they “allow uncontrolled leakage of ions into/out of the cell, destabilizing cellular ionic homeostasis” (Jang et al., 2014). A transgenic AD mouse models that expresses exclusively one N-truncated Aβ species, i.e. $Aβ_{pE3-42}$ demonstrated microglial activation and astrocytosis, developed neuron loss and behavioral alternations and revealed impaired synaptic plasticity (Alexandru et al., 2011).

Very recently, investigation of different N-truncated Aβ species attributed them a strong propensity to form stable aggregates. Among five Aβ variants the following order of aggregation propensity was obvious: $Aβ_{pE3-42}$, $Aβ_{4-42}$, $Aβ_{1-42}$/$Aβ_{4-40}$ and $Aβ_{4-38}$. Treatment of primary neurons with a variety of Aβ peptides at different concentrations revealed a comparable toxicity of N-truncated Aβ variants and full-length Aβ (Figure 6A). Furthermore, different Aβ variants were intraventricular injected in wildtype mouse brains. Subsequently performed Y-maze unveiled impairment in working memory in mice treated with N-truncated as well as full-length Aβ (Figure 6B, Bouter et al., 2013).

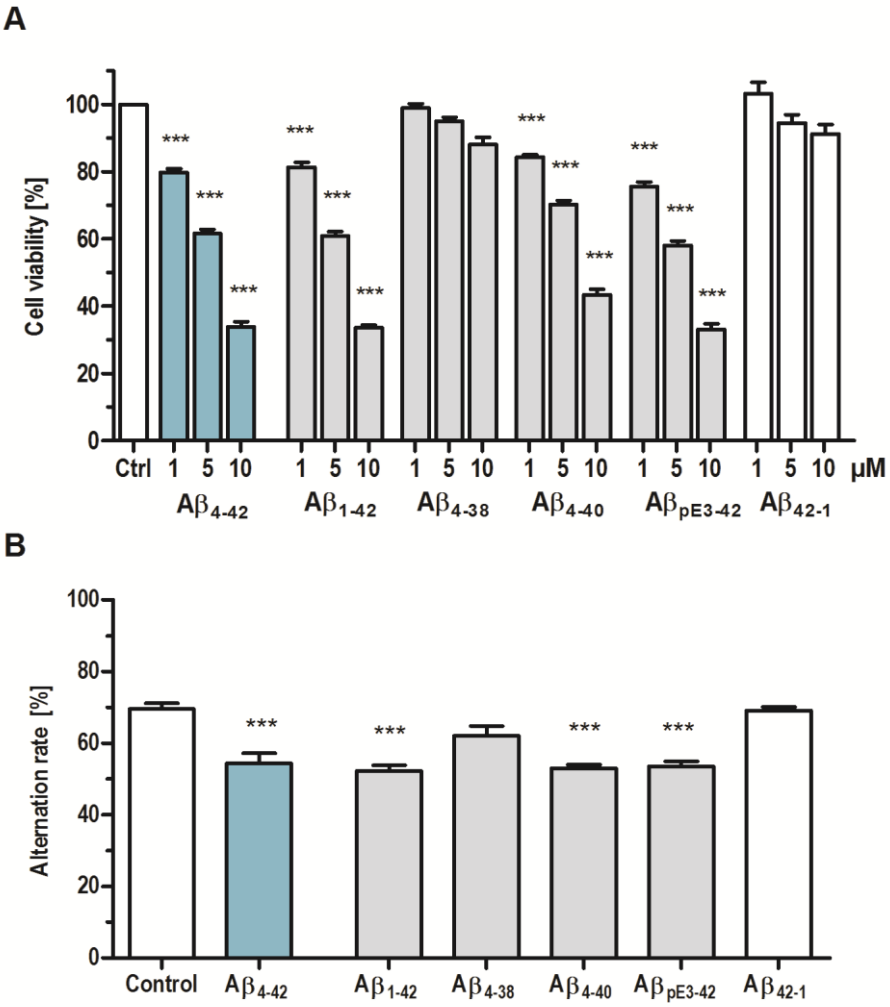

Figure 6 | N-truncated Aβ variants are toxic *in vivo* and *in vitro.*
(A) *In vitro* toxicity of Aβ species was investigated by treating primary cortical neurons with Aβ peptides at different concentrations and a following calcein-AM assay. $Aβ_{1-42}$, $Aβ_{4-42}$, $Aβ_{4-40}$ and $Aβ_{pE3-42}$ revealed comparable toxicity profiles whereas $Aβ_{4-38}$, a vehicle control and reverse $Aβ_{42-1}$ showed no toxic effects. **(B)** *In vivo* toxicity was assessed by intracerebroventricular injection of Aβ peptides into wildtype mouse brains. Afterwards, Y-maze was performed to evaluate working memory represented by alternation rate. Mice injected with $Aβ_{4-42}$, $Aβ_{1-42}$, $Aβ_{4-40}$ and $Aβ_{pE3-42}$ performed at chance level and demonstrated a robust deficit in working memory. In contrast, mice treated with vehicle control, $Aβ_{4-38}$ or $Aβ_{42-1}$ showed no impairments. Abbreviation: Ctrl – control. One-way ANOVA followed by Bonferroni multiple comparisons. ***p ≤ 0.001. Figure adapted from (Bouter et al., 2013).

1.6.2 Amyloid-$β_{4-42}$

First published in 1985, Masters *et al.* found that amyloid plaque cores of AD individuals "are composed of a single major protein component of about 4-5 kDa" that contained truncated NH_2 termini (Masters et al., 1985a). Interestingly, 64 % of the peptides isolated from amyloid plaques of AD cases started with a Phe-4 residue (Masters et al., 1985a). Näslund and colleagues analyzed amyloid from brains of individuals with either SAD or FAD as well as samples from non-demented controls. They found

“Aβ-(4-42) and Aβ-(8-42) variants […] to be the most prevalent minor Aβ variants in AD samples” (Näslund et al., 1994). More recently, Lewis and coworkers used SELDI-TOF mass spectrometry to analyze extracted peptides of AD brain samples. They detected a peak representing $Aβ_{4-42}$ which was “the most dominant peak within all the samples” tested (Lewis et al., 2006). Moreover, an additional study used immunoprecipitation in combination with mass spectrometric analysis to determine the Aβ isoform composition in three brain regions of FAD and SAD subjects as well as non-demented controls. $Aβ_{4-42}$ was found to be one of two dominant isoforms in the hippocampus and cortex in AD brains (Portelius et al., 2010). So far, the enzyme that can mediate the cleavage to generate $Aβ_{4-42}$ is not known. However, it was proposed that neprilysin is capable of cleaving between Glu-3 and Phe-4 releasing $Aβ_{4-x}$ (Howell et al., 1995, Bayer and Wirths, 2014). $Aβ_{4-42}$ showed one of the highest aggregation propensities, displayed oligomers (in contrast to other Aβ species) and revealed a strong toxic effect when studied in primary neurons. Additionally, this amino-terminal truncated species was able to induce working memory deficits after intraventricular injection into wildtype mouse brains (Figure 6, Bouter et al., 2013). Moreover, Antonios *et al.* claimed that $Aβ_{4-x}$ is the earliest N-truncated Aβ species in the 5XFAD mouse model as it precedes intraneuronal accumulation of $Aβ_{pE3-x}$ (Antonios et al., 2013).

1.7 Mouse models of Alzheimer’s disease

Besides using invertebrate models such as *Drosophila melanogaster* or *Caenorhabditis elegans* to recapitulate, at least partially, the deficits seen in human AD patients, research has largely focus on working with rodents and in particular with mouse models. Working with these animals bring along some important advantages as they are relatively easy to rear, have a shorter life-span than e.g. primates and are evolutionary closer to mammalian species than flies or nematodes. However, rodents do not spontaneously develop AD during aging. Thus, there are two possibilities for the investigation of AD in these models: either to use transgenic or non-transgenic mice.

Most transgenic mouse models are attributed to the discovery of FAD-linked mutations either in the APP and/or in the PS genes. These mutations were found to increase total Aβ production, enhance Aβ aggregation and/or increase the Aβ42/Aβ40 ratio. Assuming that FAD and SAD have a high degree of phenotypic similarity, it was reasonable to investigate mouse models that overexpress mutant human APP, PS1, PS2 and/or microtubule-associated protein tau (MAPT) (Puzzo et al., 2014). These transgenic mouse models are either single transgenic or multi-transgenic mice. The single transgenic mice possess a single mutation in the APP gene like the Swedish mutation in the Tg2576 or

APP23 models or the Indiana mutation in the PDAPP line 109 and H6 (Hsiao et al., 1996, Sturchler-Pierrat et al., 1997, Games et al., 1995). Moreover, there are mouse models which harbor multiple APP mutations like the PDAPP line J20 or the TgCRND8 model which possess both the Swedish and Indiana mutation (Mucke et al., 2000, Chishti et al., 2001). Besides models with a single mutation in the APP gene, mice with a single mutation in tau (e.g. JNPL3, MAPT mice) or presenilin 1 (e.g. PS1 (M146WL) mice) were generated and investigated (Puzzo et al., 2014). Furthermore, there are mouse models which contain multiple mutations in various genes. For example, the APP^{SL}PS1KI model (Casas et al., 2004) and the 5XFAD model (Oakley et al., 2006) harbor mutations in both the APP and the PS1 genes. The 3xTg-AD model possesses mutations in APP, PS1 and tau genes (Oddo et al., 2003). These mouse models differ not only in the number or location of their mutations but also in the used promoter (e.g. Thy-1 or PDGF promoter) and background strain (e.g. C57BL/6, DBA/2, 129/Sv). Additionally, transgenic mice were generated that overexpress several Aβ isoforms in the absence of mutant APP. This includes the TBA2 (Wirths et al., 2009), TBA2.1/2.2 (Alexandru et al., 2011), TBA42 (Wittnam et al., 2012), G2 (LaFerla et al., 1995), APP48 (Abramowski et al., 2012) and BRI-Aβ42 (McGowan et al., 2005) mice.

In order to avoid unrelated effects of the used APP or PS transgenes, non-transgenic mice are used in addition. These mouse models were generated by direct infusion of various forms of Aβ or tau into the brain (cf. Puzzo et al., 2014, Philipson et al., 2010). Furthermore, another non-transgenic mouse model was generated by intracerebroventricular (icv) administration of the diabetic compound streptozotocin (STZ). It is claimed that this icv-STZ mouse model represents sporadic AD as these mice showed similar deficits like 3xTg-AD mice (Chen et al., 2013, Wang et al., 2014). Alternatively, normally aged animals are investigated to better understand the differences between AD-dependent alterations and aging (cf. Puzzo et al., 2014, Philipson et al., 2010).

Transgenic and non-transgenic mouse models have been very helpful tools for a better understanding of AD pathophysiology and for testing mechanistic hypotheses, thereby enabling progress in novel therapeutic strategies as they model different aspects of the disease. So far, none of these mouse models recapitulate the entirety of AD seen in humans in terms of signs, symptoms and anatomicopathological hallmarks. However, at least partially, they develop amyloid plaques, extra- and/or intracellular Aβ deposits and/or neurofibrillary tangles. This neuropathology is frequently accompanied by other AD-related alterations like inflammation, cognitive and non-cognitive impairments, neuron loss

and neurodegeneration and synaptic dysfunction (cf. Puzzo et al., 2014, Webster et al., 2014).

1.7.1 Tg4-42 transgenic mice

In order to assess the effects of long-term exposure of $A\beta_{4\text{-}42}$ in mouse brain the Tg4-42 mouse line was developed. Generation of this mouse line has been initially done in our lab (Division of Molecular Psychiatry, University Medical Center Göttingen) and has been described previously (Wittnam, 2012, Bouter et al., 2013). Briefly, for the development of this novel transgenic mouse line a modified form of the TBA42 transgenic vector was used (Wittnam, 2012, Cynis et al., 2006, Wirths et al., 2009). The new transgene contains a murine Thy-1 promoter and the cDNA coding for $A\beta_{4\text{-}42}$. Transgenic mice were generated by male pronuclear microinjection of fertilized C57BL/6J oocytes. PCR analysis was used to characterize the resulting offspring for transgene integration. The identified founder animals were bred to C57BL/6J wildtype mice to establish various independent lines. Subsequently, qRT-PCR was performed to assess transgene expression in each new line. The mouse line with the highest transgene mRNA level was selected for further breeding and thereafter named Tg4-42 (Bouter et al., 2013).

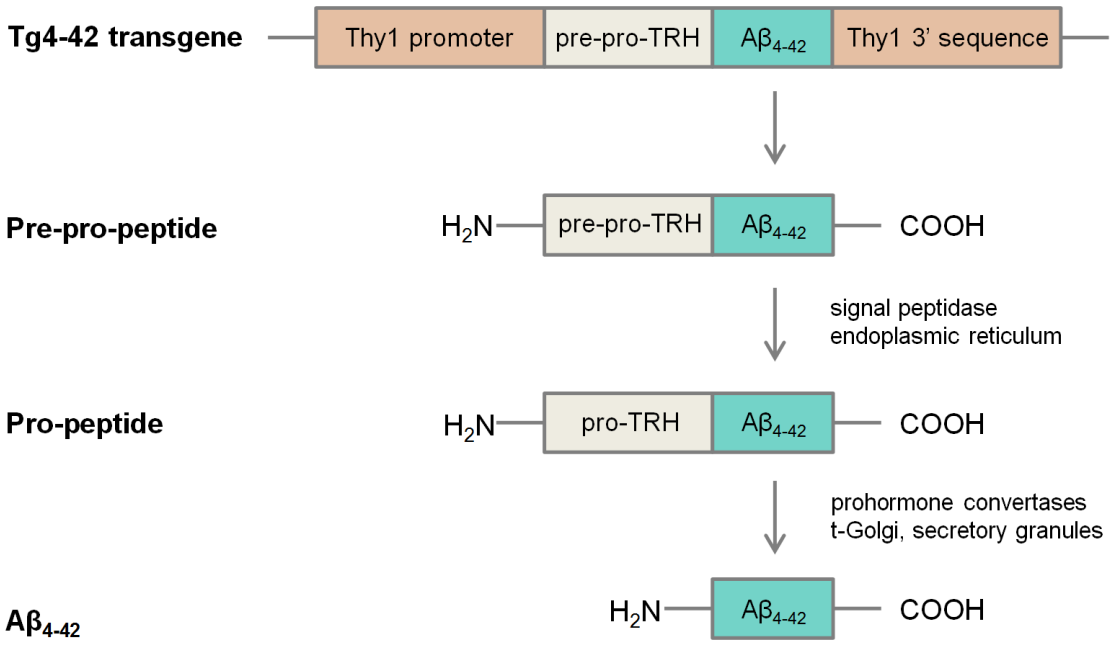

Figure 7 | Tg4-42 transgene.
N-truncated $A\beta_{4\text{-}42}$ is fused to the murine pre-pro TRH (thyrotropin-releasing hormone) signal peptide. The murine Thy-1 promoter drives the neuronal expression of these fused peptides. After liberation of the pro-TRH-$A\beta_{4\text{-}42}$-peptide from the endoplasmic reticulum the peptide is cleaved by prohormone convertases in the trans-Golgi (t-Golgi) and secretory granules. Finally, $A\beta_{4\text{-}42}$ is secreted from the cell. Figure modified from (Alexandru et al., 2011, Wittnam, 2012).

Tg4-42 mice neuronally express human $A\beta_{4-42}$ fused to the murine thyrotropin-releasing hormone (TRH) signal peptide under the control of the Thy-1 promoter. This construct was designed to route $A\beta_{4-42}$ through the secretory pathway to finally allow its extracellular release (Figure 7, Bouter et al., 2013).

1.8 The hippocampal formation in learning and memory

Research of the past years revealed a variety of neural systems involved in different forms of learning and memory. It was demonstrated that the hippocampus is essential for the formation of episodic memory as well as spatial memory and is assumed to play a key role in their long-term storage and emotional processing (Neves et al., 2008, Deng et al., 2010, Maruszak and Thuret, 2014). Furthermore, the hippocampus harbors the subgranular zone of the dentate gyrus, where adult neurogenesis occurs (Maruszak and Thuret, 2014). A plethora of studies revealed that the hippocampal formation is affected early and severely in AD pathogenesis (e.g. Hyman et al., 1984, Maruszak and Thuret, 2014).

1.8.1 Anatomy of hippocampal formation

The hippocampal formation consists of four cortical regions including the dentate gyrus (DG), the hippocampus proper with three subfields (fields of the C*ornu Ammonis* 3, 2, 1 (CA3, CA2, CA1, respectively)), the subicular complex with three subdivisions (subiculum, presubiculum, parasubiculum) and the entorhinal cortex (EC). Particularly in rodents the EC is subdivided into medial and lateral divisions (Amaral and Witter, 1989).These regions possess distinctive histological characteristics and specialized functions (Maruszak and Thuret, 2014). The principle cells of dentate gyrus and the hippocampus proper are granular cells and pyramidal cells, respectively. Both regions are organized depth-wise in several layers. Within the hippocampus proper this includes the *stratum oriens*, *stratum pyramidale*, *stratum lucidum*, *stratum radiatum* as well as *stratum lacunosum-moleculare* (Szilágyi et al., 2011). The dentate gyrus comprises the polymorphic layer, *stratum granulosum* as well as *stratum moleculare* (Amaral et al., 2007, David and Pierre, 2006).

Each of the four fields of the hippocampal formation is connected by unidirectional excitatory projections indicating a unique feature of this brain region (Amaral and Witter, 1989). Within the hippocampus the information successively passes three distinct regions: the entorhinal cortex, the dentate gyrus as well as the subfields CA3 to CA1 (Figure 8, Deng et al., 2010). This circuitry is known as the excitatory trisynaptic pathway. The dendrites of the granule cells in the dentate gyrus receive projections from axons of layer

II neurons in the entorhinal cortex via the perforant pathway (PP). This perforant pathway includes the lateral perforant pathway (LPP) and medial perforant pathway (MPP) and their axons innervate the outer and middle third of the dendritic tree (Deng et al., 2010, Neves et al., 2008). The granule cells of the EC project to mossy cells in the hilus and hilar interneurons that send excitatory and inhibitory projections back (Deng et al., 2010). The axons of the granule cells, also known as mossy fibers, project to the proximal apical dendrites of the CA3 pyramidal cells and also to cells within the polymorphic layer of the dentate gyrus (Deng et al., 2010, Neves et al., 2008, Lavenex and Amaral, 2000). In addition, CA3 is also connected with layer II of EC through the PP (Deng et al., 2010). Pyramidal neurons of CA3 send projections to ipsilateral CA1 pyramidal cells through Schaffer collaterals and to contralateral CA3 and CA1 cells through commissural connections (Deng et al., 2010, Neves et al., 2008). Moreover, CA1 pyramidal neurons also get direct input from layer III of EC through the temporoammonic pathway (TA) (Deng et al., 2010). Ultimately, CA1 neurons send projections to the subiculum and to the deep layers of the EC (Deng et al., 2010, Lavenex and Amaral, 2000).

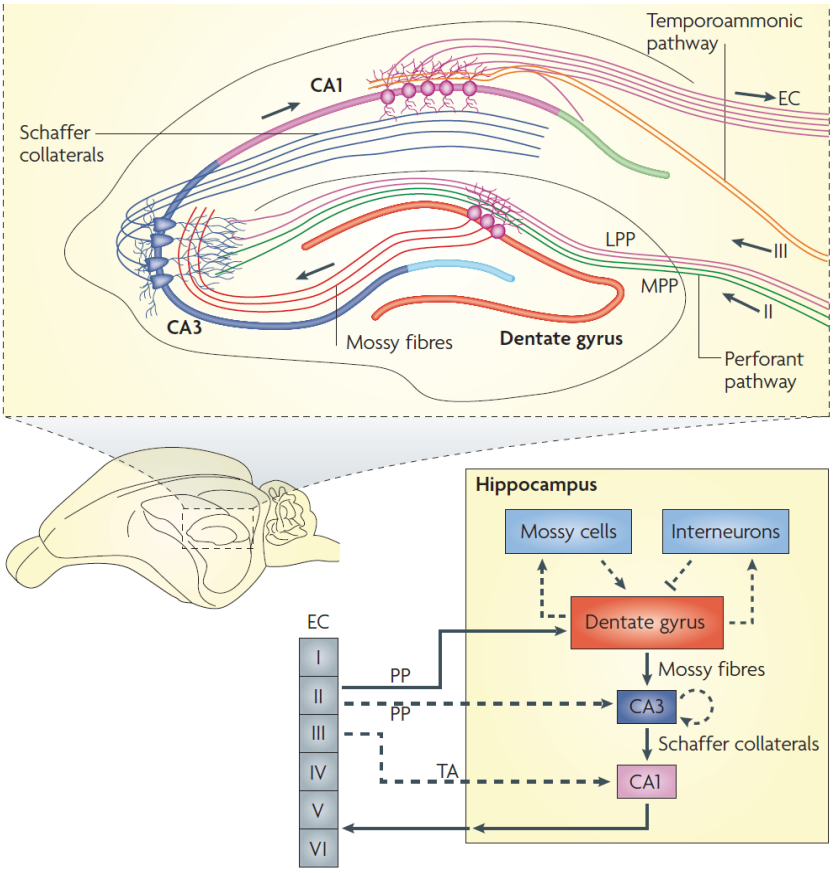

Figure 8 | The neuronal circuitry in the rodent hippocampus.
The excitatory trisynaptic pathway comprises three main pathways including the 'perforant pathway' (PP) projection to the dentate gyrus, the subsequent 'mossy fiber' (MF) path to field CA3 and finally the 'Schaffer collaterals' (SC) path to field CA1. Abbreviations: EC – entorhinal cortex; LPP – lateral perforant pathway; MPP – medial perforant pathway; CA – Cornu Ammonis; TA – temporoammonic pathway. Figure adapted from (Deng et al., 2010).

Different forms of synaptic modification are involved in storage of memories in the brain (Rosenzweig and Barnes, 2003). The “ability to undergo activity-dependent changes in synaptic strength” is defined as synaptic plasticity which is a “ubiquitous property of all synapses” (Kauer and Malenka, 2007). The hippocampus is an established key player in short-term and long-term memory. Due to the unique cellular structure and circuits, the hippocampus became a favorable area for several electrophysiological studies on short-term and long-term modifications of synaptic plasticity.

1.8.2 Short-term modifications of synaptic plasticity

Short-term modifications of synaptic plasticity include forms of synaptic enhancement like facilitation, augmentation and post-tetanic potentiation (PTP). These short-term effects usually only last for a few minutes and are due to changes in transmitter release probability, i.e. a residual elevation in presynaptic $[Ca^{2+}]_i$ (intracellular Ca^{2+}) that act on one or more molecular targets. These targets seem to be distinct from secretory triggers causing fast exocytosis and phasic release of neurotransmitter to evoke action potentials (Zucker and Regehr, 2002, Nicoll and Malenka, 1999). During facilitation the synaptic response is enhanced “on the hundreds of milliseconds time scale” (Zucker and Regehr, 2002). Paired-pulse facilitation (ppf) is of presynaptic origin (Kuhnt and Voronin, 1994) and a widely used electrophysiological paradigm. When applying a pair of stimuli separated by a certain time interval, synaptic currents are evoked in which the second response is larger than the first. If the interstimulus interval is increased, the magnitude of facilitation decreases (Zucker and Regehr, 2002). This reflects the assumption that an individual action potential has a greater chance to evoke the release of neurotransmitter when arriving within milliseconds after the first action potential due to added Ca^{2+} levels (Bliss and Collingridge, 2013). Besides ppf, two other short-term processes are noteworthy when applying an increased number of high-frequency stimuli in one train and afterwards returning to low-frequency stimulation: ‘augmentation’ that grows and decays within 5 to 10 s and ‘PTP’ that lasts between 30 s and several minutes. Both augmentation and PTP are of presynaptic origin as well (Zucker and Regehr, 2002). PTP is the first out of three phases when applying brief high-frequency trains of stimuli to the Schaffer collaterals. Presynaptic accumulation of $[Ca^{2+}]_i$ causes PTP that rapidly declines after $[Ca^{2+}]_i$ clearance. During application of tetanus in the CA1 subfield PTP is NMDA (N-methyl-D-aspartate) receptor-independent. In contrast, the following two phases that are induced by high-frequency stimulation are NMDA receptor dependent forms of long-term potentiation (Volianskis et al., 2013).

1.8.3 Long-term modifications of synaptic plasticity

Long-term potentiation (LTP) and long-term depression (LTD) are frequently studied forms of synaptic plasticity. They are considered as electrophysiological correlates of memory formation or in other words as cellular model of learning and memory. LTP is defined as an alteration of the “strength of synaptic transmission by increasing the postsynaptic response to the release of a quantum of neurotransmitter” (Volianskis et al., 2013) and was first described at CA3-CA1 synapses in 1993 (Bliss and Collingridge, 1993). While LTP is a strengthening of synaptic transmission, LTD is defined as an activity-dependent weakening of synaptic transmission. Both LTP as well as LTD are displayed by excitatory and inhibitory synapses (Kauer and Malenka, 2007). Although additional forms of LTP and LTD are present in other brain regions which might share some properties and mechanisms (e.g. amygdala, visual cortex/somatosensory/prefrontal cortex), NMDA receptor (NMDAR)-dependent LTP and LTD in the CA1 region of the hippocampus are the most extensively studied forms (Malenka and Bear, 2004, Lynch, 2004). Likewise, the focus of the present study lies on NMDAR-dependent LTP at CA3-CA1 synapses.

Basic properties of LTP include its input-specificity, associativity and cooperativity. When generating LTP at a set of synapses by applying a tetanic stimulus, the increase in synaptic strength does not normally occur in other synapses on the same cell. This input-specificity indicates an advantage as it increases the storage capacity of individual neurons. A strong activation of a set of synapses within a certain temporal period can facilitate LTP at an independent set of neighboring synapses on the same cell arguing for an associative property. Cooperativity means that there is an intensity threshold for induction as ‘weak’ tetanic stimuli can only activate a few afferent fibres and do not trigger LTP (Bliss and Collingridge, 1993, Malenka and Nicoll, 1999).

Generation of NMDAR-dependent LTP literally requires synaptic activation of postsynaptic glutamatergic NMDARs (Malenka and Nicoll, 1999). NMDARs are activated when the postsynaptic membrane is significantly depolarized (Kauer and Malenka, 2007) which is experimentally accomplished by repetitive tetanic stimulation of synapses or “by directly depolarizing the cell while continuing low-frequency synaptic activation” (Malenka and Nicoll, 1999). The neurotransmitter glutamate binds to two distinct receptor subtypes during low-frequency synaptic transmission (Figure 9A). One of these receptors is the α-amino-3-hydroxy-5-methyl-4-isoxazolepropionic acid receptor (AMPAR). Its channel is permeable to monovalent cations (Na^+ and K^+) and it is responsible for “the majority of inward current for generating synaptic responses when the cell is close to its resting membrane potential” (Malenka and Nicoll, 1999). The second of these receptors is the

NMDAR. It possesses a profound voltage dependence as its channel is blocked by extracellular Mg^{2+} avoiding the influx of Na^{+} and Ca^{2+} during low-frequency synaptic transmission. During induction of LTP (Figure 9B) the postsynaptic cell is depolarized through the AMPAR. This causes the dissociation of Mg^{2+} from its binding site within the NMDAR channel upon binding of abundant glutamate. Subsequently, Ca^{2+} and Na^{+} enter the dendritic spine (Malenka and Nicoll, 1999, Rosenzweig and Barnes, 2003). While LTD requires the activation of NR2B containing NMDAR, LTP is dependent on the activation of NR2A containing NMDAR as they have different calcium influx kinetics and influence different postsynaptic pathways (Koffie et al., 2011). In addition to NMDAR-mediated Ca^{2+} entry, activation of dendritic voltage-dependent Ca^{2+} channels (VGCC) can increase Ca^{2+} levels within the spines as well. This results in generation of LTP, STP or LTD (Malenka and Nicoll, 1999). Besides the aforementioned ionotropic receptors (NMDAR, AMPAR), metabotropic glutamate receptors (mGluR) also modulate and contribute to the induction and expression of LTP (Lynch, 2004, Collingridge et al., 2004).

The increase in postsynaptic Ca^{2+} concentration is the critical trigger for LTP and leads to activation of several intracellular signaling cascades including various protein kinases like α-calcium/calmodulin-dependent protein kinase II (CaMKII, Kauer and Malenka, 2007). In addition, other signaling pathways were suggested that enable LTP to be sustained. It was shown that they occur presynaptically and postsynaptically (Lynch, 2004). This includes protein kinase C (PKC), cyclic adenosine 3',5'-monophosphate (cAMP), cAMP-dependent protein kinase (PKA), tyrosine kinase Src, mitogen-activated protein kinase (MAPK/ERK), phosphatidylinositol 3-kinase (PI 3-kinase) and cAMP response element-binding protein (CREB) (Malenka and Nicoll, 1999, Lynch, 2004). CaMKII changes synaptic transmission through modifications of glutamate receptors. It either phosphorylates existing channels to alter their conductance state or facilitates the insertion of new receptors into the membrane (Cooke and Bliss, 2006). Interestingly, this was described for AMPAR as LTP causes both the addition of AMPAR to the postsynaptic membrane as well as phosphorylation of AMPAR and increases their single-channel conductance. Increase of available postsynaptic AMPAR elicits a larger depolarization after presynaptic release of glutamate (Rosenzweig and Barnes, 2003, Collingridge et al., 2004). cAMP initiates signaling to the nucleus via various transcription factors resulting in expression of proteins that contribute to long-lasting changes and ultimately mediate persistent LTP (Cooke and Bliss, 2006). Moreover, maintenance of LTP is accompanied by enlargements of dendritic spines and associated postsynaptic densities (Kauer and Malenka, 2007). Whereas the early phase of LTP (E-LTP) is independent of protein synthesis and only lasts for a short period, long-lasting LTP (L-LTP) is more persistent,

lasts some hours *in vitro* and weeks *in vivo,* and is dependent on *de novo* synthesis of proteins (Lynch, 2004).

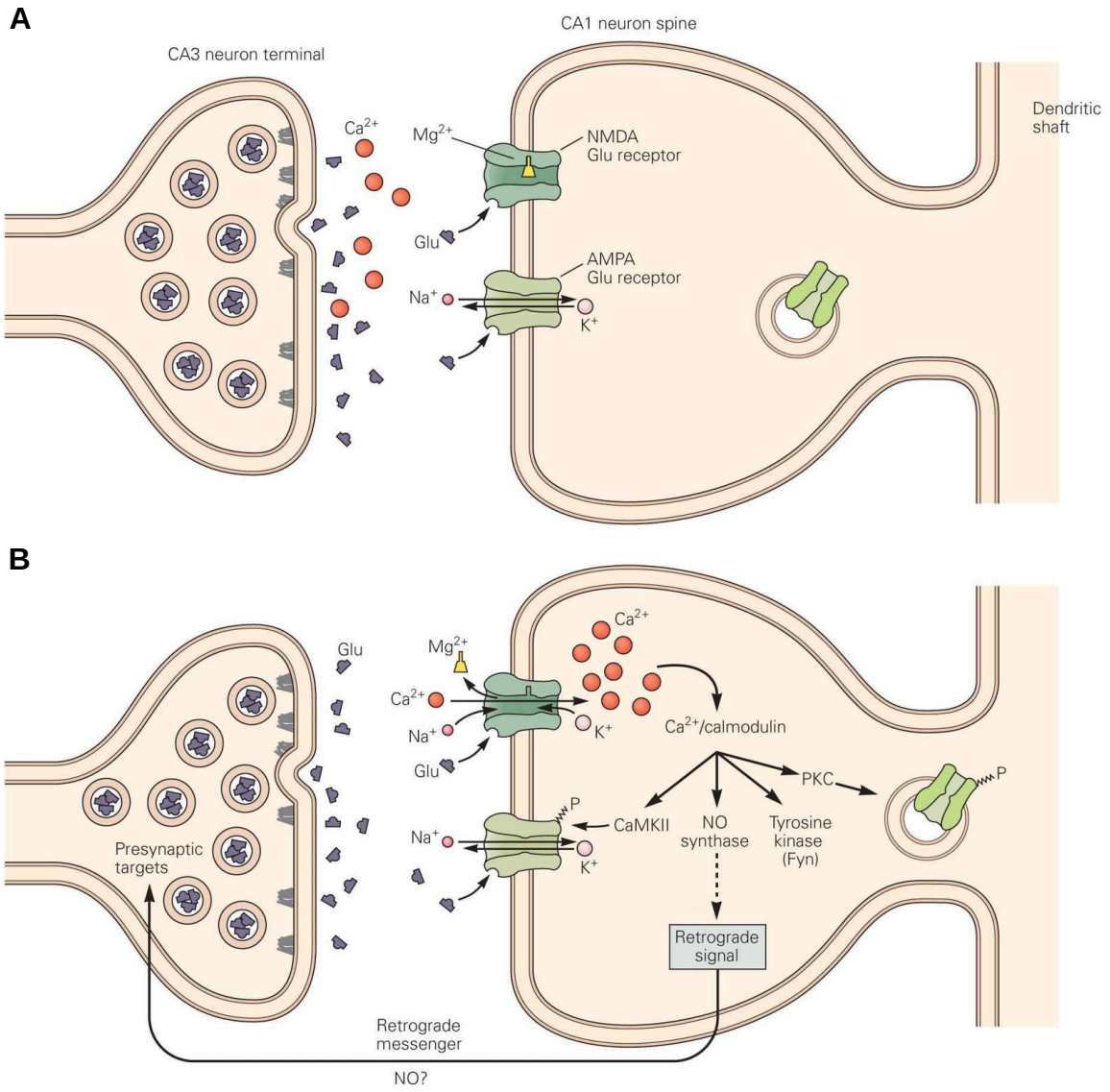

Figure 9 | Induction of long-term potentiation
(A) During normal synaptic transmission, the neurotransmitter glutamate is released from the presynapse and can act on AMPA receptors (AMPAR) and NMDA receptors (NMDAR). Since the NMDAR channel is blocked by Mg^{2+}, Na^{+} flows only through AMPAR. **(B)** Depolarization of the postsynaptic cell relieves the Mg^{2+} block allowing Na^{+} and Ca^{2+} to flow through NMDAR channels into the dendritic spine. The resulting increase in Ca^{2+} levels activates several intracellular signaling cascades leading to various LTP expression mechanisms. Figure adapted from (Siegelbaum and Kandel, 2012)

As already mentioned before, high-frequency stimulation evokes three distinct phases of potentiation including PTP and two phases of LTP. At CA3–CA1 synapses LTP consists of a stimulation-labile phase of short-term potentiation (STP) that converts into stable long-term potentiation (LTP) (Volianskis et al., 2013). Both phenomena are (very likely) of postsynaptic origin (Bliss and Collingridge, 2013) and NMDA receptor dependent (Volianskis et al., 2013). STP is considered as an “unstable phase, which declines over a period of about half an hour and leads to a sustained level of up-regulated neurotransmission” (Volianskis et al., 2013). However, the differentiation between STP and LTP is actively debated in the literature. It was argued that STP and LTP are mechanistically different parts of the potentiation process and have different consequences for the transfer of synaptic information during high-frequency stimulation (Volianskis et al., 2013, Park et al., 2014). It was described that STP and LTP can be “either co-expressed or expressed independently” (Volianskis et al., 2013). Park *et al.* suggested that different NMDAR subtypes might mediate the induction of either STP or LTP. On the basis of pharmacological and kinetic criteria they distinguished two components of STP some of which could be induced by the same NMDAR subtypes like LTP and others not. Moreover, they verified the existence of two mechanistically distinct forms of LTP that occur in addition to STP: a protein synthesis-resistant form (early LTP) and a sensitive component (late LTP). In summary, they suggested three forms of NMDAR-dependent LTP that differ in their expression: STP (also termed LTPa), early LTP (LTPb) and late LTP (LTPc) (Park et al., 2014).

1.9 Project objectives

N-terminally truncated $A\beta_{4-42}$ is highly abundant in AD brains (Portelius et al., 2010). It was demonstrated that $A\beta_{4-42}$ exhibited one of the highest aggregation propensities to form stable aggregates. Moreover, $A\beta_{4-42}$ revealed a strong toxic effect when studied in primary cortical neurons and was able to induce working memory deficits after intraventricular injection into wildtype mouse brains (Bouter et al., 2013). These results indicate that $A\beta_{4-42}$ might play a dominant role in triggering AD pathology. However, little is currently known about its effects *in vivo*.

The majority of mouse models rely on the overexpression of mutated forms of the APP and PS1 genes. However, only a minority of AD patients suffers from the hereditable form of AD. Additionally, no multiplication of mutations was observed in AD patients. Therefore, the development of a mouse model without mutations representing a situation more akin to human AD was attempted and the Tg4-42 mouse model was generated. The Tg4-42 mouse model overexpresses human $A\beta_{4-42}$ in the absence of mutant APP. Moreover, it is the first mouse model which expresses exclusively one N-terminally truncated Aβ species.

The aim of the present study was to characterize the novel transgenic mouse model Tg4-42 and thus to investigate the potential neurotoxic effects of the N-terminally truncated Aβ species $A\beta_{4-42}$ *in vivo* and *in vitro*. The following objectives were set:

- Investigate the neuropathology resulting from $A\beta_{4-42}$ expression in terms of assessing the $A\beta_{4-42}$ accumulation and gliosis as well as loss of neuronal cells in hemizygous Tg4-42 mice.
- Determine if age-dependent behavioral changes occur by assessing motor function, anxiety, working memory, spatial reference as well as associative memory in three- and 12-month-old Tg4-42 mice.
- Establish a new Morris water maze protocol in the laboratory to assess spatial learning and spatial reference memory.
- Examine the effect of $A\beta_{4-42}$ on synaptic function and plasticity in acute hippocampal tissue slices of Tg4-42 males at 3, 12 and 24 months of age.
- Analyze relative gene expression levels of several synaptic markers in hippocampal tissue of young Tg4-42 mice.

2 Material & Methods

2.1 Animals

2.1.1 Animal care and general conditions

All mouse lines were maintained at the central animal facility of the University Medical Center, Göttingen. Female and male mice were used for the present studies. Female mice were group-housed with three to five animals per cage. Male mice were individually housed to reduce stress levels and to avoid injuries due to hierarchic encounters. All mice were kept in a controlled environment on a 12 h/12 h inverted light cycle (lights off: 8 a.m. – 8 p.m.) and an average temperature of 21 °C. Food and water were provided *ad libitum*. Tissue paper was offered for nest-building. Cages were changed once a week. Cleaning the cages as well as behavioral testing was performed during dark phase. All studies were conducted according to German guidelines for animal care and approved by the local legal authorities. All feasible efforts were made to reduce animal numbers to a reasonable minimum on the one hand and to avoid the exposure to stress and suffering on the other hand.

2.1.2 Tg4-42 transgenic mice

In order to assess the effects of long-term exposure of $A\beta_{4\text{-}42}$ in mouse brain the Tg4-42 mouse line was developed. Generation of this mouse line has been initially done in our lab (Division of Molecular Psychiatry, University Medical Center Göttingen) and was described before (see section 1.7.1).

Tg4-42 mice neuronally express human $A\beta_{4\text{-}42}$ fused to the murine thyrotropin-releasing hormone (TRH) signal peptide under the control of the Thy-1 promoter. This construct was designed to route $A\beta_{4\text{-}42}$ through the secretory pathway to finally allow its extracellular release. All Tg4-42 mice were bred to C57BL/6J (Charles River Laboratories, Wilmington, MA, USA) mice to ensure an equal genetic background. Wildtype C57BL/6J mice used for the control groups were purchased from Charles River, Germany. Only hemizygous Tg4-42 mice were used for the current studies. Age, sex and numbers of all animals tested are described in the appropriate *results* sections (see chapter 3).

2.1.3 Collection of CNS tissue for immunohistochemistry

Drop-fixation - All mice were deeply anesthetized with carbon dioxide and killed via cervical dislocation. Right after decapitation the brain was rapidly extracted and dissected on ice. Skin and tissue surrounding the skull were removed and three incisions were

made. The first incision was set over the dorsal midline of the skull. The second and third incisions were made laterally. Skull bones were carefully fractured and removed. Following extraction from the skull the brain was separated at the sagittal midline. The right and/ or left hemisphere were placed into embedding cassettes (Simport, Beloeil, Canada). Hemisphere samples were fixed in 4 % phosphate-buffered formaldehyde solution (Roti®-Histofix 4 %, Roth, Karlsruhe, Germany) for at least one week. Finally, those samples were embedded in paraffin (see section 2.5.1).

Perfusion - Perfusion was done in our lab (Division of Molecular Psychiatry, University Medical Center Göttingen) as described previously (Wittnam, 2012). In brief, mice were deeply anesthetized with an intraperitoneal injection of 200 – 300 µl of an anesthesia mixture [0.2 ml ketamine (ketamine 10 %, Medistar Arzneimittelvertrieb, Ascheberg, Germany), 0.1 ml xylazine (*Xylariem*®, 20 mg, Riemser Pharma, Greifswald, Germany), 0.7 ml ddH_2O (B Braun, Melsungen, Germany)]. Perfusion was accomplished using a peristaltic pump ((*Ismatec*®) IDEX Health & Science SA, Glattbrugg, Switzerland) and two ice-cold perfusion solutions: 0.01 M PBS (Biochrom, Berlin, Germany) and 4 % paraformaldehyde (PFA, Roth, Karlsruhe, Germany) in 0.01 M PBS. Anesthetic condition of each mouse was validated using a pinching test. If the mouse did not show any response to pain stimuli it was pinned by its paws onto a foam perfusion stage. Following exposure of the beating heart an incision was made in the right atrium of the heart to allow for blood to drain from the circulatory system and a sterile needle was inserted into the left ventricle. The mouse was perfused with about 40 ml ice-cold 0.01 M PBS until the color of the mouse's liver changed from red to grayish-white. Subsequently, the mouse was perfused with 40 ml ice-cold 4 % PFA-solution. Following perfusion the mouse was decapitated and the brain was removed as described before (see section 2.1.3, drop-fixation). The right and/or left hemisphere were placed into embedding cassettes (Simport, Beloeil, Canada). Hemisphere samples were fixed in 4 % phosphate-buffered formaldehyde solution (*Roti*®-*Histofix* 4 %, Roth, Karlsruhe, Germany) for at least one week. Finally, those samples were embedded in paraffin (see section 2.5.1).

2.1.4 Collection of hippocampal tissue for biochemistry

Mice were sacrificed and brain tissue was collected as described in section 2.1.3. Following extraction from the skull the brain was separated at the sagittal midline. Cerebellum, brainstem and about one sixth of the frontal cortex were excised from the intact hemispheres and discarded. After lifting up the cortex from its caudal side the hippocampus was carefully removed from the surrounding tissue and immediately frozen on dry ice. Hippocampal samples were stored at -80 °C until further use.

2.1.5 Slice preparation for electrophysiological recordings

Preparation of slices was conducted as described previously (Fischer et al., 2009). All mice were deeply anesthetized with ether and killed via decapitation. The brain was removed from the skull (see section 2.1.3) and transferred to ice-cold chilled artificial cerebrospinal fluid (ACSF) for 1 – 2 min. Thereafter, using a vibroslicer (752 M Vibroslice, Campden Instruments, Loughborough, Leicester, UK) the brain was cut in 400 µm thick coronal slices. Tissue slices including the hippocampus were selected and separated sagittally. Hippocampal slices were placed in a submersion-style storage chamber containing oxygenated ACSF und remained there for 90 min at room temperature to recover after preparation.

The ACSF contained (in mM): 130 NaCl, 3.5 KCl, 1.25 NaH_2PO_4, 24 $NaHCO_3$, 1.2 $CaCl_2$, 1.2 $MgSO_4$, and 10 dextrose, constantly aerated with 95 % O_2 – 5 % CO_2 to adjust pH to 7.4 (all chemicals were obtained from Sigma-Aldrich, St. Louis, MO, USA or Merck, Darmstadt, Germany).

2.2 Behavioral analysis of mice

2.2.1 General considerations and testing protocol

Transgenic and wildtype control mice underwent a onetime three-week series of behavioral analysis to assess their motor abilities, memory performance and anxiety level. All female and male mice were tested either at three or 12 months of age. Behavioral tests were performed in the following chronological order: Morris water maze, balance beam, string suspension, cross maze, inverted grip hang, elevated plus maze and finally fear conditioning. To keep stress levels to a minimum the fear conditioning task was only performed on 12-month-old mice that were sacrificed after the tone trial.

Although it is inevitable to use a distinct number of mice to ensure the final statements all efforts were done to reduce the numbers of mice tested to a reasonable minimum. For that reason the wildtype group was filled up with already existing data of four to five mice that were previously tested in our research group. On the same account and due to technical limitations the Morris water maze was established and accomplished in equal shares by Yvonne Bouter and Katharina Dietrich.

2.2.2 Balance Beam

The balance beam task was used to assess balance and general motor functions and was described previously (Jawhar et al., 2010, Arendash et al., 2001). The beam consisted of a 1 cm wide and 50 cm long dowel that was attached to two columns 44 cm

above a padded surface. A 9 x 15 cm escape platform was attached at both ends of the beam. The aim of this test was for the mouse to stay on the beam and reach one of the two safe platforms within a given timeframe. Each mouse received three 60 s trials to perform the test and a minimum of 10 min between the trials for recovery. Prior to this, a test trial was given to familiarize the mouse with the beam. For each trial the mouse was placed in the center of the beam facing one of the platforms and then released. The latency to fall from the beam was recorded. If the mouse escaped to one of the platforms or stayed on the beam for the entire trial, the maximum time of 60 s was given. The average time of all three trials was taken as the final score for each mouse. The beam was cleaned with 70 % ethanol to reduce odor cues between the trials.

2.2.3 String suspension

The string suspension task was used to evaluate grip strength and general motor coordination and was described previously (Jawhar et al., 2010). The string suspension apparatus consists of a 50 cm cotton string (2 mm in diameter) tied between two wooden beams at a height of 35 cm above a padded surface. The aim of this test was for the mouse to climb across the string and reach one of the wooden beams. Each mouse received three 60 s trials to perform the test and a minimum of 10 min between the trials for recovery. For each trial the mouse was permitted to grasp the string by its forepaws and then released. The ability to climb across the string was assessed with a 0 to 5 rating score in the following way: 0 = unable to remain on the string; 1= stationary hanging only by fore- or hind paws; 2 = stationary hanging by fore- or hind paws with unsuccessful attempts to hold string by all four paws; 3 = hanging onto string by all four paws but no lateral movement (but being able to hold balance); 4 = hanging onto string using all four paws and tail and moving laterally; 5 = escaping to the edge of string and contacting wooden beam. The maximum score obtained during one trial was recorded. If the mouse felt off the string at any point during the trial it earned a score of 0. Each trial was stopped if a score of 5 was achieved. The average score of all three trials was taken as the final score for each mouse. The string was cleaned with 70 % ethanol to reduce odor cues between the trials.

2.2.4 Inverted grip hang

The inverted grip hang task was used to evaluate vestibular function as well as grip and muscle strength as described previously (Wittnam, 2012). The apparatus consisted of a wire grid (45 x 30 cm, grid spacing of 1 cm^2) that was attached to two foam supports 40 cm above a padded surface. The aim of this test was for the mouse to hang on the grid for a given time. Each mouse received a single 60 s trial. The mouse was placed onto the

center of the grid and the grid was carefully inverted. If the mouse hung on the grid for the entire 60 s or escaped over the edge of the grid, the maximum time of 60 s was given. If the mouse felt off the grid during the trial the latency to fall was recorded. The grid was cleaned with 70 % ethanol to reduce odor cues between the trials.

2.2.5 Elevated Plus Maze

The elevated plus maze was used to evaluate exploratory behavior and intensity of anxiety as described previously (Jawhar et al., 2010, Wittnam, 2012). The maze consisted of four arms (15 x 5 cm) arranged in an angle of 90° extending from a square center (5 x 5 cm). Two of those arms were closed on three sides by a 15 cm high wall of clear plastic. The other two arms were open to the surroundings on all four sides. Both the closed and the open arms alternated in their arrangement. The plus maze was elevated 75 cm above a padded surface. Each mouse received a single 5 min trial. Prior to this trial, the maze was cleaned with 70 % ethanol to reduce odor cues. The mouse was placed in the center of the maze facing one of the open arms and allowed to freely explore the different arms. A digital camera (*computar*®/CBC (America) Corp., Commack, NY, USA) connected to ANY-Maze video tracking software (Stoelting Co., Wood Dale, IL, USA) was used to record total distance traveled as well as the time spent in each arm. Subsequently, the percentage of time in open arms and the ratio of total open arm entries to total arm entries were calculated.

2.2.6 Cross maze

The Cross maze was used to assess spontaneous alternation rates as an indication for spatial working memory as described previously (Jawhar et al., 2010). The maze was made of black plastic material and had four arms (30 x 8 x 15 cm) arranged in an angle of 90° extending from a square center (8 x 8 cm). Each mouse received one single 10 min trial. Prior to this trial, the maze was cleaned with 70 % ethanol to reduce odor cues. Subsequently, the mouse was placed at the end of one arm facing the wall and allowed to freely explore the maze. In contrast to the manual analysis described in (Jawhar et al., 2010) a digital camera (computar®/ CBC (America) Corp., Commack, NY, USA) connected to ANY-Maze video tracking software (Stoelting Co., Wood Dale, IL, USA) was used in the present study to record number of arm entries and total distance traveled. A successful arm entry was reached when all four paws of the mouse crossed the entrance of one arm. Alternation was defined as consecutive entries into all four arms of the maze in overlapping quadruplet sets. The maximum number of alternations possible was calculated as the total number of arm entries minus three. Alternation percentage was

then determined as follows: (Number of alternations made/number of alternations possible) x 100 (Jawhar et al., 2010).

2.2.7 Morris water maze

Morris water maze was used to assess spatial reference memory (Morris, 1984). The aim of this test was for the mouse to learn to use spatial cues to locate a hidden, circular platform (10 cm) in a circular pool (110 cm diameter) filled with tap water. The water was made opaque by adding non-toxic white paint and maintained at 20 °C for the test duration. The pool was divided into four virtual quadrants that were defined based on their spatial relationship to the platform: left, right, opposite and target quadrant, which contains the goal platform. Non-transparent curtains were attached to three sides of the pool to reduce distracting effects. A digital camera (*computar*®/CBC (America) Corp., Commack, NY, USA) connected to ANY-Maze video tracking software (Stoelting Co., Wood Dale, IL, USA) was used to record escape latency, swimming speed and quadrant preference. Each mouse underwent a nine-day long protocol including several trials for cued and acquisition training phase as well as one for the probe trial. Mice that were unable to swim due to severe motor disabilities, an impaired vision or even blindness were immediately excluded from testing and the following analyses (termination criteria).

Testing began with three days of cued training. For these trials the platform was marked with a triangular flag. Mice were introduced into the water at the edge of the pool facing the wall. They were then given 60 s to find the submerged platform. Mice that failed to find the platform in 60 s were gently guided to it. All mice were allowed to sit on the platform for 10 s before being removed from the pool. To prevent hypothermia, all mice were kept in front of a heat lamp for 3 min before being returned to their home cage. Each mouse received four training trials per day with an average inter-trial interval of 15 min for recovery. Both the location of the platform and the position at which mice were introduced into the pool changed between trials.

Twenty-four hours after the last day of cued training, mice performed five days of acquisition training. For this part of testing, the flag was removed from the platform. In addition to the distal cues existing in the room (furniture e.g.) proximal visual cues were attached to the outside of the pool and the inside of the curtains. The platform location remained stationary for each mouse throughout training. At the start of each trial, mice were introduced into the pool from one of four predefined entry points. The order in which these entry points were used varied between training days (Vorhees and Williams, 2006). To avoid quadrant bias, the experimental cohorts were randomly split and trained to find

one of two different platform locations. Trials were conducted as during the cued training phase.

Twenty-four hours after the last acquisition trial, a probe test was performed to assess spatial reference memory. The platform was removed from the pool, and mice were introduced into the water from a novel entry point. Mice were then allowed to swim freely for 1 min while their swimming path was recorded.

2.2.8 Fear conditioning

Fear conditioning was used to assess intensity of anxiety as well as conditional learning and memory and was performed as described previously (Bouter et al., 2014). A soundproof isolation cubicle contained a standard conditioning chamber (17 x 17 x 26 cm) with a stainless steel grid floor. The walls of the conditioning chamber were covered with black and white checkered paper and the steel grid was connected to a shock generator (Sound and Shocker Generator, Ugo Basile, Gemonio, VA, Italy). An additional light was attached to the ceiling of the cubicle. A Fire-i™ digital camera (Unibrain, San Ramon, CA, USA) was connected to ANY-Maze video tracking software (Stoelting Co., Wood Dale, IL, USA) to record freezing behavior of animals. Each mouse received a 3-day lasting fear conditioning protocol to apply contextual fear conditioning and tone fear conditioning.

On the first day, each mouse was placed in the conditioning chamber and was allowed to freely explore the box for 150 s while baseline freezing was recorded. Subsequently, a tone (2000 Hz, 80 dB, conditioned stimulus) was presented for 30s. This tone was overlapped by a foot-shock (0.7 mA, unconditioned stimulus) within the last 2 s of the tone. The mouse stayed in the conditioning chamber for additional 30 s and was then returned to its home cage.

On the second day, each mouse was placed in the same conditioning chamber again to assess contextual memory. Neither tones nor foot-shocks were presented. Freezing behavior was recorded for 210 s and the mouse was finally returned to its cage.

On the last day of testing, each mouse was placed back in the conditioning chamber to assess tone memory. At that point the chamber was altered by means of white walls (instead of checkered ones), a covered floor and an acetic acid scent. After a 150 s habituation period a tone similar to the one used on the first day was presented for additional 30 s. Freezing behavior was recorded before and during the tone.

2.3 Molecular Biology

2.3.1 DNA isolation for genotyping of transgenic mice

Genomic DNA isolated from tail biopsies was used to genotype all transgenic mice. Tail biopsies of each mouse were collected in the central animal facility of the University Medical Center, Göttingen at about six to eight weeks of age. Lysis buffer [100 mM Tris/HCl (pH 8.5, Roth, Karlsruhe, Germany), 5 mM EDTA (AppliChem, Darmstadt, Germany), 0.2 % SDS (Biomol, Hamburg, Germany), 200 mM NaCl (Roth, Karlsruhe, Germany) ad 200 ml ddH_2O and 10 µl/ml peqGOLD Proteinase K (PEQLAB Biotechnologie, Erlangen, Germany)] was added to each tail biopsy sample at a volume of 500 µl. Samples were incubated at 400 rpm for 20 h at 56 °C in a Thermomixer Compact (Eppendorf, Hamburg, Germany). The next day, samples were centrifuged at 17 000 rpm for 20 min at 4 °C (Heraeus™Biofuge™Stratos™Centrifuge, Thermo Fisher Scientific Inc., Waltham, MA, USA). Subsequently, the supernatant of each sample was transferred to a new microcentrifuge tube with 500 µl of ice-cold isopropanol (Roth, Karlsruhe, Germany) and gently mixed. Samples were again centrifuged at 13 000 rpm for 10 min at RT (Heraeus™Pico™Centrifuge, Thermo Fisher Scientific Inc., Waltham, MA, USA). Afterwards, supernatants were discarded and each pellet was washed with 500 µl 70 % ice-cold EtOH (absolute ethanol, Merck, Darmstadt, Germany). Samples were again centrifuged at 13 000 rpm for 10 min at RT. Supernatants were discarded and pellets were dried at 55 °C (Thermomixer Compact, Eppendorf, Hamburg, Germany) for about 2 h. Subsequently, each pellet was dissolved in 30 µl molecular-grade water (B Braun, Melsungen, Germany). Samples remained at 55 °C (Thermomixer Compact, Eppendorf, Hamburg, Germany) over night and were then stored at 4 °C. Prior to genotyping PCR all DNA samples were diluted to a concentration of 20 ng/µl in a total volume of 30 µl molecular-grade water.

2.3.2 RNA isolation for qRT-PCR

RNA was isolated from hippocampal tissue of male Tg4-42 mice as described previously (Bouter et al., 2014) and subsequently used for qRT-PCR. After weighing the frozen hippocampal tissue 1 ml *peqGOLD TriFast™/Trizol* (PEQLAB Biotechnologie, Erlangen, Germany) per 100 mg tissue was added. Samples were homogenized at 800 rpm with about 10 strokes at RT using a Precision Overhead Stirrer (CAT Scientific, Paso Robles, CA, USA). After adding 0.2 ml Chloroform (Merck, Darmstadt, Germany) per 1 ml *TriFast™/Trizol* to each homogenate samples were shaken by hand for 15 s and then incubated for 10 min at RT. For separation of RNA samples were centrifuged at 12 000 g for 15 min at 4 °C (Heraeus™Biofuge™Stratos™Centrifuge, Thermo Fisher

Scientific Inc., Waltham, MA, USA). The upper clear phase contained the RNA and was transferred to a new microcentrifuge tube. To precipitate the RNA 0.5 ml isopropanol (Roth, Karlsruhe, Germany) per 1 ml *TriFast™/Trizol* were added. Samples were gently mixed and incubated for 15 min on ice. After centrifugation at 12 000 g for 10 min at 4 °C the supernatants were discarded. Each RNA pellet was washed twice by adding 0.5 ml 75 % EtOH (absolute ethanol, Merck, Darmstadt, Germany) and centrifuged at 12 000 g for 10 min at 4 °C. After washing the ethanol supernatants were removed and pellets were air-dried for 30 min at RT. Finally, RNA was dissolved in 30 µl RNase free water (B Braun, Melsungen, Germany), mixed well and stored at 4 °C over night.

2.3.3 Preparation of DNA-free RNA (DNase digestion)

RNA samples (see section 2.3.2) were subjected to digestion by desoxyribonucleases (DNases) using the following mixture: 3 µl 10X reaction buffer with $MgCl_2$ for DNase I (Thermo Fisher Scientific Inc., Waltham, MA, USA), 2 µl DNase I (1 U/µl; Thermo Fisher Scientific Inc., Waltham, MA, USA), 1 µl *Recombinant RNasin® Ribonuclease Inhibitor* (Promega, Madison, WI, USA). Six µl of this digestion mix were added to 24 µl of each previously prepared RNA sample, gently mixed and incubated at 37 °C for 1.5 h (Thermomixer Compact, Eppendorf, Hamburg, Germany). After incubation 70 µl of RNase free water (B Braun, Melsungen, Germany) and 0.4 ml *TriFast™/Trizol* (PEQLAB Biotechnologie, Erlangen, Germany) were added to each sample, again carefully mixed and incubated for 5 min at RT. Afterwards, 60 µl chloroform (Merck, Darmstadt, Germany) per sample were added. Samples were shaken by hand for 15 s and incubated for 3 min at RT. For separation of RNA samples were centrifuged at 12 000 g for 15 min at 4 °C (Heraeus™Biofuge™Stratos™Centrifuge, Thermo Fisher Scientific Inc., Waltham, MA, USA). The upper aqueous phase contained the RNA and was transferred to new a microcentrifuge tube. To precipitate the RNA 0.2 ml isopropanol (Roth, Karlsruhe, Germany) per sample were added. Samples were gently mixed and incubated for 15 min on ice. After centrifugation at 12 000 g for 10 min at 4 °C the supernatant was discarded. Each RNA pellet was washed twice by adding 0.5 ml 75 % EtOH (absolute ethanol, Merck, Darmstadt, Germany) and centrifuged at 12 000 g for 10 min at 4 °C. After washing the ethanol supernatants were removed and pellets were air-dried for 30 min at RT. Finally, RNA was dissolved in 30 µl RNase free water, mixed well and stored at -80 °C until further use. Prior to cDNA synthesis all RNA samples were diluted to a concentration of 1 µg/µl in a total volume of 20 µl RNase free water.

2.3.4 Determination of nucleic acid concentration

Purity and concentration of DNA and RNA were measured using a Biophotometer (Eppendorf, Hamburg, Germany) and *Eppendorf UVette® cuvettes* (Eppendorf, Hamburg, Germany). Prior to determination of nucleic acid concentration molecular grade water (B Braun, Melsungen, Germany) was used as a blank for photometry readings. Concentration ratios were considered accurate if the 260/280 and 260/230 absorbance ratios were between 1.6 and 2.2.

2.3.5 Reverse transcription

Total RNA isolated from hippocampal tissue (see sections 2.3.2, 2.3.3) was subjected to reverse transcription to synthesize cDNA using the *RevertAid First Strand cDNA Synthesis Kit* (Thermo Fisher Scientific Inc., Waltham, MA, USA). Reaction mixtures were prepared as described in Table 1 and incubated for 5 min at 25 °C, 1 h at 37 °C and 5 min at 70 °C in a labcycler (SensoQuest, Göttingen, Germany). Generated cDNA was diluted 1:10 in RNase free water (B Braun, Melsungen, Germany) and used as the sample template for qRT-PCR. Obtained cDNA samples and dilutions were stored at -20 °C until further use.

Table 1 │ Reaction mixture for reverse transcription.

Reagent	Volume
Random Hexamer Primer (100 µM)	1.0 µl
5X Reaction Buffer	4.0 µl
RiboLock RNase Inhibitor (20 U/µl)	1.0 µl
dNTP Mix (10 mM)	2.0 µl
RevertAid Reverse Transcriptase (200 U/µl)	1.0 µl
DNase digested RNA template (1 µg/µl)	11.0 µl
Total volume per sample	**20.0 µl**

2.3.6 Primers

All primers (Table 2) were used at a final concentration of 10 pmol/µl (100 pmol/µl primer stock was diluted 1:10 ddH_2O) and were purchased from Eurofins (Eurofins MWG Operon, Ebersberg, Germany)

Table 2 | List of primers used for qRT-PCR and mouse genotyping.

Name	Sequence (5' → 3')	Usage
Synpr for	CAA ATG CAA ACA TTG CAA AAA	qRT-PCR
Synpr rev	GAC AGA GTA CGG GAG AGC CA	qRT-PCR
Nlgn1 for	AGA ACC CAA TGT TCT CGC TG	qRT-PCR
Nlgn1 rev	TCA ACT ATC GGC TTG GGG TA	qRT-PCR
Actb for	ATG GAG GGG AAT ACA GCC C	qRT-PCR
Actb rev	TTC TTT GCA GCT CCT TCG TT	qRT-PCR
Dlgh4 for	TGT CTT CAT CTT GGT AGC GG	qRT-PCR
Dlgh4 rev	CTC CAA TGA AGT CAG AGC CC	qRT-PCR
SNAP25 pan (for)	CAG CTG GCT GAT GAG TCC CTG GAA A	qRT-PCR
SNAP25a rev	TTG GTT GAT ATG GTT CAT GCC TTC TTC GAC ACG ATC	qRT-PCR
SNAP25b rev	CAC ACA AAG CCC GCA GAA TTT TCC TAG GTC CGT C	qRT-PCR
Aβ3-42v4 for	GTGACTCCTGACCTTCCAG	mouse genotyping
Aβ3-42v4 rev	GTTACGCTATGACAACACC	mouse genotyping

2.3.7 Quantitative real-time polymerase chain reaction (qRT-PCR)

All qRT-PCR experiments were conducted in collaboration with the Department of Neuropathology (University Medical Center, Göttingen). Gene expression levels of synaptic coding genes were analyzed using the DyNAmo Flash SYBR green qPCR Kit (Thermo Fisher Scientific Inc., Waltham, MA, USA) containing ROX as an internal passive reference dye. Prepared cDNA (see section 2.3.5) was used as the sample template for qRT-PCR. Quantitative RT-PCR reaction mixture was prepared on ice as described in Table 3. Forward and reverse primers are listed in Table 2. First, dilutions of cDNA were pipetted in *96-Well Multiply® PCR Plates* (Sarstedt, Nürnbrecht, Germany) followed by the qRT-PCR reaction mix and finally sealed up a with transparent adhesive tape for PCR and sample storage (Sarstedt, Nürnbrecht, Germany). Plates were briefly centrifuged to avoid air bubbles in the reaction mix. The mouse β-Actin gene served as internal reference for normalizing transgene CT values. All reactions were performed with cycling parameters

described in Table 4 using the iQ5 Multicolor Real-Time PCR Detection System (Bio-Rad Laboratories, Hercules, CA, USA).

Table 3 | Reaction mixture for qRT-PCR.

Reagent	Company	Volume
2X qPCR master mix	Thermo Fisher Scientific Inc., Waltham, MA, USA	12.5 µl
ROX dye	Thermo Fisher Scientific Inc., Waltham, MA, USA	0.3 µl
Forward Primer	Eurofins MWG Operon, Ebersberg, Germany	1.5 µl
Reverse Primer	Eurofins MWG Operon, Ebersberg, Germany	1.5 µl
ddH_2O	B Braun, Melsungen, Germany	4,2 µl
cDNA (1:10 dilution)	-	5.0 µl
Total volume per sample		**25.0 µl**

Table 4 | Cycling Parameters for qRT-PCR.

Step	Temperature	Time
1	95 °C	10 min
2	95 °C	15 s
3	59 °C/ 62 °C	30 s
4	repeat steps 2-3 for 40 cycles	
5	95 °C	1 min
6	55 °C	30 s
7	95 °C	30 s

2.3.8 Polymerase chain reaction (PCR)

Polymerase chain reaction for mouse genotyping was performed using reagents described in Table 5 as well as prepared dilutions of DNA samples (see section 2.3.1). PCR reaction mixtures were set up on ice as described in Table 5. Forward and reverse primers are listed in Table 2. First, DNA was pipetted in PCR tubes (Biozym Scientific, Hessisch Oldendorf, Germany) followed by PCR reaction mixture. Tubes were shortly mixed to avoid air bubbles. PCR reactions were performed with cycling parameters described in Table 6 using a labcycler (SensoQuest, Göttingen, Germany).

Table 5 | Reaction mixture for genotyping PCR.

Reagent	Company	Volume
Forward primer	Eurofins MWG Operon, Ebersberg, Germany	1.0 µl
Reverse primer	Eurofins MWG Operon, Ebersberg, Germany	1.0 µl
dNTP Mix (100 mM)	PEQLAB Biotechnologie, Erlangen, Germany	2.0 µl
$MgCl_2$ (25 mM)	Axon Laboratories, Kaiserslautern, Germany	1.6 µl
10X Reaction Buffer B	Axon Laboratories, Kaiserslautern, Germany	2.0 µl
ddH_2O	B Braun, Melsungen, Germany	10.2 µl
Taq DNA Polymerase (5 U/µl)	Axon Laboratories, Kaiserslautern, Germany	0.2 µl
DNA (20 ng/µl)	-	2.0 µl
Total volume per sample		**20.0 µl**

Table 6 | Cycling Parameters for genotyping PCR.

Step	Temperature	Time
1	94 °C	3 min
2	94 °C	45 s
3	58 °C	1 min
4	72 °C	1 min
5	repeat steps 2 - 4 for 35 cycles	
6	72 °C	5 min
7	4 °C	∞

2.3.9 DNA electrophoresis

Products of PCR (see section 2.3.8) were analyzed using agarose gel electrophoresis. To get a 2 % gel 4 g agarose (SeaKem®LE Agarose, Lonza, Basel, Switzerland) were added to 200 ml previously prepared 1x TBE buffer [5x TBE buffer: 54 g Tris (base) (Roth, Karlsruhe, Germany), 26.5 g boric acid (Roth, Karlsruhe, Germany), 20 ml EDTA (AppliChem, Darmstadt, Germany) ad 1000 ml ddH_2O]. This solution was boiled in a microwave at 560 W until the agarose was completely dissolved. After a brief cooling down 6 µl ethidium bromide (Roth, Karlsruhe, Germany) were added and the total solution was poured in a casting tray. A 20-pocket sample comb was plugged in, air bubbles were carefully removed and solution was allowed to solidify. Subsequently, the comb was

removed and the gel was placed in an electrophoresis chamber containing 1x TBE buffer. One µl of 10x agarose gel sample buffer were mixed with 10 µl PCR product and immediately pipetted into a well. Five µl DNA ladder (100 bp DNA ladder (no stain) 0.2 mg/ml; Bioron, Ludwigshafen, Germany) were used and pipetted into a separate well. Electrophoresis was done using a Power Pack P25 power supply (Biometra, Göttingen, Germany) at 120 V for about 45 min to resolve the DNA. Afterwards, gels were analyzed under UV light with the help of the Gel Doc 2000 system (Bio-Rad, Hercules, CA, USA) and Quantity One software version 4.3.0 (Bio-Rad, Hercules, CA, USA).

2.4 Electrophysiological recordings

Hippocampal slices (see section 2.1.5) of Tg4-42 males and same-sex wildtype (C57BL/6J) littermate controls were tested at three, 12 and 24 months of age. Up to two slices from each brain were used. To make sure that these observations are independent each experimental series was performed on at least six to eight different animals of each genotype and age.

All electrical recordings were conducted in collaboration with the Institute of Neuro- and Sensory Physiology (University Medical Center, Göttingen) and were performed as described previously (Fischer et al., 2009, Janc and Müller, 2014). An Oslo-style interface recording chamber that was kept at a temperature of 31 – 33 °C, continuously aerated with 95 % O_2 – 5 % CO_2 and perfused with oxygenated ACSF (3 - 4 ml/min; see section 2.1.5 for chemical composition) was used for recording evoked field potentials. To prevent hippocampal slices from draining during the electrical recordings the slice chamber was covered by a lid with a small vent for positioning of the electrodes. Field excitatory postsynaptic potentials (fEPSPs) were evoked by 0.1 ms unipolar stimuli (S88 stimulator with PSIU6 stimulus isolation units, Grass Instruments, Warwick, RI, USA) and delivered via steel micro wire electrodes (50 µm in diameter, A-M Systems, Carlsborg, WA, USA) that were placed at the CA3/CA1 junction in acute hippocampal tissue slices. Stimulation of Schaffer collaterals elicited orthodromic responses that were recorded in *stratum radiatum* of the CA1 region using a glass electrode and a locally constructed extracellular DC potential amplifier. Recording electrodes were pulled from thin-walled borosilicate glass (GC150TF-10, Harvard Apparatus, Holliston, MA, USA) using a horizontal electrode puller (Model P-97, Sutter Instrument, Novato, CA, USA). Those electrodes were filled with ACSF solution and their tips were carefully trimmed to a resistance of about 5 MΩ. All electrophysiological data were sampled using an Axon Instruments Digitizer 1322A and pClamp 9.2 software (Molecular Devices, Sunnyvale, CA, USA). Sampling rate was 20 kHz.

In the present study input-output curves, paired-pulse facilitation and post-tetanic potentiation (PTP), short-term potentiation (STP) as well as long-term potentiation (LTP) were recorded to assess neuronal excitability and synaptic plasticity. Applied stimulation protocols for those recordings are described in the appropriate *results* sections (see section 3.5).

2.5 Immunohistochemistry

2.5.1 Paraffin-embedding of mouse brains

Hemisphere samples were prepared as described earlier (see section 2.1.3). After fixation in a 4 % phosphate-buffered formaldehyde solution (Roti®-Histofix 4 %, Roth, Karlsruhe, Germany) for at least one week samples were placed in an automatic tissue processor (TP 1020, Leica Biosystems, Nussloch, Germany) to dehydrate the tissue and immerse it in paraffin (Roth, Karlsruhe, Germany). In detail the following protocol was used: 4 % PBS-buffered formalin for 5 min, ddH_2O for 30 min, 50%, 60%, 70%, 80% and 90% EtOH (Chemie-Vertrieb, Hannover, Germany) for 1 h respectively, 2 x 1 h in 100% EtOH, Xylene (Roth, Karlsruhe, Germany) for 1 h, 2 x 1 h in melted Paraffin. Using a heated paraffin embedding module (Leica Biosystems, Nussloch, Germany) and embedding cassettes (Simport, Beloeil, Canada) hemisphere samples were embedded in solid paraffin blocks.

2.5.2 Slice preparation of paraffin-embedded hemispheres

Paraffin-embedded tissue blocks (see section 2.5.1) were cut in 4 µm thick sagittal sections using a microtome (microm cool-cut HM 335 E; Thermo Fisher Scientific Inc., Waltham, MA, USA). Slices were then mounted on microscope Superfrost®Plus slides (Menzel-Gläser, Braunschweig, Germany) in a 55 °C ddH_2O bath (paraffin tissue floating bath, Medax Nagel, Kiel, Germany), dried on a 55 °C hot plate for about 20 min and incubated at 37 °C over night (Thermo Fisher Scientific Inc., Waltham, MA, USA).

2.5.3 Antibodies

All antibodies used for immunohistochemistry are listed in Table 7 and Table 8.

Table 7 | Primary antibodies used for DAB immunohistochemistry.

Name	Host	Immunogen	Isotype	Company	Working dilution
24311	rabbit	pan-Aβ	polyclonal	Synaptic Systems, Göttingen, Germany	1:500
Aβ42	rabbit	C-terminus of Aβ42	polyclonal	Synaptic Systems, Göttingen, Germany	1:500
GFAP	rabbit	GFAP	polyclonal	Dako Denmark A/S, Glostrup, Denmark	1:1000
Iba-1	rabbit	Iba-1	polyclonal	Synaptic Systems, Göttingen, Germany	1:500

Table 8 | Secondary antibodies used for DAB immunohistochemistry.

Name	Company	Working dilution
Polyclonal swine anti-rabbit immunoglobulins, biotinylated	Dako Denmark A/S, Glostrup, Denmark	1:200

2.5.4 3,3'-Diaminobenzidine (DAB) immunohistochemistry

DAB immunohistochemistry was performed on 4 µm sagittal paraffin sections (see section 2.5.2) from either perfused (for stainings with antibodies against GFAP and Iba-1) or non-perfused (for stainings with antibodies against Aβ) wild-type and transgenic mice. First, sections were deparaffinized and rehydrated using various incubations as follows: 2 x 5 min xylene (Roth, Karlsruhe, Germany), 10 min 100 % EtOH (Chemie-Vertrieb, Hannover, Germany), 5 min 95 % EtOH, 5 min 70 % EtOH, 1 min ddH_2O. Blocking of endogenous peroxidase was done by incubating sections in 30 % H_2O_2 (Roth, Karlsruhe, Germany) in 0.01 M PBS (Biochrom, Berlin, Germany) for 30 min. After washing in ddH_2O for 1 min antigen retrieval was performed. For this purpose sections were boiled in 0.01 M citrate buffer (pH 6.0; Roth, Karlsruhe, Germany) for 10 min using a microwave (at 800 W until boiling, then at 80 W). Sections were allowed to cool down for 15 min. Permeabilisation of membranes was achieved by washing the sections with ddH_2O for 1 min, incubate them in 0.1 % Triton X 100 (Roth, Karlsruhe, Germany) in 0.01 M PBS for 15 min and finally wash them with 0.01 M PBS for 1 min. Sections were additionally incubated in 88 % formic acid (Roth, Karlsruhe, Germany) for 3 min and washed with 0.01 M PBS for 6 min to reveal intracellular Aβ. Unspecific protein binding sites were

blocked for 1 h at RT using 90 µl of milk blocking solution [4 % powdered milk (Roth, Karlsruhe, Germany) in 0.01 M PBS and 10 % FCS (Biochrom, Berlin, Germany)]. Prior to this, sections were circled with a lipid pen (Pap pen, Kisker Biotech, Steinfurt, Germany) to divide slides into discrete areas. Next to blocking incubation with primary antibodies (see Table 7) diluted to the desired concentration in 10 % FCS in 0.01 M PBS (90 µl per section) was done overnight at RT.

On the second day sections were washed 3 times for 5 min with 0.1 % Triton X 100 in 0.01 M PBS and once with 0.01 PBS for 1 min. Subsequently, sections were incubated for 1 h at 37 °C with a biotinylated secondary antibody (see Table 8) diluted to the appropriate concentration in 10 % FCS in 0.01 M PBS (90 µl per section). After an additional washing step with 0.01 M PBS slices were subjected to avidin-biotin complex (ABC) incubation [VECTASTAIN® Elite® ABC Kit (Vector Laboratories, Burlingame, CA, USA): components A and B in 10 % FCS in 0.01 M PBS at a dilution of 1:100 each] for 1.5 h at 37 °C. Following a further washing step (0.01 M PBS) staining was visualized using DAB as a chromagen [DAB solution: 5 ml 0.05 M Tris/HCl (pH 7.5, Roth, Karlsruhe, Germany), 0.1 ml DAB stock solution (25 mg/ml, Roth, Karlsruhe, Germany), 0.0025 ml 30 % H_2O_2]. Incubation time with DAB varied depending on the type of antibody used. Remaining DAB solution was washed off using 0.01 M PBS. Filtered hematoxylin (Roth, Karlsruhe, Germany) was used for counterstaining and was applied for 40 s. After a last washing step with tap water to remove the remaining hematoxylin sections were dehydrated as follows: 1 min 70 % EtOH, 5 min 95 % EtOH, 10 min 100 % EtOH, 2 x 5 min Xylene. Sections were embedded using *Roti*®-*Histokitt* (Roth, Karlsruhe, Germany) and microscope cover slips (Menzel-Gläser, Braunschweig, Germany).

2.5.5 4‘,6-Diamidino-2-phenylindol (DAPI) staining

DAPI staining was performed on 4 µm sagittal paraffin sections (see section 2.5.2) from perfused wild-type and transgenic mice (see section 2.1.3). First, sections were deparaffinized and rehydrated using various incubations as follows: 2 x 5 min xylene (Roth, Karlsruhe, Germany), 10 min 100 % EtOH (Chemie-Vertrieb, Hannover, Germany), 5 min 95 % EtOH, 1 min 70 % EtOH, 1 min ddH2O. Subsequently, sections were incubated in 4‘,6-Diamidino-2-phenylindol [DAPI (Roth, Karlsruhe, Germany), 15 mg/l] and washed with 0.01 M PBS (Biochrom, Berlin, Germany) for 1 min, respectively. Sections were embedded using Fluorescence Mounting Medium (Dako North America Inc., Carpinteria, CA, USA) and microscope cover slips (Menzel-Gläser, Braunschweig, Germany).

2.5.6 Image acquisition

Images of DAB-stained sections were acquired using an Olympus BX51 microscope (Olympus, Shinjuku-ku, Tokyo, Japan), a Moticam Pro 282 B camera and MoticImages Plus 2.0 software (Motic, Hong Kong). Arrangement of images was done with GIMP software (GNU Image Manipulation Program, version 2.8.10 for windows).

2.6 Data analysis

2.6.1 Analysis of behavioral data

Collection of data for each behavioral test was performed as described in section 2.2. Except for the Morris water maze and fear conditioning, differences between groups were tested using a two-way analysis of variance (ANOVA) followed by a *t-test for independent samples* (unpaired t-test).

For the Morris water maze as well as the fear conditioning, differences between groups were tested using *repeated measure analysis of variance* (RM-ANOVA) and *t-test for dependent samples* (paired t-test) considering different parameters as indicated. First, a RM-ANOVA was performed on each data set to test for higher order interactions. If RM-ANOVA revealed a main effect for one of the parameters tested, analysis was completed by *t-tests for dependent samples*.

Statistical analyses were calculated using STATISTICA for windows version 10.0 (StatSoft, Inc., Tulsa, OK, USA). All data are given as mean ± standard error of the mean (SEM). Significance levels are indicated as follows: ***$p \leq 0.001$; **$p \leq 0.01$; *$p \leq 0.05$.

2.6.2 Analysis of electrophysiological data

Collection of data was performed as described in section 2.4 and section 3.5. In general, data sets were excluded from analyses if the position of the electrode shifted during measurement, the shape of a single curve was excessively unstable (due to hypoxia, e.g.) and did not show a clear potentiation after high-frequency stimulation or the absolute value for the baseline measurement was greater than -0.5.

Differences between groups were tested using *repeated measures analysis of variance* (RM-ANOVA) and *t-test for independent samples* considering different parameters as indicated. First, a RM-ANOVA was performed on each data set to test for higher order interactions. If RM-ANOVA revealed a main effect for one of the parameters tested, analysis was completed by *t-tests for independent samples*. Statistical analyses were calculated using *STATISTICA* for windows version 10.0 (StatSoft, Inc., Tulsa, OK, USA).

All data are given as mean ± standard deviation (SD). Significance levels are indicated as follows: **p ≤ 0.01; *p ≤ 0.05.

2.6.3 Analysis of qRT-PCR data

Data of qRT-PCR was collected as described earlier (see section 2.3.7). Data sets were excluded if the melting curve profile showed additional peaks. Expression levels were measured in duplicates for each gene and mouse genotype. The obtained CT values were averaged and statistical analyses were calculated using the Relative Expression Software Tool V2.0.13 (REST 2009, Qiagen, Hilden, Germany) (Pfaffl et al., 2002). The expression ratio results of the studied transcripts were tested for significance by *Pair Wise Fixed Reallocation Randomization Test*. All data are given as mean ± 95 % CI. Significance levels are indicated as follows: *p ≤ 0.05.

3 Results

The aim of the present study was to characterize the recently generated Tg4-42 mouse model. The Tg4-42 line is the first mouse model expressing exclusively N-terminally truncated $A\beta_{4-42}$. In a first step, the neuropathology resulting from $A\beta_{4-42}$ expression was investigated. Afterwards, the potential neurotoxic effects of $A\beta_{4-42}$ *in vivo* and *in vitro* were analyzed regarding the behavioral phenotype, effects on synaptic function and plasticity as well as possible alternations in the expression levels of selected genes. All of the following analyses were performed with hemizygous Tg4-42 male and female mice at three (young) and 12 (old) months of age unless indicated otherwise. Age- and sex-matched wildtype (WT) C57BL/6J mice were used as a control group.

3.1 $A\beta_{4-42}$ expression in Tg4-42 mice

DAB immunohistochemistry was applied to assess Aβ expression in Tg4-42 mice. Using the pan-Aβ antibody 24311 an abundant intraneuronal Aβ immunoreactivity was found in the CA1 pyramidal cell layer of the hippocampus in three-month-old Tg4-42 mice (Figure 10A). This immunoreactivity was even more pronounced when using an Aβ42-specific antiserum (Figure 10B). The expression of Aβ in the CA1 region declined during aging as seen in 12-month-old Tg4-42 mice (Figure 10C). As in the hippocampus, intraneuronal Aβ aggregation was also initially detected in the striatum (Figure 10D), piriform cortex (Figure 10E) and inferior colliculus (Figure 10F) at three months of age. No extracellular plaque deposition was detected in either young or aged mice.

3.2 Gliosis in Tg4-42 mice

DAB immunohistochemistry was also used to assess astrogliosis and microgliosis in Tg4-42 mice. Reactive microglial cells and astrocytes were detected in areas showing aggregation of Aβ, i.e. the hippocampus, as early as three months of age (Figure 11). Microgliosis was even more pronounced in three-month-old Tg4-42 mice (Figure 11B) compared to age-matched WT mice (Figure 11A). Likewise, an increased amount of astroglia was found in three-month-old Tg4-42 mice (Figure 11D) compared to same-aged control mice (Figure 11C).

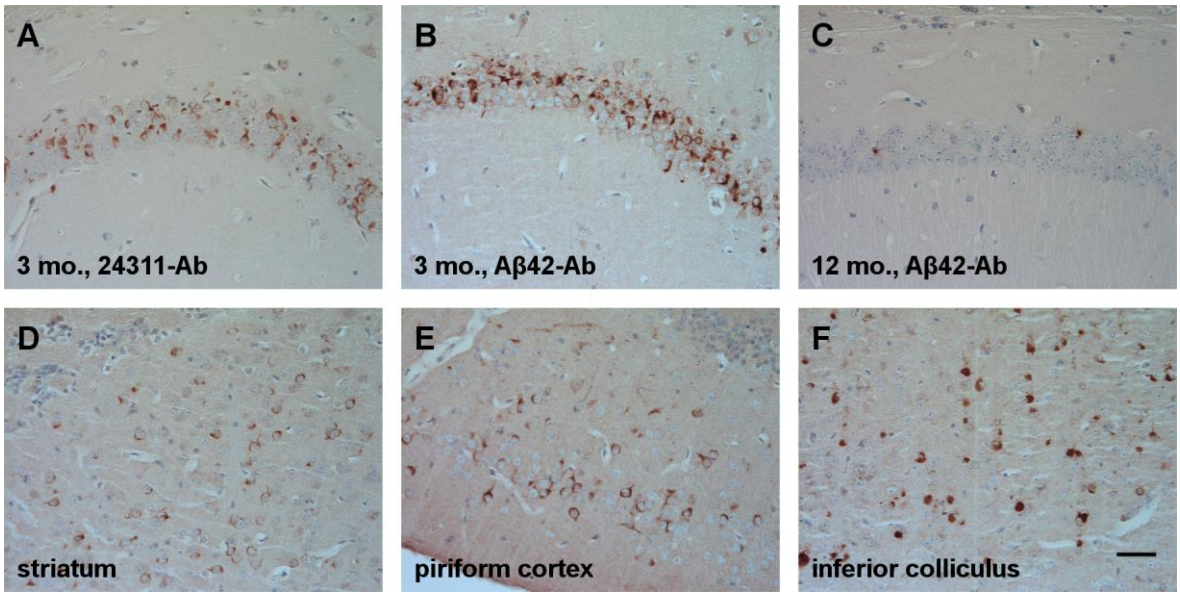

Figure 10 │ Aβ expression in Tg4-42 mice.
DAB immunohistochemistry was performed on the brains of 3- and 12-month-old Tg4-42 mice. **(A-B)** Abundant intraneuronal Aβ immunoreactivity was found in the CA1 region of the hippocampus in 3-month-old Tg4-42 mice using the polyclonal antiserum 24311 (A) and the polyclonal Aβ42 antibody (B). **(C)** An age-dependent reduction in positive cells was obvious in 12-month-old Tg4-42 mice (Aβ42 antibody). **(D-F)** Additionally, Aβ accumulations were detected in striatum (D), piriform cortex (E) and inferior colliculus (F) using the Aβ42 antibody. Scale bar: 50 µm.

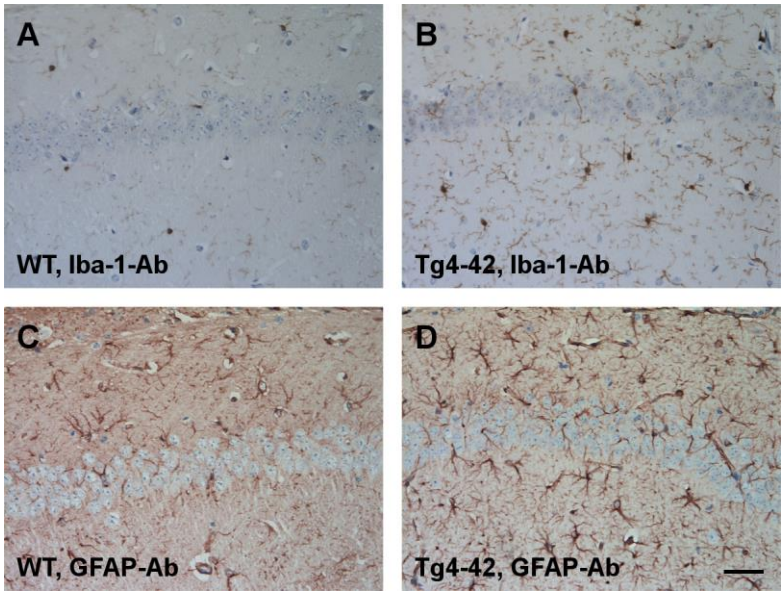

Figure 11 │ Increased microgliosis and astrogliosis in Tg4-42 mice.
DAB immunohistochemistry was performed on the brains of 3-month-old Tg4-42 mice. **(A-B)** Increased microgliosis with Iba-1 staining was found in 3-month-old Tg4-42 (B) mice compared to age-matched wildtype mice (A). **(C-D)** Increased astrogliosis was observed in 3-month-old Tg4-42 (D) mice compared to same-aged control mice (C) using a GFAP antibody. Scale bar: 50 µm.

3.3 Neuron loss in Tg4-42 mice

The fluorescent DNA stain 4‘,6-Diamidino-2-phenylindol (DAPI) was used to analyze loss of neuronal cells in the hippocampal CA1 region in young and aged Tg4-42 mice. Number of neurons was not altered comparing three-month-old Tg4-42 mice (Figure 12B) with WT mice (Figure 12A). In contrast, number of neuronal cells was affected in Tg4-42 mice (Figure 12D) at 12 months of age as seen by a thinner CA1 pyramidal cell layer of the hippocampus compared to WT mice (Figure 12C).

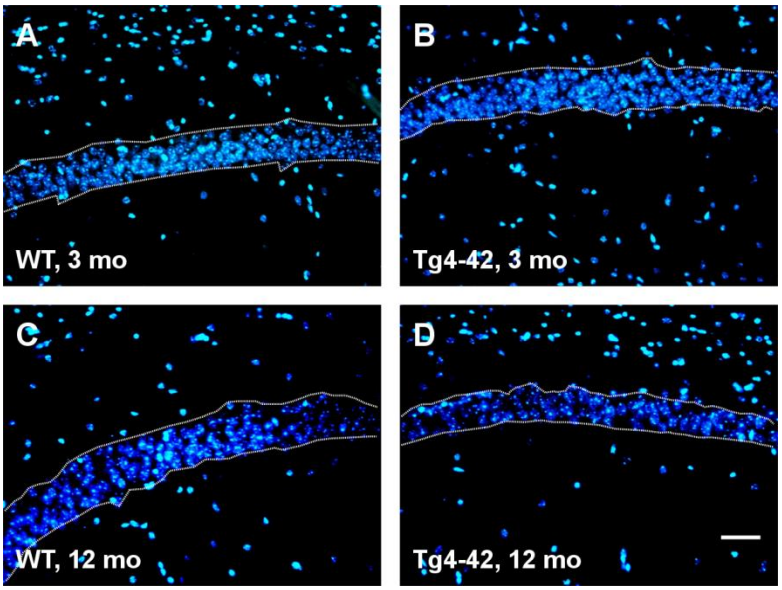

Figure 12 │ Age-dependent loss of neuronal cells in CA1 region in Tg4-42 mice.
Fluorescent immunohistochemistry was performed on the brains of 3- and 12-month-old Tg4-42 and WT mice using DAPI staining. **(A-B)** No change in number of neuronal cells was found between WT (A) and Tg4-42 (B) mice at 3 months of age. **(C-D)** In contrast, 12-month-old Tg4-42 (D) mice revealed a loss in neuron number in the hippocampal CA1 region as seen by a thinner cell layer in comparison to age-matched WT (C) mice. Scale bar: 50 µm.

Taken together, Tg4-42 mice develop intraneuronal Aβ accumulations, a pronounced inflammatory response as well as a reduction of neuronal cells in hippocampal CA1 region. In order to determine if the present Aβ pathology was sufficient to cause behavioral impairments, groups of young and old Tg4-42 mice performed a battery of behavioral tests.

3.4 Behavioral characterization of Tg4-42 mice

The standard battery of behavioral tests included balance beam, string suspension and inverted grip hang tasks to assess motor function. Furthermore, elevated plus maze and cross maze were performed to analyze anxiety and exploratory behavior as well as working memory, respectively. Spatial reference memory and associative memory were evaluated using the Morris water maze and the fear conditioning paradigm. In general, differences between groups were tested using *two-way analysis of varianc*e (two-way ANOVA). If the ANOVA revealed a significant difference, a *t-test for independent samples* (unpaired t-test) was performed.

3.4.1 Motor function of Tg4-42 mice

In the present study, motor capabilities were analyzed using the balance beam, string suspension and inverted grip hang task (Figure 13).

Balance beam was used to assess balance and general motor abilities. The aim of this test was for the mouse to stay on the beam and reach one of two safe platforms within a given timeframe. This test revealed no significant differences between the genotypes at all ages tested (Figure 13A, two-way ANOVA, main effect of genotype: $p = 0.3403$). However, the age affected the performance on the balance beam (Figure 13A, two-way ANOVA, main effect of age: $p = 0.0003$). Both groups of three-month-old Tg4-42 and WT mice stayed significantly longer on the beam than the 12-month-old mice, respectively (Figure 13A, unpaired t-test (3 vs. 12 mo.): $p = 0.0248$ (WT), $p = 0.0074$ (Tg4-42)).

Grip strength and motor coordination was analyzed with the string suspension task. The aim of this test was for the mouse to climb on the string and reach one of the wooden beams. Three- and 12-month-old Tg4-42 mice exhibited no impairments compared to the control animals (Figure 13B, two-way ANOVA, main effect of genotype: $p = 0.4596$). As with the balance beam, the performance on the string suspension was affected by age (Figure 13B, two-way ANOVA, main effect of age: $p = 0.0266$). In this test, transgenic animals performed worse at 12 months of age in comparison to three-month-old animals of the same group (Figure 13B, unpaired t-test (3 vs. 12 mo.): $p = 0.3960$ (WT), $p = 0.0315$ (Tg4-42)).

The inverted grip hang task is a test of vestibular function and muscle strength. The aim of this test was for the mouse to hang on the inverted grid for a given time. No differences were found between wildtype and transgenic mice at both ages tested (Figure 13C, two-way ANOVA, main effect of genotype and age: $p = 0.1726$).

In summary, behavioral testing demonstrated that motor functions are unaffected in young and aged Tg4-42 mice.

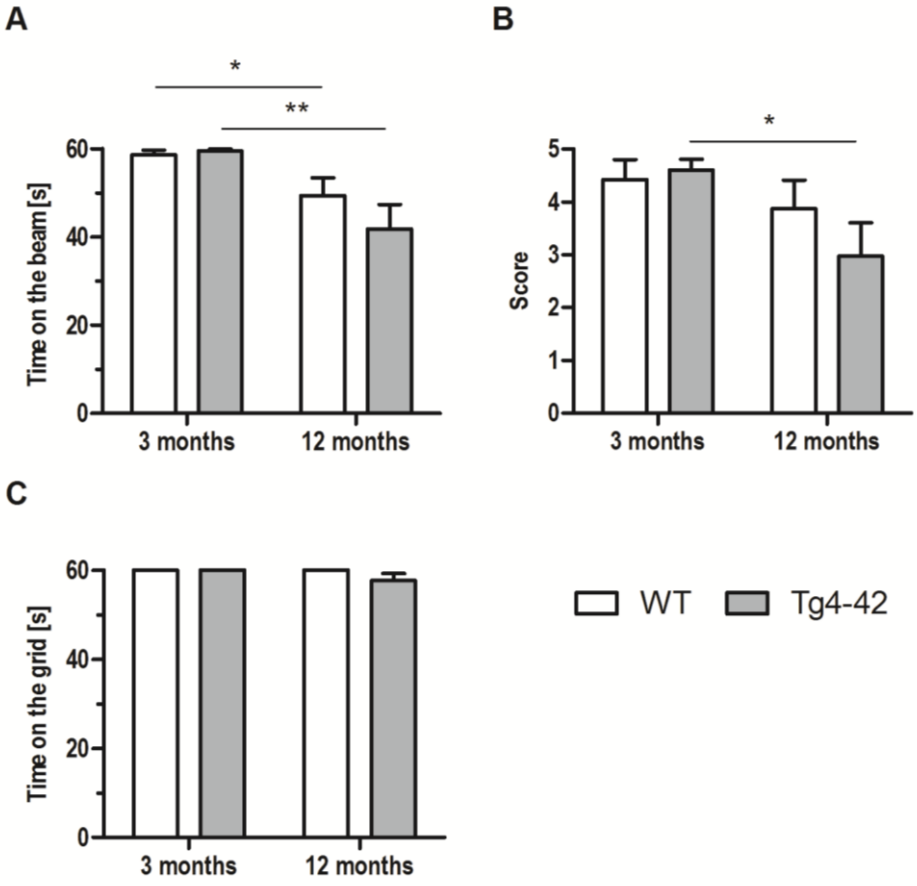

Figure 13 │ Intact motor functions were demonstrated in Tg4-42 mice.
Balance beam, string suspension as well as inverted grip hang task were performed to analyze general motor functions, balance and grip strength. Tg4-42 and wildtype mice were tested at 3 and 12 months of age. **(A)** Balance beam, **(B)** string suspension and **(C)** inverted grip hang revealed no significant differences between WT and transgenic mice at both ages tested. n = 10 – 15 mice per group (groups: sex- and age-matched). Mean ± SEM. Two-way ANOVA and unpaired t-test. Significance levels: **p ≤ 0.01, *p ≤ 0.05.

3.4.2 Anxiety and exploratory behavior of Tg4-42 mice

Basal anxiety and exploratory behavior were assessed using the elevated plus maze task. This maze consists of two closed and two open arms that alternates around a center and is elevated above the surface. Mice have to choose between their tendency to explore a new environment and their tendency to avoid a bright and open setting. The time spent in the open arms was unaltered between control and transgenic mice at all age tested (Figure 14A, Two-way ANOVA, main effect of genotype: $p = 0.0593$). However, the age affected the performance on the elevated plus maze (Figure 14A, two-way ANOVA, main effect of age: $p = 0.0000$). WT as well as transgenic mice spent significant less time in the open arms at 12 months of age compared to the earlier time point (Figure 14A, unpaired t-test (3 vs. 12 mo.): $p = 0.0000$ (WT), $p = 0.0173$ (Tg4-42)). Additionally, the total distance traveled was affected in transgenic mice at three months of age (Figure 14B, unpaired t-test, WT vs. Tg4-42, 3 mo.: $p = 0.038$). Moreover, both WT as well as transgenic mice exhibited reduced distance traveled at 12 months of age compared to three months of age, respectively (Figure 14B, unpaired t-test (3 vs. 12 mo.): $p = 0.0000$ (WT), $p = 0.0000$ (Tg4-42)).

The elevated plus maze task revealed that basal anxiety and exploratory behavior are not affected in Tg4-42 mice at both ages tested.

3.4.3 Working memory of Tg4-42 mice

The cross-maze alternation task was used to assess spatial working memory. Alternation rates in the cross-maze were equivalent between control and transgenic mice at both ages examined (Figure 15A, two-way ANOVA, main effect of genotype: $p = 0.464$; main effect of age: $p = 0.4848$). Analyzing the total distance traveled, no significant differences between WT and Tg4-42 mice were found at three or 12 months of age (Figure 15B, two-way ANOVA, main effect of genotype: $p = 0.3728$). However, transgenic and wildtype mice showed a reduction in total distance traveled at 12 months of age in comparison to the 3-month time point (Figure 15B, two-way ANOVA, main effect of age: $p = 0.0000$, unpaired t-test (3 vs. 12 mo.): $p = 0.0002$ (WT), $p = 0.0006$ (Tg4-42)).

The cross-maze task demonstrated that working memory is not impaired in young and aged Tg4-42 mice.

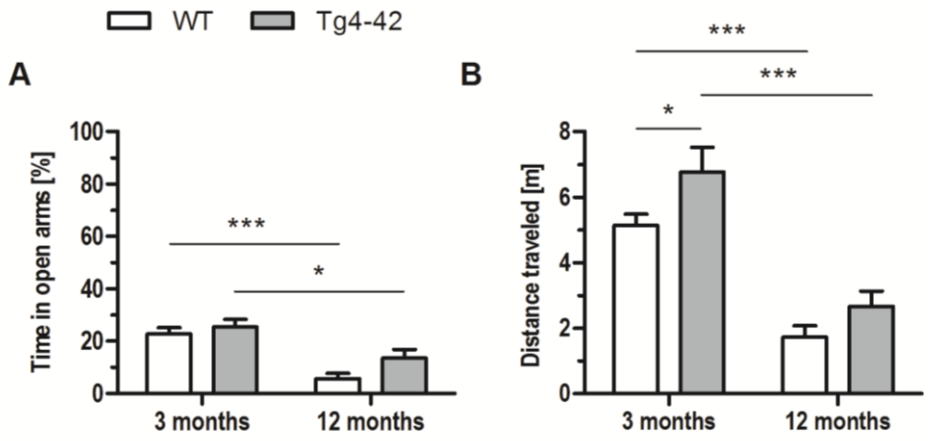

Figure 14 | Basal anxiety was unaffected in Tg4-42 mice.
Time spent in the open arms as well as distance traveled was assessed. Tg4-42 and wildtype mice were tested at 3 and 12 months of age. **(A)** Mice of both genotypes spent a similar percentage of time in the open arms at 3 and 12 months of age. **(B)** However, 3-month-old transgenic mice covered a greater distance compared to the age-matched control group. Distance traveled was not different between the 12-month-old groups. n = 10 – 15 mice per group (groups: sex- and age-matched). Mean ± SEM. Two-way ANOVA and unpaired t-test. Significance levels: ***p ≤ 0.001, *p ≤ 0.05.

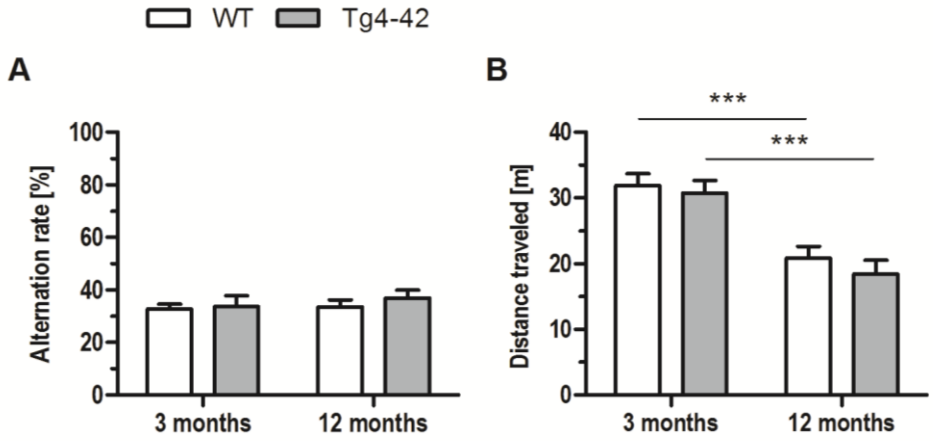

Figure 15 | No deficits in working memory were found in Tg4-42 mice.
Spontaneous alternation rates were analyzed as an indication for spatial working memory. Tg4-42 and wildtype mice were tested at 3 and 12 months of age. **(A)** Alternation rates were equivalent between WT and Tg4-42 mice at both 3 and 12 months of age. **(B)** Further, distance traveled revealed no significant differences between control and transgenic mice at both ages tested. n = 10 – 15 mice per group (groups: sex- and age-matched). Mean ± SEM. Two-way ANOVA and unpaired t-test. Significance levels: ***p ≤ 0.001.

3.4.4 Spatial reference memory of Tg4-42 mice

Spatial reference memory was assessed using the Morris water maze (MWM). The aim of this test was for the mouse to learn to use spatial cues to find a direct path to a hidden platform in a circular pool (Figure 16A). Each mouse was subjected to a nine-day long protocol including cued and acquisition training as well as one probe trial on the last day (Figure 16B).

For the Morris water maze, differences between groups were tested using *repeated measure analysis of variance* (RM-ANOVA) and *t-test for dependent samples* (paired t-test) considering different parameters as indicated. First, a RM-ANOVA was performed on each data set to test for higher order interactions. If RM-ANOVA revealed a main effect for one of the parameters tested, analysis was completed by *t-tests for dependent samples*.

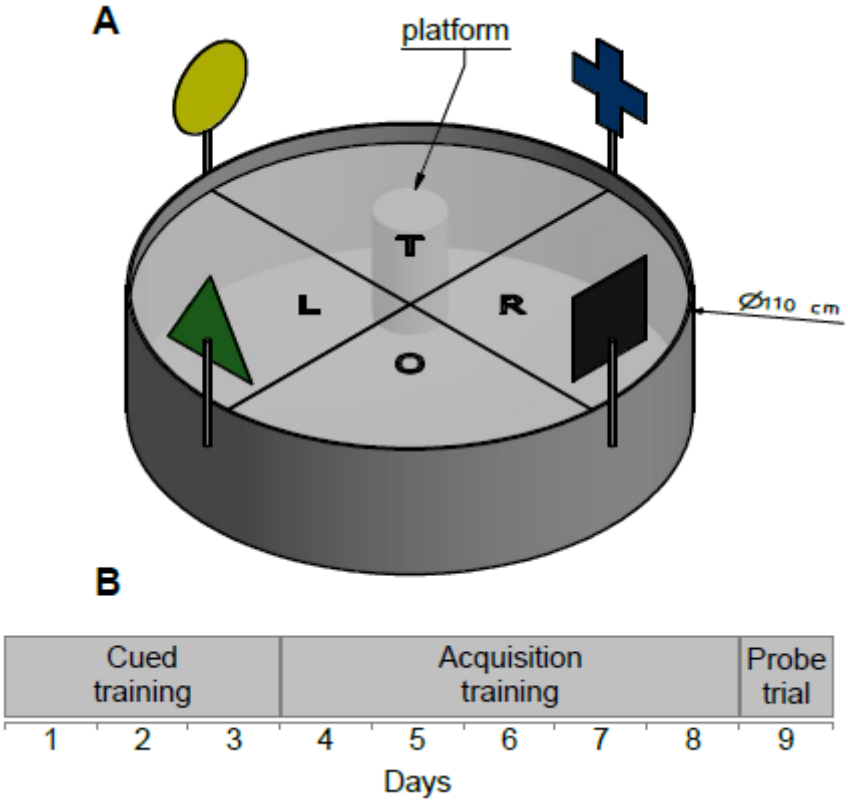

Figure 16 | Schematic setup and diagram of trial sequences of Morris water maze.
(A) Morris water maze procedure was used to analyze spatial reference memory in Tg4-42 mice. The setup was composed of a hidden circular platform in a circular pool filled with tap water. The pool was divided into 4 virtual quadrants that were defined based on their relationship to the platform: left (L), right (R), opposite (O) and target (T) quadrant which contains the goal platform. Proximal cues were attached to the outside of the pool. **(B)** Each mouse underwent a nine-day long protocol including 3 days of cued training, 5 days of acquisition training and 1 day for the probe trial.

Testing began with three days of cued training with a marked platform to familiarize the mice with the pool and to exclude effects from possible sensory and/or motor deficits. Wildtype and Tg4-42 mice showed successively decreased escape latencies over the three days of training at both ages tested (Figure 17A+C, RM-ANOVA, main effect of days: $p = 0.0000$; paired t-test (1. vs. 3. day): $p = 0.0000$ (WT, 3 mo.), $p = 0.0002$ (Tg4-42, 3 mo.), $p = 0.0033$ (WT, 3 mo.), $p = 0.0348$ (Tg4-42, 12 mo.)). Additionally, escape latencies were similar for WT and transgenic mice in response to training at both three and 12 months of age (Figure 17A+C, RM-ANOVA, main effect of genotype: $p = 0.0801$). Moreover, a significant main effect of age was found for all groups at both ages tested (Figure 17A+C, RM-ANOVA, main effect of age: $p = 0.0017$). In detail, we found a significant difference between three-month-old Tg4-42 and 12-month-old Tg4-42 mice (Figure 17A+C, RM-ANOVA, main effect of age: $p =0.0057$). Swimming speed did neither differ between transgenic and wildtype mice (Figure 17B+D, RM-ANOVA, main effect of genotype: $p = 0.1553$) nor within one genotype over the three days of training (Figure 17B+D, RM-ANOVA, main effect of days: $p = 0.3104$). Thus, cued training confirmed that all mice had intact vision and the appropriate motor abilities to swim.

Twenty-four hours after the last cued training trial, mice started to perform acquisition training. The marked platform was replaced by a submerged platform and proximal cues were attached to the outside of the pool and the inside of the curtains. Mice were tested for their learning abilities to find the location of the platform by using those proximal and additional distal cues. Progressively decreased escape latencies over the five days of training were found for wildtype and Tg4-42 mice at three months of age as well as for 12-month-old Tg4-42 mice (Figure 18A+C, RM-ANOVA, main effect of days: $p = 0.0000$; paired t-test (1. vs. 5. day): $p = 0.0123$ (WT, 3 mo.), $p = 0.0052$ (Tg4-42, 3 mo.), $p = 0.0484$ (Tg4-42, 12 mo.)). Since 12-month-old WT mice already reached the goal platform in less than 17 s on the first day of testing they were not able to show a decrease in escape latencies (Figure 18C, paired t-test (1. vs. 5. day): $p = 0.0924$). Escape latencies were similar between wildtype and Tg4-42 mice in response to training at three months of age (Figure 18A, RM-ANOVA, main effect of genotype: $p = 0.0748$). In contrast, escape latencies were significantly different between WT and transgenic mice in response to training at 12 months of age (Figure 18C, RM-ANOVA, main effect of genotype: $p = 0.0379$). Thus, aged Tg4-42 mice showed a slightly impaired spatial learning compared to same-aged wildtype animals. Although, swimming speed did not differ between transgenic and wildtype mice at both ages tested (Figure 18B+D, RM-ANOVA, main effect of genotype: $p = 0.0853$) a significant main effect of days was detectable within the 12-month-old Tg4-42 group (Figure 18D, paired t-test (1. vs. 5. day): $p = 0.0483$).

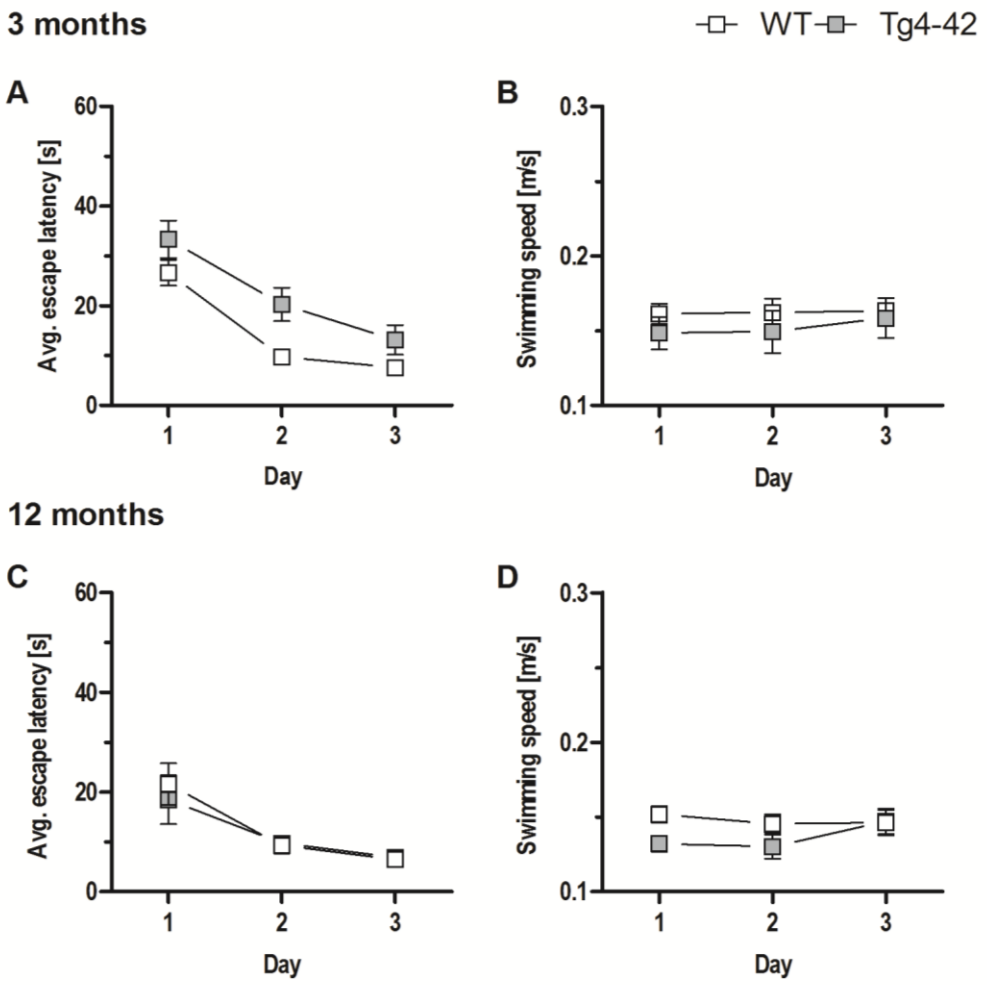

Figure 17 | Intact vision and motor abilities were found in Tg4-42 mice.
Cued training was performed to familiarize the mice with the pool and to rule out effects from potential motor and/ or sensory deficits. Tg4-42 and wildtype mice were tested at 3 and 12 months of age. **(A+C)** All mice showed successively decreased escape latencies over 3 days of training. Escape latencies were similar for wildtype and transgenic mice in response to training. **(B+D)** Swimming speed did not differ between wildtype and transgenic mice and was not affected at both ages tested. n = 10 – 15 mice per group (groups: sex- and age-matched). Mean ± SEM. RM-ANOVA and paired t-test.

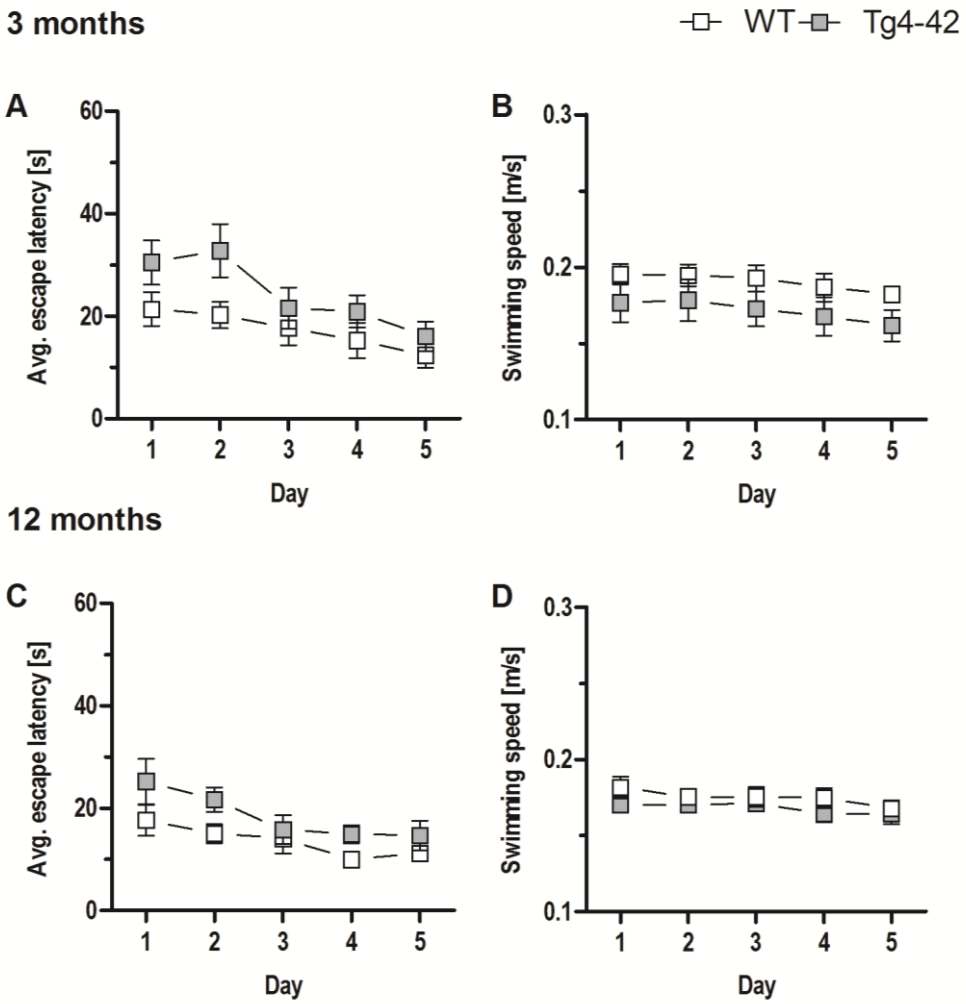

Figure 18 │ Subtle effects on spatial learning were demonstrated in aged Tg4-42 mice.
Mice performed acquisition training to learn to use proximal and distal cues to navigate a direct path to the hidden platform. Tg4-42 and wildtype mice were tested at 3 and 12 months of age. **(A+C)** Mice showed progressively reduced escape latencies over 5 days of training. However, 12-month-old Tg4-42 mice displayed a slightly impaired spatial learning compared to the age-matched wildtype animals as seen by higher escape latencies. **(B+D)** Swimming speed did not differ between the genotypes at 3 and 12 months of age. n = 10 – 15 mice per group (groups: sex- and age-matched). Mean ± SEM. RM-ANOVA and paired t-test.

Twenty-four hours after the last acquisition training trial, mice performed one probe trial to assess their spatial reference memory. The platform was removed from the pool and the swimming path was recorded for each mouse (see Figure 16). At three months of age Tg4-42 mice as well as wildtype controls showed no impairment in spatial reference memory as they spent a significant higher percentage of time in the target quadrant (Figure 19A, RM-ANOVA, main effect of quadrants: $p = 0.0000$; paired t-test: WT: $p = 0.0123$ T vs. L, $p = 0.0001$ T vs. R & O; Tg4-42: $p = 0.003$ T vs. L, $p = 0.0148$ T vs. R, $p = 0.0242$ T vs. O). Swimming speed was not affected at this age (Figure 19B, unpaired t-test: $p = 0.2598$). A repeated-measures ANOVA revealed a significant main effect of quadrants and additionally of the interaction between quadrants and genotype at 12 months of age (Figure 19C, RM-ANOVA, main effect of quadrants: $p = 0.0000$, main effect of quadrants*genotype: $p = 0.0221$). This means that 12-month-old wildtype mice still displayed a significant preference for the target quadrant (Figure 19C, RM-ANOVA, main effect of quadrants: $p = 0.0000$ paired t-test: $p = 0.0001$ T vs. L & R, $p = 0.0002$ T vs. O). In contrast, Tg4-42 mice demonstrated a significantly reduced learning behavior as they showed no preference for the target quadrant (Figure 19C, RM-ANOVA, main effect of quadrants: $p = 0.1463$). Again, swimming speed did not differ between both genotypes at 12 months of age (Figure 19D, unpaired t-test: $p = 0.2398$).

Taken together, the Morris water maze test revealed impairments in spatial learning as well as spatial reference memory in aged Tg4-42 mice.

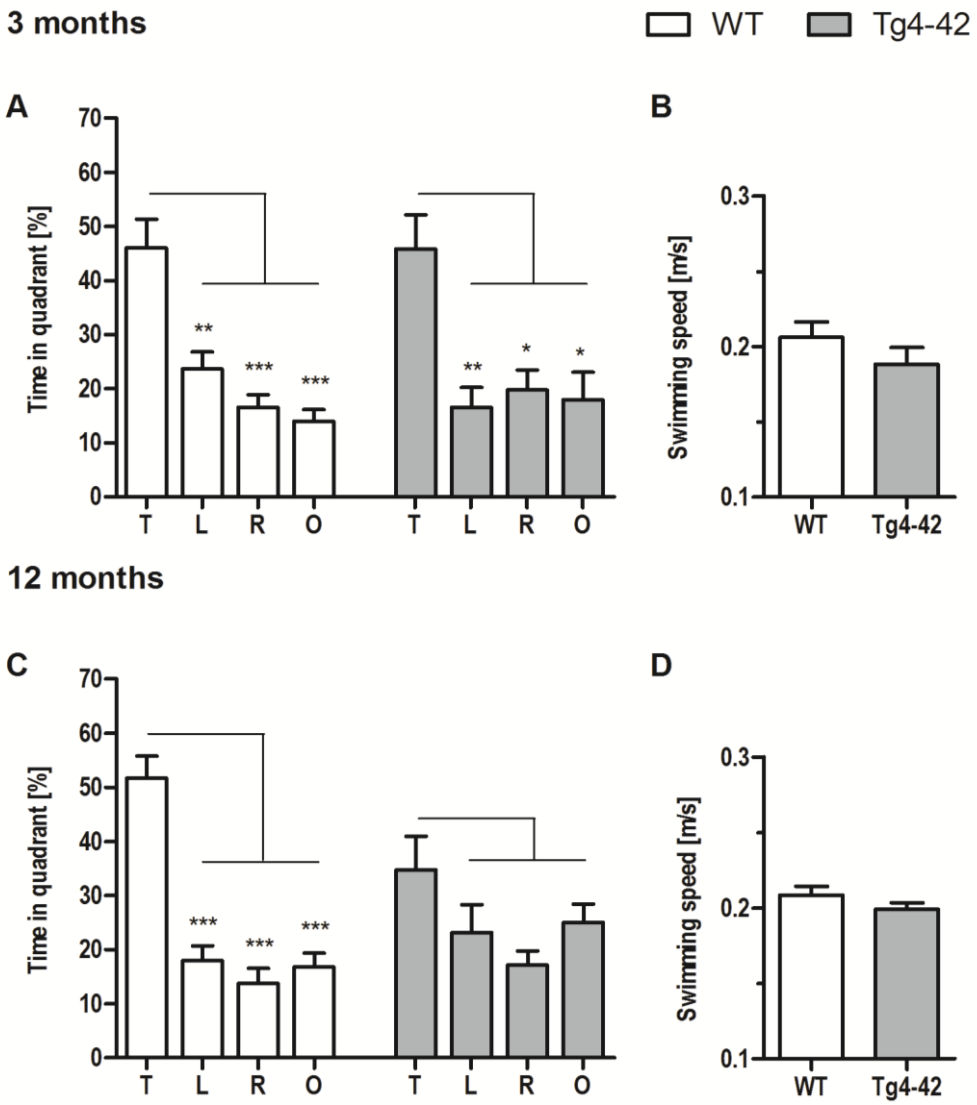

Figure 19 │ Aged Tg4-42 mice displayed an impaired spatial reference memory.
The probe trial was given at the end of the learning phase (AT) to assess spatial reference memory. Tg4-42 and wildtype mice were tested at 3 and 12 months of age. Quadrant preference and swimming speed are plotted for the first 30 s of the probe trial. **(A)** Wildtype and transgenic mice showed no impairment in spatial reference memory at 3 months of age. All mice spent a significant greater percentage of time in the target quadrant. **(C)** In contrast, Tg4-42 mice displayed distinct spatial reference deficits at 12 months of age as they showed no preference for the target quadrant. Wildtype mice still revealed an intact spatial reference memory at the same age. **(B+D)** No differences in swimming speed between wildtype and transgenic mice were detected at any age tested. Abbreviations: T – target, L – left, R – right, O – opposite quadrant. n = 10 – 15 mice per group (groups: sex- and age-matched). Mean ± SEM. RM-ANOVA and paired t-test (quadrant preference), unpaired t-test (swimming speed). Significance levels refer to the corresponding target quadrant: ***p ≤ 0.001; **p ≤ 0.01, *p ≤ 0.05.

3.4.5 Associative memory of Tg4-42 mice

Conditional learning and associative memory was assessed using the fear conditioning test. Each mouse was subjected to a three-day long protocol including one training trial as well as one test for contextual and tone memory respectively (Figure 20). This protocol contained the pairing of a conditioned stimulus (CS) with an unconditioned stimulus (US) within the initial training session.

For the fear conditioning task, differences between groups were tested using *repeated measure analysis of variance* (RM-ANOVA) and *t-test for dependent samples* (paired t-test) considering different parameters as indicated. First, a RM-ANOVA was performed on each data set to test for higher order interactions. If RM-ANOVA revealed a main effect for one of the parameters tested, analysis was completed by *t-tests for dependent samples*.

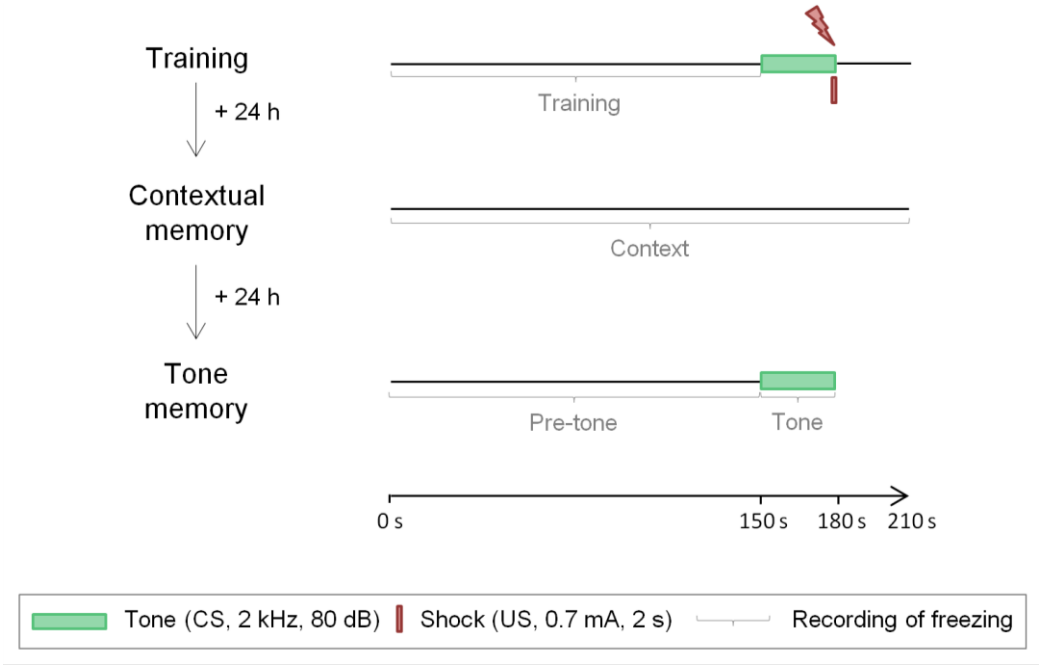

Figure 20 | Schematic diagram of fear conditioning procedure.
The fear conditioning task was used to analyze conditional learning and memory in Tg4-42 mice. Mice received one day of training including a time period to familiarize with the conditioning chamber followed by the presentation of a tone for 30 s that was overlapped by a foot-shock (red lightning) within the last two seconds of the tone. On the second day mice were placed in the same chamber to assess contextual memory (without tone or foot-shock). Twenty-four hours later tone memory was assessed in an altered conditioning chamber by presenting the tone that was already given on the first day. Freezing behavior was recorded on all days as indicated: training, context, pre-tone, tone. Abbreviations: CS – conditioned stimulus, US – unconditioned stimulus.

Twenty-four hours after the initial training session mice were placed in the same conditioning chamber. However, no tone or foot shock was given on this day. Analyzing the freezing behavior of all mice revealed that both the test phase as well as the genotype are important (Figure 21A, RM-ANOVA, main effect of test phase: $p = 0.0041$, main effect of test phase*genotype: $p = 0.0197$). This means that WT mice were still able to recognize the familiar chamber as they displayed a significantly higher percentage of freezing behavior in the context testing (Figure 21A, paired t-test, $p = 0.0006$ (training vs. context)). In contrast, transgenic mice maintained a similar percentage of freezing behavior for training and context testing (Figure 21A, paired t-test, $p = 0.6718$ (training vs. context)) and thus showed an impaired context memory.

Tone testing was performed on day three in an altered conditioning chamber. In contrast to the previous context testing a tone similar to the one used on the first day was presented. The test also showed an impact on freezing behavior (Figure 21B, RM-ANOVA, main effect of test phase: $p = 0.0000$). Both WT and transgenic mice were able to recognize the striking tone as they displayed a significantly higher freezing behavior during the tone period compared to the pre-tone period (Figure 21B, paired t-test (pre-tone vs. tone), $p = 0.002$ (WT), $p = 0.0001$ (Tg4-42)). As a consequence, this test revealed no deficits in tone memory in both groups.

Taken together, the fear conditioning task demonstrated that associative memory is impaired in aged Tg4-42 mice as seen by an altered context memory. However, tone memory was unaffected in Tg4-42 mice.

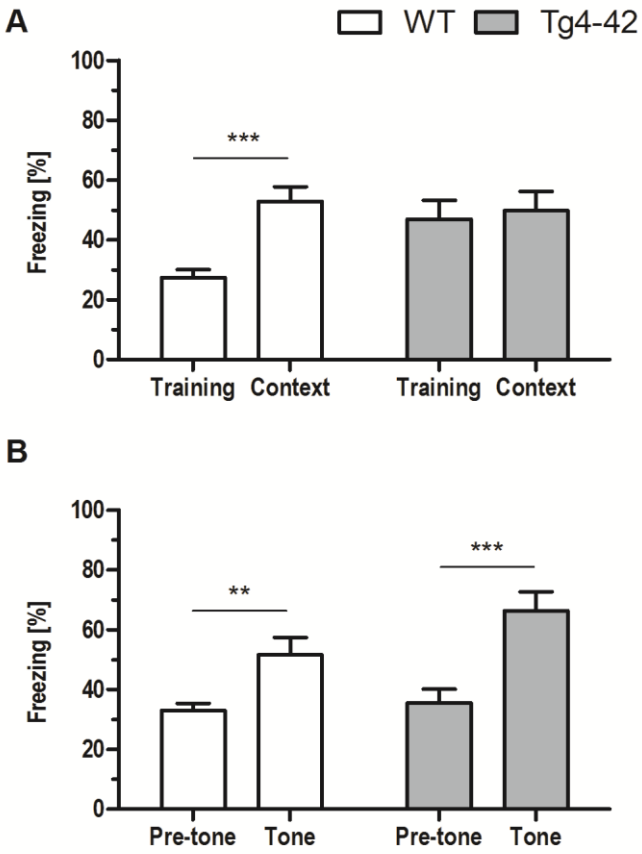

Figure 21 | Impaired contextual, but intact tone memory was found in aged Tg4-42 mice. Tg4-42 and wildtype mice were tested at 12 months of age **(A)** Tg4-42 mice showed an impaired contextual memory as they did not display a significant difference in freezing between training and context. Same-aged WT mice were still able to remember the conditioning chamber on the second day. **(B)** Both WT and Tg4-42 mice demonstrated an intact tone memory as seen by a significant increase in freezing behavior between pre-tone and tone period. n = 12 – 16 mice per group (groups: sex-matched). Mean ± SEM. RM-ANOVA and paired t-test. Significance levels: ***p ≤ 0.001; **p ≤ 0.01.

3.5 Electrophysiological recordings in Tg4-42 hippocampal tissue slices

The behavioral characterization of Tg4-42 mice revealed deficits in spatial learning, spatial reference memory and context memory. Hence, it was examined whether $A\beta_{4\text{-}42}$ is capable of inducing impairments in synaptic plasticity.

Synaptic function and plasticity were assessed using electrophysiological recordings in acute hippocampal tissue slices. Field EPSPs were evoked by unipolar stimuli that were delivered via steel micro wire electrodes. Those electrodes were placed at the CA3/CA1 junction and elicited orthodromic responses by stimulating the Schaffer collaterals. Field EPSPs were recorded in *stratum radiatum* of the CA1 region using a glass electrode filled with ACSF solution (Figure 22A). Acute hippocampal tissue slices of Tg4-42 males and same-sex wildtype littermate controls at three, 12 and 24 months of age were subjected to three different test paradigms, i.e. input-output curves, paired-pulse facilitation as well as recordings for short-term and long-term potentiation (Figure 22B).

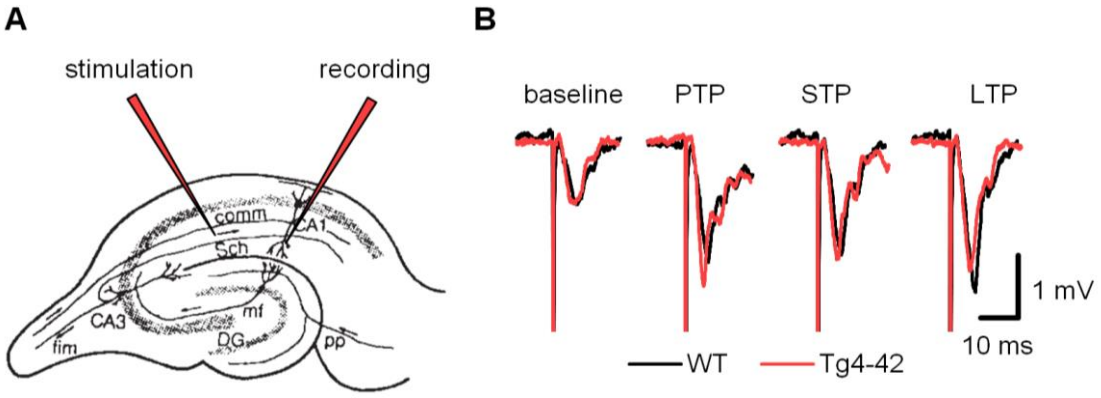

Figure 22 | Schematic illustration of electrode positioning and representative recordings. **(A)** Experiments were performed using acute hippocampal tissue slices of Tg4-42 mice. Field EPSPs were evoked by 0.1 ms unipolar stimuli delivered via an electrode that was placed at the CA3/ CA1 junction ('stimulation'). Orthodromic response was recorded in *stratum radiatum* of CA1 region using a glass electrode ('recording'). Figure adapted from (Bliss and Collingridge, 1993) **(B)** Sample traces of fEPSPs are shown before (baseline) and after (PTP, STP, LTP) high frequency stimulation for 3-month-old WT and Tg4-42 slices.

Differences between groups were tested using *repeated measures analysis of variance* (RM-ANOVA) and *t-test for independent samples* considering different parameters as indicated. First, a RM-ANOVA was performed on each data set to test for higher order interactions. If RM-ANOVA revealed a main effect for one of the parameters tested, analysis was completed by *t-tests for independent samples*.

3.5.1 Neuronal excitability in Tg4-42 mice

Responses to a single pulse stimulation, also referred to as input–output (IO) curves were recorded for stimulation intensities of 10 – 150 µA to assess neuronal excitability and basal synaptic function. Recorded fEPSP amplitudes were normalized to their absolute minimum. Four consecutive stimulus trains were pooled and averaged for each stimulus intensity.

Recordings revealed a characteristic run of all input-output curves as seen by higher normalized fEPSP amplitudes with increasing stimuli (Figure 23A-C, RM-ANOVA, main effect of stimuli: $p = 0.0000$). Furthermore, overall statistical analyses yielded various impacts on the behavior of the curve (Figure 23A-C, RM-ANOVA, main effect of stimulus*genotype: $p = 0.0000$, main effect of stimulus*age: $p = 0.0001$, main effect of genotype: $p = 0.0081$). More precisely, only three-month-old Tg4-42 mice showed a left shift of the input-output curve and hence an altered basal excitatory synaptic transmission as seen by significantly higher normalized fEPSP amplitudes compared to age-matched wildtype mice (Figure 23A, RM-ANOVA, main effect of genotypes $p = 0.0031$). In contrast, this increased neuronal excitability was not obvious in 12- and 24-month-old Tg4-42 mice compared to wildtype controls (Figure 23B-C, RM-ANOVA, main effect of genotypes $p = 0.1273$ (12 mo.) and $p = 0.9286$ (24 mo.)). Additional analysis of half-maximal stimulus intensity confirmed this increased neuronal excitability in three-month-old Tg4-42 mice compared to the age-matched control group (Figure 23D, unpaired t-test, $p = 0.0041$).

An additional analysis was performed comparing the IO curves of wildtype and transgenic mice with advancing age, respectively. Normalized fEPSP amplitudes of Tg4-42 mice were at similar levels between three and 24 months of age (Figure 23A-C, RM-ANOVA, main effect of age $p = 0.6260$). In contrast, wildtype mice revealed a left shift of the IO curves between three and 24 months of age (Figure 23A-C, RM-ANOVA, main effect of age $p = 0.012$).

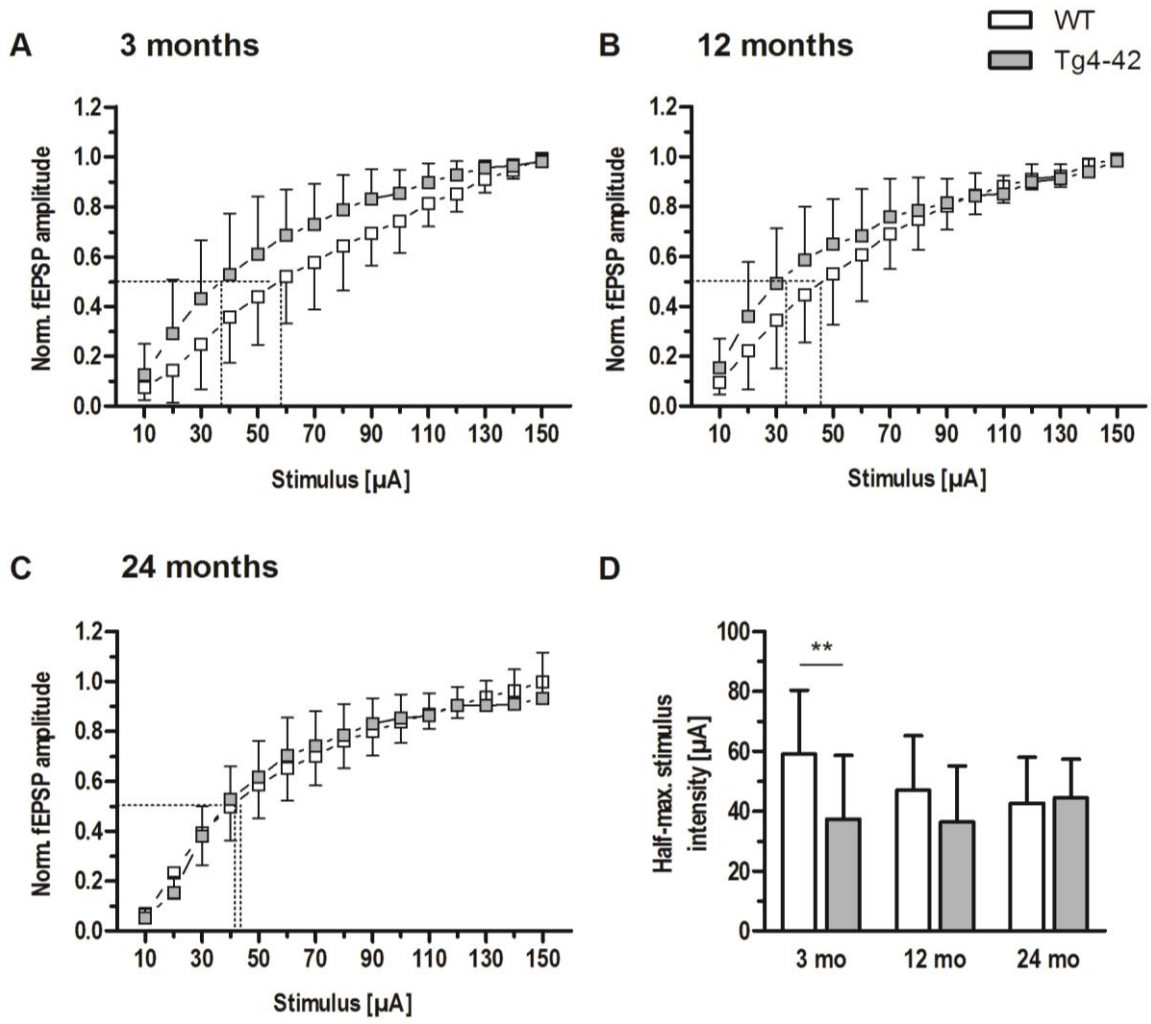

Figure 23 │ Alterations in basal synaptic transmission were evident in young Tg4-42 mice. Acute hippocampal tissue slices of Tg4-42 males and same-sex wildtype controls were used to assess neuronal excitability and basal synaptic function. Input–output curves were recorded for stimulation intensities of 10–150 µA. **(A)** 3-month-old Tg4-42 mice showed an altered basal excitatory synaptic transmission compared to age-matched wildtype mice as seen by a left shift of the input-output curve. **(B+C)** This increased neuronal excitability was not found in 12- and 24-month-old Tg4-42 mice compared to age-matched wildtype controls. **(D)** Analyzing the half-maximal stimulus intensity (dashed lines in A-C) revealed a variation in synaptic transmission only in 3-month-old Tg4-42 mice. n = 10 - 22 slices per group. Mean ± SD. Significance level refers to the age-matched WT group. RM-ANOVA and unpaired t-test. Significance level: ** $p \leq 0.01$.

3.5.2 Synaptic short-term plasticity in Tg4-42 mice

Paired-pulse facilitation (ppf) was quantified as a paradigm for synaptic short-term plasticity (Zucker, 1989) using the half maximal stimulus intensity obtained from input-output recordings. This twin-pulse stimulation was measured at eight different interstimulus intervals (25 – 200 ms) in 25 ms increments as the ratio of the second fEPSP to the first fEPSP amplitude. Four consecutive stimulus trains were pooled and averaged for each interstimulus interval.

Recordings revealed a characteristic run of ppf curves as the amplitudes decayed rapidly with interstimulus interval duration (Figure 24A-C, RM-ANOVA, main effect of interval: $p = 0.0000$). Moreover, shape of the curves were found to be dependent on the interactions of interval and genotype as well as interval and age (Figure 24A-C, RM-ANOVA, main effect of interval*genotype: $p = 0.0003$, main effect of interval*age: $p = 0.0078$). This means that three-month-old Tg4-42 mice showed a significantly decreased short-term plasticity at the shortest interpulse duration of 25 ms (Figure 24A+D, unpaired t-test, $p=0.0439$). However, long-term exposure to N-truncated $A\beta_{4-42}$ did not affect short-term plasticity in 12- as well as in 24-month-old Tg4-42 compared to wildtype mice (Figure 24B+C, RM-ANOVA, main effect of genotypes $p=0.1635$ (12 mo.) and $p=0.785$ (24 mo.)).

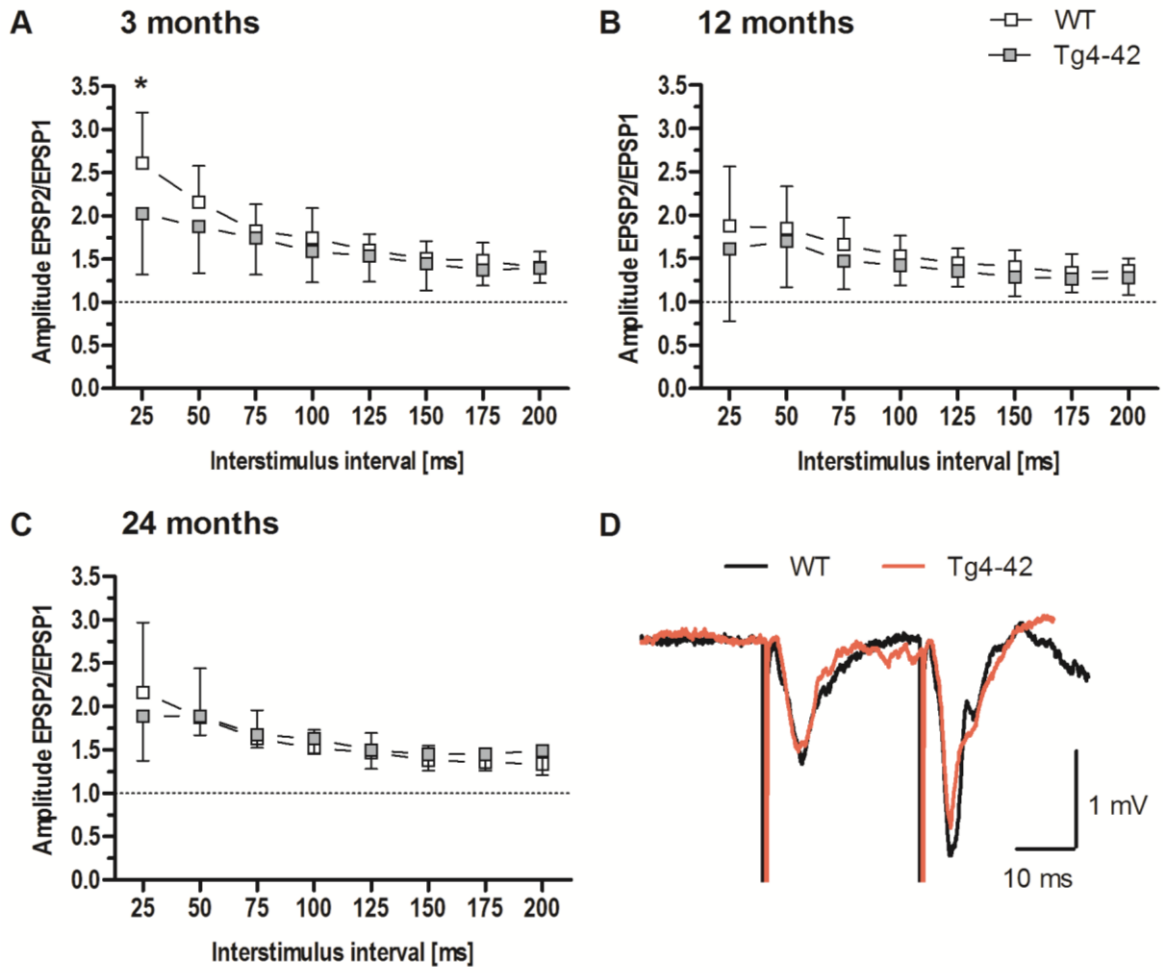

Figure 24 | Subtle effects on short-term plasticity were found in young Tg4-42 mice.
Paired-pulse facilitation (ppf) was quantified as a paradigm for synaptic short-term plasticity in Tg4-42 males and same-sex wildtype controls. This twin-pulse stimulation was measured at various interstimulus intervals (25–200 ms) as the ratio of the second fEPSP to the first fEPSP amplitude. **(A)** The overall short-term plasticity was affected in 3-month-old Tg4-42 mice compared to wildtype controls. Note that the amplitudes differ significantly between wildtype and Tg4-42 at an interpulse interval of 25 ms. **(B+C)** No difference in ppf was found between Tg4-42 and wildtype mice at 12 and 24 months of age. **(D)** Representative sample traces of ppf (interstimulus interval: 25 ms) recorded in 3-month old WT and Tg4-42 slices. n = 10 – 21 slices per group. Mean ± SD. Significance level refers to age-matched WT group (at 25 ms). RM-ANOVA and unpaired t-test. Significance level: *p ≤ 0.05.

3.5.3 Short-term and long-term plasticity in Tg4-42 mice

Effects of N-truncated $A\beta_{4-42}$ on post-tetanic potentiation (PTP), short-term (STP) as well as long-term potentiation (LTP) were examined at the Schaffer collateral CA1 pathway. Baseline fEPSP was determined using the half-maximal stimulus intensity obtained from input-output recordings as well as a low stimulation frequency and was recorded for 10 minutes. Potentials were measured every 15 s and 4 traces were averaged for one minute. Different forms of potentiation were induced by applying three tetanic stimulus trains of 100 Hz for one second every five minutes. After the third tetanic stimulus, recordings were continued for additional 65 minutes. Absolute fEPSP amplitudes were normalized to the average of pre-tetanus baseline fEPSP amplitudes. Post-tetanic potentiation was defined as the maximal response within one minute after the third tetanic stimulus. Short-term potentiation (STP) and long-term potentiation (LTP) were defined as the period between 12^{th} – 21^{st} min and 65^{th} – 75^{th} min after induction, respectively.

Induction of potentiation by three high-frequency stimuli caused a clear PTP of fEPSP amplitudes in all groups tested (Figure 25A-C). Using a repeated measures ANOVA, analysis revealed a main effect of genotype for PTP (Figure 25A-C, D, RM-ANOVA, main effect of genotypes: $p = 0.0218$). However, when comparing each single WT group with the age-matched transgenic group this effect was no longer obvious (Figure 25D, unpaired t-test, WT vs. Tg4-42, $p = 0.3461$ (3 mo.), $p = 0.2781$ (12 mo.), $p = 0.0727$ (24 mo.)).

Following PTP, short-term potentiation was analyzed in these recordings. Short-term potentiation remained stable in Tg4-42 and WT slices (Figure 25A-C). Further, STP was unaltered in Tg4-42 slices compared to WT slices at three, 12 and 24 months of age (Figure 25A-C, E, RM-ANOVA, main effect of genotypes $p = 0.2331$ (3 mo.), $p = 0.1489$ (12 mo.), p = 0,0533 (24 mo.)).

Besides, slices of wildtype and transgenic mice showed stable LTP after the high-frequency stimulation at all ages tested (Figure 25A-C). Remarkably, long-term potentiation was not affected in three-, 12- and 24-month-old Tg4-42 mice compared to wildtype controls (Figure 25A-C, F, RM-ANOVA, main effect of genotypes $p = 0.1925$).

Taken together, neurophysiological recordings revealed that basal synaptic transmission is altered in young Tg4-42 mice. However, neither short-term nor long-term potentiation was affected in Tg4-42 mice at any age tested.

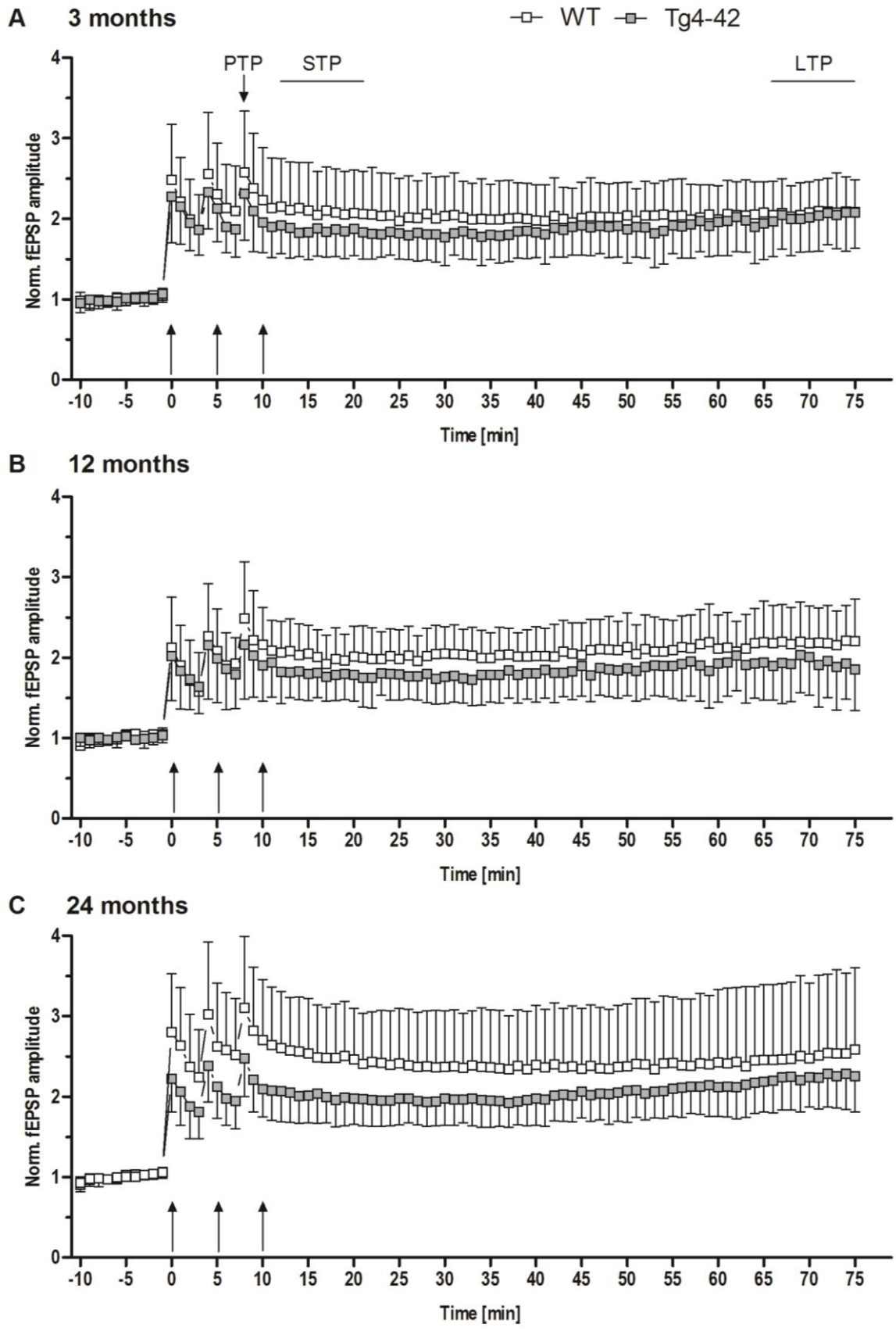

Figure 25 | No deficits in STP and LTP were found in Tg4-42 mice at any age tested.
Figure is continued and described on the next page.

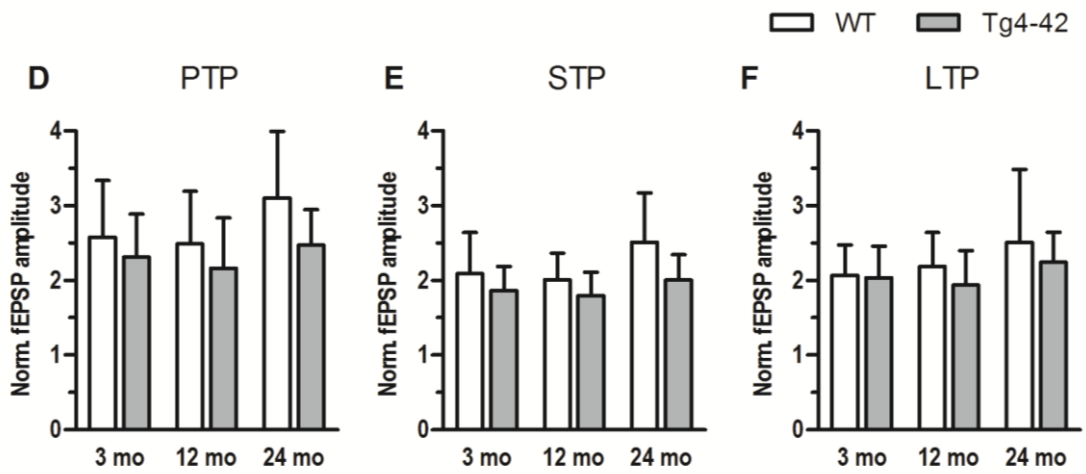

Figure 25 │ No deficits in STP and LTP were found in Tg4-42 mice at any age tested.
Effects of $A\beta_{4-42}$ on synaptic plasticity were assessed in hippocampal slices of Tg4-42 males and same-sex wildtype controls. PTP was defined as the maximal response within 1 min after the third tetanic stimulus. STP and LTP were defined as the period between 12^{th} – 21^{st} min and 65^{th} – 75^{th} min after induction, respectively. **(A-C)** Induction of potentiation by three high-frequency stimulus trains (filled arrows) caused a clear PTP of fEPSP amplitudes that did not differ among the groups at 3, 12 and 24 months of age. Recordings of STP revealed stable amplitudes in hippocampal slices of Tg4-42 and WT mice at all ages tested. Moreover, STP was not significantly different between the groups tested. Slices of wildtype and transgenic mice showed stable LTP after the high-frequency stimulation at all ages tested. Notably, long-term potentiation was not affected in 3-, 12- and 24-month-old Tg4-42 mice compared to wildtype controls **(D-F)** Summarized bar graphs for effects of $A\beta_{4-42}$ on PTP (D), STP (E) and LTP (F). No significant differences were found between WT and transgenic mice at any age evaluated neither for PTP nor for STP and LTP. Abbreviations: PTP – Post-tetanic potentiation, STP – Short-term potentiation, LTP – Long-term potentiation, mo – age in months. n = 10 – 12 slices per group. Mean ± SD. RM-ANOVA and unpaired t-test.

3.6 Gene expression analysis of synaptic markers

Neurophysiological recordings revealed an increased neuronal excitability in three-month-old Tg4-42 mice. Therefore, relative gene expression levels of selected synaptic markers were analyzed using qRT-PCR in three-month-old mice. In a pilot study, synaptoporin (Synpr) and SNAP25 (SNAP25a, SNAP25b) as well as neuroligin 1 (Nlgn) and PSD95 (Dlgh4) were examined as presynaptic and postsynaptic markers, respectively.

Analysis of gene expression levels revealed a significant down-regulation of synaptoporin and neuroligin 1 in Tg4-42 mice compared to the control group (Figure 26, Pairwise fixed reallocation randomization test, p = 0.037 (Synpr), p = 0.035 (Nlgn)). Expression levels of SNAP25 and PSD95 showed no significant changes between wildtype and transgenic mice (Figure 26, Pairwise fixed reallocation randomization test, p = 0.842 (SNAP25a), p =0.495 (SNAP25b), p = 0.743 (Dlgh4)).

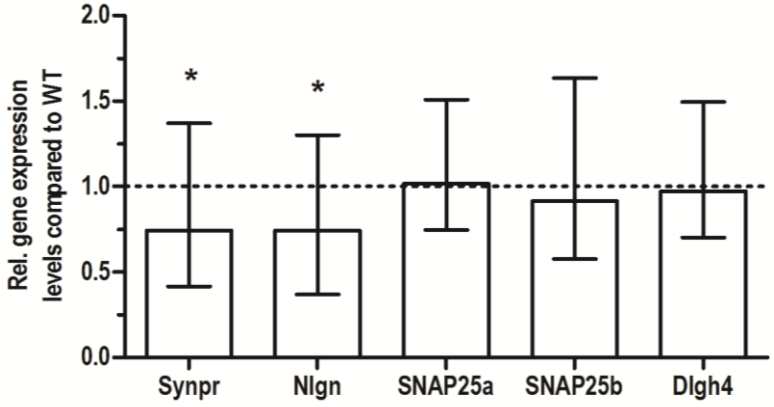

Figure 26 | Changes in gene expression of synaptic markers were shown in Tg4-42 mice. Analysis of expression levels of synaptic markers were performed using hippocampal tissue of 3-month-old male Tg4-42 and WT mice. Normalization was performed against the housekeeping gene β-Actin. Expression levels of Synpr and Nlgn were significantly down-regulated in Tg4-42 mice compared to control group. No changes in expression levels of 2 isoforms of SNAP25 and Dlgh4 were found between wildtype and transgenic mice. n = 7 – 8 mice per group. Mean ± 95 % CI. Pairwise Fixed Reallocation Randomization Test. Significance levels refer to Tg4-42 mice compared to WT animals (dashed line represents WT standard). Significance level: *p ≤ 0.05.

4 Discussion

4.1 N-truncated Aβ variants in AD etiology

In addition to the knowledge about various C-terminal modifications (e.g. Prelli et al., 1988, Miller et al., 1993, Näslund et al., 1994) mounting evidence suggested a role of N-truncated Aβ species in the etiology of AD since the eighties of the last century. Masters and colleagues demonstrated that the amyloid plaque cores of AD individuals are composed of a single major protein component of about 4-5 kDa that contained a truncated NH_2 terminus (Masters et al., 1985a). In the following years, many groups discovered various N-truncated Aβ species, $Aβ_{4-42}$ i.a., in brain samples of AD patients (Miller et al., 1993, Roher et al., 1993, Näslund et al., 1994, Saido et al., 1995, Gouras et al., 2000, Sergeant et al., 2003, Guzmán et al., 2014). Lewis and coworkers used SELDI-TOF (surface-enhanced laser desorption/ionization time-of-flight) mass spectrometry to analyze extracted peptides of AD samples. They detected a peak representing $Aβ_{4-42}$ which was the most dominant peak within all samples tested (Lewis et al., 2006). Beyond that, an additional study used immunoprecipitation in combination with mass spectrometric analysis to determine the Aβ isoform composition in three brain regions of FAD and SAD subjects as well as non-demented controls. $Aβ_{4-42}$ was found to be one of the most dominant isoforms in the hippocampus and cortex in AD brains (Portelius et al., 2010).

Based on those findings the question arose if the occurrence of N-truncated species has an influence on AD pathology. Using sedimentation analyses, electron microscopy, circular dichroism and cell culture, it was shown that “N-terminal deletions enhance aggregation of Aβ into neurotoxic, β-sheet fibrils” (Pike et al., 1995b). Furthermore, the authors suggested that those amino-terminal deletions initiate or at least contribute to Aβ deposition (Pike et al., 1995b). Additional studies analyzing Aβ isoforms with a pyroglutamate at position 3 revealed that N-truncated peptides displayed an increased toxicity *in vitro* and had a higher aggregation propensity, an increased hydrophobicity and an altered pH-dependent solubility profile (Russo et al., 2002, Schilling et al., 2006, Schlenzig et al., 2009). N-truncated Aβ species demonstrated a strong propensity to form stable aggregates as well as a high toxicity *in vitro* and *in vivo*. Particularly, $Aβ_{4-42}$ showed one of the highest aggregation propensities and displayed the formation of oligomers. The $Aβ_{4-42}$ peptide had a strong toxic effect when studied in primary cortical neurons and induced working memory deficits after intraventricular injection into wildtype mouse brains (Bouter et al., 2013).

In the last few years, the generation of mouse models harboring N-terminal truncated Aβ variants has gained more and more attention. Especially the N-terminally modified Aβ species pyroglutamate-amyloid-β (pE3-Aβ) has been extensively analyzed in the TBA2, TBA2.1/2.2, APP^{SL}PS1KI, 5XFAD, TBA42 and FAD42 mouse models (Wirths et al., 2009, Alexandru et al., 2011, Casas et al., 2004, Wittnam et al., 2012). However, other N-truncated Aβ variants, such as the highly abundant $Aβ_{4-42}$ form, were neglected and little is known about the toxic effects of these Aβ forms *in vivo*.

4.2 N-truncated $Aβ_{4-42}$ in a new mouse model

The aim of the present study was to analyze the neurotoxic effects of $Aβ_{4-42}$ in a novel mouse model which had been recently generated in our lab (Bouter et al., 2013). The Tg4-42 mouse line is the first model expressing exclusively N-truncated $Aβ_{4-42}$ without having any mutations which is in sharp contrast to most mouse models analyzed so far. The transgene construct consisting of a Thy-1 promoter and a TRH signal peptide directs $Aβ_{4-42}$ through the secretory pathway and enables its extracellular release (Bouter et al., 2013). Finally, due to the characteristics of the Thy-1 promoter (Caroni, 1997) human $Aβ_{4-42}$ is expressed in neurons. The effectiveness of using such a Thy-1 – TRH construct was shown in other mouse models like TBA2 (Wirths et al., 2009), TBA2.1 and TBA2.2 (Alexandru et al., 2011), TBA42 (Wittnam et al., 2012) as well as ETNA (Becker et al., 2013). Unlike other mouse models such as TBA42 and TBA2 the new Tg4-42 line does not need the activity of QC to form N-truncated Aβ (Wittnam et al., 2012, Wirths et al., 2009). In these aforementioned mouse lines at least two different Aβ isoforms are produced. Therefore, the Tg4-42 mice represent a more “cleaner” mouse model as they initially generate only $Aβ_{4-42}$. However, the possibility that $Aβ_{4-42}$ is further cleaved cannot be excluded.

Young Tg4-42 mice revealed a distinct pattern of Aβ deposition. This accumulation was demonstrated in a region-specific manner correlating with the expression pattern of the Thy-1 promoter (Caroni, 1997). Aside from intracellular Aβ deposits found in striatum, piriform cortex and inferior colliculus Tg4-42 mice revealed a strong Aβ pathology in the CA1 region of the hippocampus. Accumulation of intraneuronal Aβ declined with advancing age in these mice. This is well in line with other mouse models showing a decrease in intracellular Aβ deposits while aging (e.g. Wirths et al., 2001, Oddo et al., 2003, Christensen et al., 2008b, Jawhar et al., 2010). However, it should be mentioned that all those aforementioned mouse models displayed an age-dependent plaque pathology, while this is not the case in the Tg4-42 mouse model. Even at late age Tg4-42 mice do not develop plaques. As mentioned before, only minor Aβ deposits were

detectable in the hippocampal CA1 region at 12 months of age. It was suggested that the reduction in intracellular Aβ reactivity is due to the severe neuron loss shown in these mice and that these small deposits are left fragments of disintegrated cells which contained Aβ (Bouter et al., 2013). A similar pathology was also seen in the TBA2.1 mouse model which showed intracellularly high Aβ reactivity in intact cells at young ages and a severe neuron loss as well as extracellular deposits at later stages (Alexandru et al., 2011).

4.3 Gliosis in Tg4-42 mice

Inflammation is known to be a characteristic feature of AD (Akiyama et al., 2000). Microglia and astrocytes were investigated in Tg4-42 mice as cellular mediators of inflammation. Previously, diverse studies showed that Aβ is capable of stimulating microglia resulting in an activation of different inflammatory signaling pathways (Akiyama et al., 2000). Likewise, exposure of cultured astrocytes to Aβ increased the production of a wide range of inflammation-related factors (Wyss-Coray and Rogers, 2012). Increased astrogliosis as well as microgliosis were found in the Tg4-42 line as early as three months of age. Iba1 and GFAP positive cells were present in brain regions with Aβ accumulations, notably in the CA1 region of the hippocampus.

Previously, several studies reported that reactive microglia and astrocytes appeared in close vicinity to (extracellular) Aβ deposits both in human AD brains (Combs, 2009, Sofroniew and Vinters, 2010, respectively) as well as in brains of transgenic mouse models (e.g. Games et al., 1995, Frautschy et al., 1998, Stalder et al., 1999, Oakley et al., 2006). In addition, astrogliosis and/or microgliosis were also observed in mouse models showing less extracellular but high intracellular Aβ levels, e.g. APP^{SL}PS1KI (Casas et al., 2004), TBA2 (Wirths et al., 2009), TBA2.1/TBA2.2 (Alexandru et al., 2011) and TBA42 (Wittnam et al., 2012). This is in good agreement with our observations in Tg4-42 mice since reactive astrocytes as well as microglia were detected in parallel to intraneuronal Aβ accumulations. Thus, irrespective of the question about the causal connection, it could be stated that there is a direct link between Aβ and inflammation. Moreover, since the Tg4-42 mouse model expresses exclusively one N-truncated Aβ species the work of Thal and colleagues cannot be ignored (Thal et al., 2000). This group found that astrocytes containing N-truncated Aβ fragments predominantly appeared in the vicinity of N-truncated Aβ deposits. In contrast, Aβ-containing astrocytes were rarely detected in close proximity of full-length Aβ. The authors concluded that astrocyte-driven removal of extracellular Aβ may be possible that is followed by lysosomal processing. However, astrocytes may only take up N-truncated Aβ whereas full-length Aβ cannot be processed

(Thal et al., 2000). On the contrary, Russo *et al.* described a significant resistance of AβN3(pE)-40/42 peptides to degradation by astrocytes thereby increasing the time period where toxic effects can appear (Russo et al., 2002). However, the questions if astrocytes are capable of taking up $Aβ_{4-42}$ or if this N-truncated species develop a similar resistance to degradation by the mentioned mediators still remained unclear. Yet, the present data suggests that the specific characteristics of Aβ accumulations found in Tg4-42 promote the formation of a severe astro- and microgliosis that might exacerbate the ongoing neuropathology. Nevertheless, a positive role of inflammation in terms of a contribution to Aβ clearance cannot be excluded and further analyses are required.

4.4 Neuron loss in Tg4-42 mice

One of the main objectives in understanding AD-related pathologies is the investigation of neuron loss. Several attempts were taken to reproduce this known hallmark in transgenic mice. However, especially the first APP transgenic mice were not successful in this regard. Neither Tg2576 (Irizarry et al., 1997a) nor PDAPP (line 109) mice (Irizarry et al., 1997b) developed neuronal loss even at late ages. In contrast, APP23 mice exhibited a loss of neurons in the CA1 region of the hippocampus although this was relatively minor (~ 14 %) compared to what is observed in AD patients (Calhoun et al., 1998). Beyond that, mice harboring multiple mutations in both the APP gene and the PS1 gene displayed a more substantial neuron loss. For example, APP^{SL}PS1KI mice revealed an age-dependent neuron loss of about 33 – 49 % in hippocampal CA1 area (Casas et al., 2004, Breyhan et al., 2009, Brasnjevic et al., 2013). Similar to this, the number of neurons in the fifth cortical layer was decreased by 38 % in the multi-transgenic 5XFAD mouse model (Jawhar et al., 2010).

In the present study, Tg4-42 and WT mice demonstrated a comparable number of neuronal cells at three months of age using DAPI-staining. However, at 12 months of age the CA1 layer was visibly thinner in Tg4-42 mice compared to WT mice. This observation was analyzed in more detail in our lab employing unbiased stereology. The neuron number was determined in the hippocampal CA1 region of young and aged Tg4-42 mice. Three-month-old Tg4-42 mice showed no differences in the number of neurons, whereas a severe neuron loss of 49 % was detectable in Tg4-42 at 12 months of age (Bouter et al., 2013).

These findings are in good agreement with other mouse models expressing N-truncated Aβ variants. Wirths *et al.* detected a loss of calbindin-positive Purkinje cells in TBA2 mice (Wirths et al., 2009). A similar mouse model showed a severe loss of hippocampal cells (CA1) ranging from 35 % in three-month-old mice to almost 50 % at five

months of age (Alexandru et al., 2011). Likewise, 6-month-old homozygous ETNA mice demonstrated a striatal cell loss of 45 % (Becker et al., 2013).

The prominent neuronal loss occurred in a brain region which previously displayed an abundant accumulation of intraneuronal Aβ. This was not surprising since various studies established a direct causal relationship between intraneuronal Aβ accumulation and subsequent neuron loss (e.g. Wirths and Bayer, 2010). For example, in the aforementioned APP^{SL}PS1KI the age-dependent neuron loss was directly correlated with accumulation of intraneuronal Aβ, Thioflavin-S positive intracellular material and an atrophy of the entire hippocampus (Casas et al., 2004, Breyhan et al., 2009). Strikingly, this hypothesis was underlined by findings in the 5XFAD mouse model. In these mice substantial neuron loss was found in a brain region (fifth cortical layer) with abundant intracellular Aβ accumulation. In contrast, the CA1 region revealed neither intraneuronal Aβ nor a decrease in the number of neurons (Jawhar et al., 2010). Additionally, all mouse models expressing N-truncated Aβ species (TBA2, TBA2.1hom, ETNA) exhibited intraneuronal Aβ accumulations prior to a loss of neuronal cells (Wirths et al., 2009, Alexandru et al., 2011, Becker et al., 2013). Furthermore, an APP transgenic mouse model was described that did not develop any plaques until 24 months of age but displayed intraneuronal Aβ accumulations and a severe neuron loss (Tomiyama et al., 2010). Thus, it can be concluded that the neuron loss in Tg4-42 is a direct consequence of the intraneuronal Aβ accumulations.

Taken together, the Tg4-42 mice develop intraneuronal Aβ accumulations, severe inflammation as well as a distinct neuron loss. In a next step we evaluated possible behavioral changes in these mice assessing motor function, anxiety levels and cognitive functions.

4.5 Behavioral characterization of Tg4-42 mice

4.5.1 Motor function of Tg4-42 mice

Motoric abnormalities are common in AD patients and worsen as the disease progresses (Scarmeas et al., 2004, Wang et al., 2006). Since impairments in posture and gait appertain to the neurologic symptoms even in early stages of AD (Lalonde et al., 2012), various mouse models have been used to model motor dysfunctions and difficulties in coordinating movements. In sum, these analyses revealed a list of conflicting results. On one hand, several APP or APP/PS1 transgenic mice showed motor deficits as they were not able to achieve balance and reach a platform, grasp on a string or stay on a rotarod for a given time. This was true e.g. in 5XFAD (Jawhar et al., 2010), TBA42

(Wittnam et al., 2012), Tg2576 (King and Arendash, 2002), APP23 (van Dam et al., 2003) as well as in APP^{SL}PS1KI (Wirths et al., 2006) mice. On the other hand, some studies could not detect such motor deficits in transgenic mouse models. Normal performances on balance beam, string suspension or rotarod were found in 3xTg-AD (Giménez-Llort et al., 2007), APPSwe (line E1-2; Savonenko et al., 2003) and APP23 (Lalonde et al., 2002a) mice, for example. Likewise, Tg4-42 mice showed no development of motor dysfunction as they performed equally to age-matched control animals in all applied motor tests. Apart from methodological factors such as different apparatuses, age and genetic background of mice, the unequal distribution of intraneuronal Aβ accumulations and Aβ plaques in motor-related brain areas may explain these contrasting data. However, an intact motor performance in Tg4-42 also facilitates the accomplishment of more challenging and complex tests that rely on different forms of memory.

4.5.2 Anxiety and exploratory behavior of Tg4-42 mice

Alongside with cognitive decline a vast majority of MCI and AD patients suffer from neuropsychiatric symptoms like delusions, hallucinations, agitation/aggression, depression, apathy as well as anxiety (Lyketsos et al., 2002). These symptoms are mostly summarized as “behavioral and psychological symptoms of dementia (BPSD)” (Giménez-Llort et al., 2007). It is self-evident that modeling these non-cognitive symptoms in transgenic mice is an even more ambitious goal. Apart from human behavior traits like delusion and hallucination being impossible to recapitulate in mice other symptoms such as agitation or anxiety might be easier to address.

The present study used the elevated plus maze task to assess anxiety and exploratory behavior. This maze consists of two closed and two open arms that alternates around a center and is elevated above the surface. Mice have to choose between their tendency to explore a new environment and their tendency to avoid a bright and open setting. Increased entries and time spent in the open arms indicate a reduced anxious behavior (Karl et al., 2003). It is believed that this altered behavior is similar to the disinhibition seen in AD patients (cf. Webster et al., 2014). Young and aged Tg4-42 mice showed no alterations in their anxiety levels when compared to aged-matched control mice.

Similar results were obtained in studies with Tg2576 (Arendash et al., 2004), 3xTg-AD (Giménez-Llort et al., 2007), PD-APP (line J20, Wright et al., 2013), APP23 (Lalonde et al., 2002a), and APPSwe (line C3-3, E1-2, Savonenko et al., 2003) mice. In contrast, it was also reported that mice demonstrated a decreased anxiety phenotype such as the 5XFAD (Jawhar et al., 2010), TBA42 (Wittnam et al., 2012) and APP^{SL}PS1KI (Faure et al., 2011) models. In light of these results it remains unclear whether or not these differences

are due to methodological variations, the various distribution patterns of Aβ accumulations or age differences. Moreover, the difficulties in replicating BPSD seem to persist and additional tests are required to investigate these AD-related neuropsychiatric symptoms.

The emphasis in modeling AD pathologies in transgenic mice has widely been set on the investigation of memory impairments since cognitive decline is the most prominent hallmark of AD. In the present study, various tests were used to assess different cognitive domains like working memory, spatial learning, spatial reference memory as well as associative (i.e. context and tone) memory.

4.5.3 Working memory of Tg4-42 mice

Often used paradigms for working memory in mice are maze type tasks like T-maze, Y-maze or X-maze that become more challenging with increasing number of arms. Based on their natural exploratory behavior, mice are prone to alternate their arm entries when walking in a maze (Dudchenko, 2004). The calculated alternation rate is then assumed to be an indication for working memory. The present study takes the definition of Dudchenko as a basis as he “define[s] working memory as a short term memory for an object, stimulus, or location that is used within a testing session, but not typically between sessions.” (Dudchenko, 2004). It was shown that spontaneous alternation is sensitive to brain lesions including those in hippocampus and different cortical regions (Lalonde, 2002b). Therefore, it is assumed that spontaneous alternation is an appropriate paradigm for investigating AD-related memory deficits.

As with the motor function and anxiety level, assessment of working memory in AD mouse models revealed diverse results. Decreased performances in alternation were shown in 5XFAD (Oakley et al., 2006), TBA42 (Wittnam et al., 2012), Tg2576 (Hsiao et al., 1996) and APP^{SL}PS1KI (Wirths et al., 2006) mice. In contrast, this kind of short term memory was unaffected in PD-APP (line J20, Karl et al., 2012), APP23 (Lalonde et al., 2002a) and APPSwe (line C3-3, Savonenko et al., 2003) mice.

Neither young nor aged Tg4-42 mice demonstrated impairments in working memory as seen by similar alternation rates of transgenic and control animals in the cross maze. Again, methodological differences may explain the observed differences between the aforementioned mouse models since they differ in age, transgene promoter and expression levels as well as in their background strain. Moreover, working memory was assessed using dissimilar types of maze that impose different requirements. However, it should be noted that the cross maze used in the present study does not place a very high demand on hippocampus-dependent learning. As a consequence, the Morris water maze

was additionally used as a more sensitive test to assess hippocampal-dependent memory deficits.

4.5.4 Spatial reference memory of Tg4-42 mice

The Morris water maze (MWM), a test initially designed for rats, is meanwhile widely used to assess place learning or spatial (reference) memory (Morris, 1984). In this test, rodents must learn to find a direct path to a hidden platform in a circular pool. Navigation is supported by providing spatial cues around and attached to the pool. Lesion studies revealed that learning strategies used in the MWM are dependent on the dorsal hippocampus (Moser et al., 1995). Moreover, it was shown that other brain regions are involved as well, e.g. entorhinal and perirhinal cortices, prefrontal and cingulate cortex, neostriatum and potentially cerebellum (Vorhees and Williams, 2006).

Protocols for MWM exist in a large variety modifying number of test days, order of test parts, application and position of platform as well as changing the usage of certain analyses or the definition of types of memory. In the present study, the protocol was based on the description of Vorhees and Williams (Vorhees and Williams, 2006) and contained a cued as well as acquisition training and finally a probe trial. First, cued training was performed to familiarize the mice with the pool (pre-training) and to determine whether impairments that are unrelated to place learning are present, e.g. sensory and motor deficits. Subsequently, spatial learning was assessed across repeated trials within the acquisition training where platform location remained stationary and additional cues were provided. Finally, the probe trial was used to evaluate spatial reference memory by analyzing the preference for the target quadrant in comparison to all other quadrants when the platform is absent (Vorhees and Williams, 2006). In order to be able to differentiate between short- and long-term memory the probe trial was performed 24 hours after the last trial of the acquisition training. Based on such a long interval it is possible to determine reference memory independent of the memory of the last session (Vorhees and Williams, 2006).

In the present study, cued training confirmed that no deficits that are unrelated to place learning are present. Young and aged Tg4-42 mice revealed decreasing escape latencies over three days of training as well as swimming speeds that were both comparable to wildtype mice. In this way, they demonstrated intact eyesight, the motoric ability to swim, the presence of basic strategies (e.g. learning to swim away from the wall, learning to climb on the platform) and the motivation to escape from water. Therefore, there was no doubt on their capacity to learn to use distal cues in the following acquisition training. The

results of the cued training also corroborated the outcome of the motor tests in view of the total absence of motor constraints in Tg4-42 mice.

The acquisition training was performed to assess spatial learning. Again, swimming speed was similar between Tg4-42 and wildtype mice confirming the absence of motor impairments. Young Tg4-42 and wildtype mice demonstrated progressively decreased escape latencies over five days of acquisition training that were undistinguishable between both genotypes. This indicates an intact spatial learning behavior. The same was true for 12-month-old wildtype mice. In contrast, escape latencies of aged Tg4-42 were significantly different from age-matched wildtype mice as they needed more time to find the submerged platform indicating an impaired spatial learning in aged Tg4-42 mice.

At the end of the learning phase a probe trial was performed to assess spatial reference memory. The aim of this test was to determine if mice are able to remember the previous platform position. Young and aged wildtype as well as young Tg4-42 mice showed an explicit preference for the target quadrant indicating an intact spatial reference memory. However, aged Tg4-42 mice were unable to remember the previous platform position and spent an equal percentage of time in each quadrant. Since there were no differences in swimming speed between the genotypes it can be concluded that aged Tg4-42 mice developed severe impairments in their spatial reference memory.

Previous experiments showed a hippocampus-specific expression of $A\beta_{4\text{-}42}$ and a severe neuron loss in the CA1 region. These pathological features of the Tg4-42 mice correlate well with the age-dependent deficits in spatial learning and spatial reference memory. Almost all transgenic mouse models for AD have been tested in the MWM. Besides the Tg4-42 mice, other mouse models also revealed impairments in spatial learning and/or spatial reference memory, e.g. 5XFAD (Bouter et al., 2014), Tg2576 (Hsiao et al., 1996), APP^{SL}PS1KI (Faure et al., 2011), 3xTg-AD (Billings et al., 2005, Chen et al., 2013), PD-APP (line 109, Chen et al., 2000, line J20, Palop et al., 2003) and APP23 (van Dam et al., 2003). Nevertheless, some reports failed to verify impairments in the MWM, e.g. in APPSwe mice (line C3-3, Savonenko et al., 2003). Mouse models expressing N-truncated pE3-Aβ have not been investigated in the MWM so far. Thus, it remains difficult to draw comparable conclusions from the impact of N-truncated Aβ variants on spatial (reference) memory. However, since all aforementioned mouse models revealed intraneuronal Aβ accumulations and at least partially N-truncated Aβ species a correlation with impairments in spatial (reference) memory cannot be denied. This is noteworthy as accumulation of intraneuronal Aβ often precedes memory deficits and difficulties occur in directly correlating plaques and cognitive impairments (cf. Cheng et al., 2007).

4.5.5 Associative memory of Tg4-42 mice

Fear conditioning to a cue or a context is widely used to assess associative memory (Curzon et al., 2009, Puzzo et al., 2014). In this experimental setup, an unconditioned stimulus (US, e.g. foot shock) is paired with a conditioned stimulus (CS, e.g. tone). The aim of this test is for the mice to learn to associate this characteristic context (CS) with the aversive foot shock (US) (Fanselow, 2000). The successful association is then expressed in an increased freezing response. At this, freezing is defined as “the absence of all movement except […] for breathing” (Ohno, 2009). Additionally, mice with an intact associative memory do not only learn the tone but also the surrounding area (context).

It was shown that different brain regions are involved in contextual and cued fear conditioning, in particular amygdala, hippocampus, frontal and cingulate cortex (Curzon et al., 2009). Studies in rats revealed that an intact hippocampal formation is necessary for conditioning to a context while an undamaged amygdala causes an association between an auditory cue and a food reward (Sutherland and McDonald, 1990). Another study in rats claimed that the amygdala is involved in both the cue and the context memory, whereas the hippocampus is only needed for conditioning to a context (Phillips and LeDoux, 1992). Moreover, different studies verified an impact of hippocampal NMDA receptors on associative memory (Bast et al., 2003, Nakazawa et al., 2004).

In the present study an experimental design including context as well as cue (tone) fear conditioning was chosen. This three-day delay test began with a training session in which a tone that was overlapped by a foot shock was presented. Twenty-four hours after this training trial aged mice were again placed in the conditioning chamber. At this time neither a tone nor a foot shock was given. Wildtype mice were still able to remember the conditioning chamber as indicated by a significantly higher percentage of freezing. In contrast, aged Tg4-42 mice did not reveal such a behavior as they showed comparable levels of freezing behavior during the training and the context trial. Therefore, it is assumed that these mice developed impairments in associative memory in terms of context learning. Based on previous findings claiming context memory to be hippocampal-dependent these results are well in line with the region-specific $A\beta_{4\text{-}42}$ expression in the CA1 region in Tg4-42.

On the last day of testing, the tone memory was assessed in an altered conditioning chamber. At this time mice of both genotypes were able to remember the characteristic tone that had been presented during training session. Wildtype and Tg4-42 mice demonstrated an increased freezing behavior in response to the tone indicating an intact tone/ cue memory. Since the amygdala was shown to be involved in tone learning it can

be concluded that this brain region is not affected in Tg4-42 mice. This is also supported by the fact that Aβ accumulation was not evident in this area.

Several other AD transgenic mouse models have been tested in the fear condition paradigm revealing a variety of results. Impaired associative memory was found e.g. in 5XFAD (Kimura and Ohno, 2009, Bouter et al., 2014), Tg2576 (Jacobsen et al., 2006) and 3xTg-AD (Billings et al., 2005) mice. In contrast, PD-APP mice presented normal contextual memory (line J20, Wright et al., 2013). Despite the occurrence of methodological differences these dissimilar results might be due to the distribution pattern of Aβ in those mouse models. It is assumed that impairments in memory arise in those brain regions that are affected by Aβ accumulations. This was also corroborated by findings of España and colleagues that correlated fear conditioning symptoms with enhanced intraneuronal Aβ accumulation (España et al., 2010).

In general, the analysis of motor function, BPSDs or memory performance in AD transgenic mouse models often revealed controversial results. These differences might be due to the transgene itself, the expression of the transgene, the background strain and/ or the distribution pattern of plaques and intraneuronal Aβ accumulations. Moreover, a high methodological variation can influence the results of behavioral analyses. Mice are tested at different ages and ‘disease’ stages, analyzed brain regions are not coincided and protocols for behavioral experiments are often controversial.

In spite of that, it seems to be reasonable to conclude that $A\beta_{4-42}$ is capable of inducing AD-typical changes. Behavioral characterization of aged Tg4-42 mice revealed deficits in spatial learning, spatial reference memory and context memory. These impairments highly correlate with the hippocampus-specific expression of $A\beta_{4-42}$ and the observed neuron loss in same region. Based on these results it was assessed whether $A\beta_{4-42}$ has the ability to induce deficits in synaptic plasticity.

4.6 Neurophysiological alterations in Tg4-42 mice

Impairments in synaptic transmission and plasticity are well-known hallmarks of AD. Synaptic loss is an early event that occurs in the hippocampus and neocortex of AD patients and is assumed to be the major structural correlate to cognitive dysfunction (Marcello et al., 2012). Based on early versions of the amyloid cascade hypothesis it was initially thought that extracellular Aβ accumulations and amyloid plaques induce synaptic dysfunction (cf. Wirths et al., 2004, Mucke and Selkoe, 2012).

However, during the last years the detection of buffer-soluble bioactive oligomers (e.g. dimers, trimers, tetramers, dodecamers, higher oligomers) led to the concept that soluble

Aβ plays a key role in progressive synaptic injury (Mucke and Selkoe, 2012). This was supported by finding accumulations of oligomeric Aβ around neurons in human brains already at very early disease stages (Pozueta et al., 2013). A verification of this concept was achieved by different studies (using synthetic and natural oligomers) some of which shall be mentioned hereafter. Microinjection of cell medium containing natural oligomers of human Aβ into the brain of wildtype rats markedly inhibited hippocampal long-term potentiation (LTP) *in vivo*. Thus, Walsh *et al.* were able to proof that Aβ oligomers can interact with neurons and impair synaptic plasticity (Walsh et al., 2002). Another study described the inhibition of LTP, enhancement of long-term depression (LTD) and reduction of dendritic spine density in normal mouse hippocampus after administration of soluble Aβ oligomers that were directly extracted from cortices of AD patients. Additionally, Shankar *et al.* found that Aβ monomers and insoluble amyloid plaque cores were not capable of altering synaptic plasticity. They concluded “that dimers are the smallest synaptotoxic species” (Shankar et al., 2008). Trimers were also found to be potent inhibitors of hippocampal LTP (Townsend et al., 2006). In addition, Schlenzig and colleagues showed that N-terminal modifications of Aβ lead to rapid formation of oligomers that were able to inhibit hippocampal LTP in murine slices (Schlenzig et al., 2012). These and a plenty of other studies emphasize that Aβ oligomers can cause neuronal damage and that they are able to impair synaptic structure and function although it is still under debate which aggregation state represents the most synaptotoxic species (Benilova et al., 2012, Haass and Selkoe, 2007,Selkoe, 2008, Klyubin et al., 2012). However, it was also described that Aβ peptides can differentially affect synaptic function and also act as a positive regulator at the presynaptic level (Abramov et al., 2009). A study showed that synaptic plasticity was positively modulated by picomolar levels of Aβ (Puzzo et al., 2008). Hence, it was suggested that the pre- and postsynaptic regulation of synaptic transmission and plasticity by Aβ highly depends on its concentration (Mucke and Selkoe, 2012, Carrillo-Mora et al., 2014). Intermediate levels of Aβ enhance synaptic activity on the presynaptic terminal, whereas abnormal high or low levels of Aβ impair synaptic activity either on the presynaptic or postsynaptic terminal (Mucke and Selkoe, 2012).

Formation of Aβ oligomers was found primarily intracellular in both mouse and human brains (Walsh et al., 2000, Takahashi et al., 2004). This is of particular interest for this study as Tg4-42 mice developed massive intraneuronal Aβ accumulations. Moreover, it was shown that N-truncated Aβ peptides rapidly form stable aggregates, in particular monomers, dimers, trimers/tetramers and higher molecular weight oligomers (Bouter et al., 2013). Taking the distinct memory impairments in Tg4-42 into account it was examined whether the $A\beta_{4\text{-}42}$-induced deficits are also detectable on a synaptic level

indicating functional changes. Therefore, input-output curves, paired-pulse facilitation as well as short-term and long-term potentiation were recorded. These measurements are considered as electrophysiological correlates of neuronal excitability and learning and memory formation. Recordings were performed in *stratum radiatum* of the CA1 subfield in acute hippocampal tissue slices of Tg4-42 males.

4.6.1 Neuronal excitability in Tg4-42 mice

Input-output curves were recorded to assess the synaptic response to single pulse stimulation. Analyses were performed comparing Tg4-42 with respective wildtype mice. Basal synaptic transmission was altered in young Tg4-42 mice as seen by a left shift of the IO-curve, i.e. higher normalized fEPSP amplitudes. One can conclude that the neuronal excitability must be increased in terms of a neuronal hyperexcitability in these slices. This was also confirmed by analyzing the half-maximal stimulus intensity that was significantly increased in Tg4-42 slices compared to wildtype slices. Tg4-42 slices were faster excitable than wildtype slices. However, a comparable alteration was not found in 12- and 24-month-old Tg4-42 slices when analyzing either the entire IO curves or the half-maximal stimulus intensities.

Certain levels of Aβ may alter synaptic activity in young Tg4-42 mice as described above. It was suggested that intermediate levels of Aβ enhance synaptic activity presynaptically (cf. Mucke and Selkoe, 2012). Unfortunately, a lack of appropriate ELISA antibodies has prevented a quantitative assessment of Aβ levels in Tg4-42 so far. Thus, further studies are necessary to evaluate Aβ levels in this transgenic line both at one time point as well as within the course of time, i.e. during aging. Thereby, it might be possible to validate the hypothesis that increased excitability in Tg4-42 mice is due to high $Aβ_{4-42}$ levels. Alternatively, this altered excitability might be due to the oligomerization state of Aβ. So far, the molecular origin of this increased excitability in Tg4-42 mice remains unknown especially since further detailed pharmacological trials were not performed yet. Hippocampal hyperactivity was also observed in another mouse model that overexpresses both mutated APP_{swe} and mutated $PS1_{G384A}$ in neurons (Busche et al., 2012). Neuronal activity in the hippocampus was not only altered in plaque-bearing transgenic mice at the age of six to seven months but also in predepositing mice at one to two months of age. Moreover, application of nanomolar concentrations of Aβ dimers to hippocampal CA1 neurons in wildtype mice induced hyperactivity. They concluded that soluble Aβ is able to directly evoke neuronal hyperactivity by inducing inward currents in hippocampal neurons that lead to increased action potential firing and intracellular Ca^{2+} elevations (Busche et al., 2012). Previously, Kamenetz *et al.* showed that activity-dependent Aβ production participates in a negative feedback that regulates neuronal

hyperactivity indicating a role of Aβ in homeostatic plasticity (Kamenetz et al., 2003). Another study suggested that hyperexcitability within the hippocampus activates compensatory inhibitory mechanisms in order to weaken this aberrant activity. Furthermore, Palop *et al*. assumed that this hyperactivity as well as the compensatory mechanisms may lead to the observed network dysfunctions (Palop et al., 2007). Interestingly, it was also reported that "MCI patients exhibit hyperactivity in the hippocampus/parahippocampal region" (Maruszak and Thuret, 2014). Since it is also possible that hyperexcitability is caused by acute effects of Aβ at synapses this phenomenon needs additional studies.

An additional data analysis was performed comparing the IO curves of each genotype with advancing age. Wildtype mice revealed a left shift of the IO curves between three and 24 months of age. This implies that the same normalized fEPSP amplitude is evoked by decreased stimulation strength. In contrast, normalized fEPSP amplitudes of Tg4-42 slices were at similar levels at three, 12 and 24 months of age. The reason for these differences remains unclear. Several maturation or development processes in wildtype mice may alter the neuronal excitability during aging. An interaction of developmental programs of gene expression and experience-dependent plasticity, i.e. neural activity, is attributed for construction and deconstruction of synapses as well as for the characteristics on the presynaptic and postsynaptic level (Bagley and Westbrook, 2012). On the postsynaptic level, this can include an increase in receptor density or total receptor number (Sanes and Lichtman, 2001) as well as an altered subunit composition of e.g. AMPA or NMDA receptors (Bagley and Westbrook, 2012). Likewise, changes on the presynaptic level may affect the probability of transmitter release (Bagley and Westbrook, 2012). These mentioned changes might then contribute to an altered neuronal excitability in wildtype mice. Hippocampal hyperexcitability was also found in naturally aged, nontransgenic rats. Wilson and colleagues reported increasing firing rates, i.e. hyperactivity of CA3 place cells in aged rats while CA1 place cells had similar firing characteristics in aged and young animals (Wilson et al., 2005). They assumed that a combination of three age-related changes might be responsible for this hyperactivity: reduced function of interneurons in stratum radiatum, "decreased cholinergic modulation from basal forebrain innervation" (Wilson et al., 2005) as well as a reduced input from entorhinal cortex to dentate gyrus. Additionally, they found that CA3 cells were not able to rapidly encode changes in their environment indicating a key role of CA3 subregion in age-related changes, i.e. deficits in spatial memory (Wilson et al., 2005). However, the reason for the discrepancies between the Wilson study and the observations in our wildtype cohort remain unclear and further studies are required.

4.6.2 Synaptic short-term plasticity in Tg4-42 mice

Paired-pulse facilitation (ppf) was quantified in hippocampal tissue slices of Tg4-42 and wildtype males. Paired-pulse facilitation is known as a type of short-term plasticity and the synaptic response is enhanced “on the hundreds of milliseconds time scale” (Zucker and Regehr, 2002). Applying a pair of stimuli separated by a certain time interval evokes synaptic currents in which the second response is larger than the first. The magnitude of this facilitation decreases if the interstimulus interval is increased (Zucker and Regehr, 2002). It was shown that “paired-pulse facilitation is of presynaptic origin” (Kuhnt and Voronin, 1994) and reflects an increase in the probability of transmitter release (Zucker and Regehr, 2002). In the present study, interstimulus intervals ranging from 25 to 200 ms in 25 ms increments were used. Subsequent comparisons between wildtype and transgenic mice revealed a subtle effect on short-term plasticity in three-month-old Tg4-42 mice as seen by a lower EPSP2/EPSP1 ratio for the shortest interstimulus interval of 25 ms. Amplitude EPSP2/EPSP1 ratios were not altered for any other interstimulus interval in Tg4-42 mice at three months of age. Likewise, facilitation was not affected either at 12 or 24 months of age. Since only young Tg4-42 mice revealed a deficit and this difference between wildtype and transgenic mice appears to be extremely slight it can be concluded that short-term potentiation, i.e. facilitation is not primarily affected in this mouse line.

4.6.3 Short-term and long-term plasticity in Tg4-42 mice

Post-tetanic potentiation (PTP), short-term potentiation (STP) and long-term potentiation (LTP) were assessed in Tg4-42 and wildtype hippocampal slices. These neurophysiological measurements are widely used to investigate the occurrence and manifestation of synaptic dysfunction. Like PPF, post-tetanic potentiation is a type of enhancement of transmission of presynaptic origin. When applying a train of high-frequency stimuli, enhancement is gradually increased. After turning back to low-frequency stimulation this enhancement persists and lasts for 30 s to several minutes. However, it has to be considered that PTP is sometimes hard to identify since several enhancement processes may interfere, e.g. augmentation and PTP (Zucker and Regehr, 2002). In the present study, induction of potentiation caused a clear and immediate PTP in wildtype and transgenic slices that was undistinguishable between both genotypes at all ages tested. Thus, $A\beta_{4\text{-}42}$ has no effect on this type of enhancement.

Besides PTP, STP and LTP were evaluated. In general, at CA3 – CA1 synapses LTP consists of two phases: a stimulation-labile phase of short-term potentiation (STP) that converts into stable long-term potentiation (LTP) (Volianskis et al., 2013). Moreover it was described that both phenomena are (very likely) of postsynaptic origin (Bliss and

Collingridge, 2013). Here, after high-frequency stimulation induction and maintenance of stable LTP was detectable in wildtype and transgenic slices at all ages tested. Contrary to expectations, neither STP nor LTP were affected in aged Tg4-42 mice indicating that $A\beta_{4\text{-}42}$ is not capable of inducing substantial impairments in short-term or long-term plasticity in these mice. Further studies are necessary to clarify whether $A\beta_{4\text{-}42}$ is able to affect long-term depression as several studies revealed that elevated secretion of Aβ contributes to synaptic depression (e.g. Kamenetz et al., 2003, Hsieh et al., 2006, Kessels et al., 2013).

4.6.4 Comparison of neurophysiological alterations in AD mouse models

In order to assess AD-related changes in synaptic plasticity electrophysiological examinations were performed in other AD mouse models as well. Strikingly, these analyses revealed contradictory results. Outcomes ranged from reduced to enhanced to unaltered LTP, ppf and basal synaptic transmission. An overview of neurophysiological alterations in hippocampal slices from various mouse models is given in Table 9. Self-evidently, this table merely provides a limited selection since other mouse models revealed alterations in synaptic function as well, e.g. CRND8 (Jolas et al., 2002), PS2APP (Richards et al., 2003), SAMP8 (Lin et al., 2014), $PLB1_{Triple}$ (Koss et al., 2013), etc. To avoid going beyond the scope of this discussion, only studies were chosen that used similar experimental settings as we employed in the current study, including measurements in the hippocampal CA1 region *in vitro* (Table 9).

Most studies revealed a reduction of synaptic function in these mouse models. Interestingly, this is in sharp contrast to the Tg4-42 mouse model showing an increased excitability and no impairments in short-term or long-term plasticity. Several mouse models also revealed no impairments in neuronal excitability and/or synaptic plasticity. Moreover, various laboratories working with the same mouse models gained opposing results, e.g. in Tg2576 or PD-APP line J20 mice. Other studies found alterations that were no longer detectable at later time points, e.g. in APP23 mice (Table 9). Nevertheless, when comparing the synaptic function of different mouse models, it was often reduced in relatively young mice. More importantly this appeared (almost always) prior to extracellular Aβ deposition. Thus, it seems to be obvious that soluble, intracellular Aβ is a critical key player in inducing AD-related synaptic deficits. This was further affirmed by a study of Tomiyama and colleagues (Tomiyama et al., 2010). The characterization of the APP E693Δ mouse model revealed an enhanced Aβ oligomerization, an age-dependent accumulation of intraneuronal Aβ oligomers and the absence of extracellular Aβ deposits even at 24 months of age. *In vivo* electrophysiological recordings in the granular cell body layer of the *dentate* gyrus revealed a significant reduction of paired-pulse facilitation and

LTP, while the basal synaptic transmission was not affected. These impairments were detectable at a time point when Aβ oligomers have begun to accumulate and memory deficits as well as reduced synaptophysin levels were noticed. Thus, the group verified that Aβ oligomers can "cause early synaptic pathology in the absence of amyloid plaques" (Tomiyama et al., 2010). A correlation between intracellular Aβ or at least pre-plaque conditions and synaptic pathology was also depicted in other transgenic mouse models, e.g. PD-APP (Hsia et al., 1999), 3xTg-AD (Oddo et al., 2003), arcAβ (Knobloch et al., 2007) or APP^{SL}PS1KI (Bayer and Wirths, 2010). Although, it cannot be excluded that small amounts of extracellular Aβ are responsible for these synaptic deficits, it seems to be unlikely because a plethora of Aβ-specific antibodies could not detect extracellular Aβ at the time points used for electrophysiological experiments (cf. Oddo et al., 2003). Therefore, these findings highly support the intraneuronal Aβ-hypothesis.

The discrepancies both between different studies for the same line and between different mouse models may arise from several factors. As with the varieties in behavioral assessments this includes different transgenes, expression levels of transgenes, background strains and ages or rather 'disease' stages. Furthermore, the presence of intraneuronal Aβ or plaques, the prevalence and assembly forms of different Aβ variants as well as the general Aβ levels at the time points tested are apparently crucial factors since their impacts can differ. It was shown that the effects of Aβ are highly dependent on the applied or present concentration (Abramov et al., 2009) since low levels might also facilitate the maintenance of LTP (Puzzo et al., 2008, Pozueta et al., 2013). Furthermore, methodological variations might have an influence on the results. Differences appear in the precise stimulus protocols, definition of parameters as well as data analysis, e.g. type of normalization of fEPSP. In addition, the health of the *in vitro* preparations and the additive application of (stimulating) chemicals (e.g. kynurenate, physiological abnormal levels of Ca^{2+}) are not to be underestimated.

Table 9 | Overview of neurophysiological alterations in hippocampal slices from transgenic mouse models.
This selection only comprises electrophysiological recordings of fEPSPs in CA1 subfield *in vitro* thus enabling comparisons with the results of the present study.

Mouse line (mutations) (promoter)	Intra-neuronal Aβ	Plaques	Tangles	IO curve	ppf	PTP	STP	LTP	Reference
Tg4-42 (none) (Thy-1)	>2mo: yes	none	none	3mo: yes ↑ >12mo: none	3mo: yes ↓ >12mo: none	>3mo: none	>3mo: none	>3mo: none	(Bouter et al., 2013)
TBA2.1hom ($Aβ_{3E-42}$ → $Aβ_{3Q-42}$) (Thy-1.2)	>1mo: yes	>1mo: yes	none	2mo: none 5mo: yes ↓	n.a.	n.a.	n.a.	2mo: none 5mo: yes ↓	(Alexandru et al., 2011)
Tg2576 (APP: Swe) (PrP)	>2mo: yes	>6mo: yes	none	3mo: none[1] 2-8mo: none[2] 15-17mo: none[2] 12mo: none/yes[3]↓ 18mo: yes[3] ↓	3mo: none[1] <17mo: none[2] <18mo: none[3]	n.a.	n.a.	3mo: none[1] 2-8mo: none[2] 15-17mo: yes[2] ↓ <18mo: none[3]	(Hsiao et al., 1996); (Takahashi et al., 2013); (D'Amelio et al., 2011)[1]; (Chapman et al., 1999)[2]; (Fitzjohn et al., 2001)[3]
PD-APP line H6 (APP: Ind) (PDGF-β)	n.a.	2-5mo: none 8-10mo: yes	none	1-4mo: yes ↓ 8-10mo: yes ↓	1-4mo: n.a. 8-10mo: none	n.a.	n.a.	1-4mo: n.a. 8-10mo: none	(Games et al., 1995); (Hsia et al., 1999)
PD-APP line 109 (APP: Ind) (PDGF-β)	n.a.	27mo: yes	none	4-5mo: none 27-29mo: yes ↓	4-5mo: yes ↑ 27-29mo: yes ↓	n.a.	n.a.	4-5mo: yes ↓ 27-29mo: none	(Games et al., 1995); (Larson et al., 1999)

Table 9 | continued

Mouse line (mutations) (promoter)	Intra-neuronal Aβ	Plaques	Tangles	IO curve	ppf	PTP	STP	LTP	Reference
PD-APP line J9 (APP: Ind, Swe) (PDGF-β)	n.a.	2-4mo: none 8-10mo: yes	none	2-4mo: yes ↓	n.a.	n.a.	n.a.	n.a.	(Games et al., 1995); (Hsia et al., 1999)
PD-APP line J20 (APP: Ind, Swe) (PDGF-β)	n.a.	>2mo: yes	none	3-6mo: yes ↓ 4-7mo: yes ↓	3-6mo: none 4-7mo: none	n.a.	n.a.	3-6mo: yes ↓ 4-7mo: none	(Mucke et al., 2000); (Saganich et al., 2006); (Palop et al., 2007)
APP23 (APP: Swe) (Thy-1.2)	4mo: yes	>9mo: yes	none	3-9mo: none 12-18mo: yes ↓ 24mo: none	n.a.	n.a.	n.a.	3mo: none 6mo: yes ↓ 9-12mo: none 18mo: yes ↑ 24mo: none	(Sturchler-Pierrat et al., 1997); (Kuo et al., 2001); (Roder et al., 2003)
5XFAD (APP: Swe, Flo, Lon, PS1: M146L, L286V) (Thy-1)	>1.5mo: yes	>2mo: yes	none	4mo: none 5.5mo: yes ↓	<6mo: none	n.a.	n.a.	4mo: none 5.5mo: yes ↓	(Oakley et al., 2006); (Jawhar et al., 2010); (Wittnam et al., 2012); (Kimura and Ohno, 2009); (Crouzin et al., 2013)

Table 9 | continued

Mouse line (mutations) (promoter)	Intra-neuronal Aβ	Plaques	Tangles	IO curve	ppf	PTP	STP	LTP	Reference
APP^{SL}PS1KI (APP: Lon, Swe, PS1: M233T/ L235P) (Thy-1 (APP), PS1 knock-in)	>1.5mo: yes	>2mo: yes	none	n.a.	2-4mo: n.a. 6mo: yes ↓	n.a.	n.a.	2-4mo: none 6mo: yes ↓	(Casas et al., 2004); (Christensen et al., 2008b); (Breyhan et al., 2009)
3xTg-AD (APP: Swe, tau: P301L, PS1: M146V) (Thy-1.2 (APP, tau), PS1 knock-in)	>3mo: yes	>6mo: yes	>12mo: yes	1mo: none 6mo: yes ↓	1-6mo: none	n.a.	1-6mo: none	1mo: none 6mo: yes ↓	(Oddo et al., 2003)
icv-STZ (none) (none)	n.a.	n.a.	yes	6-7mo: none	6-7mo: none	n.a.	n.a.	6-7mo: yes ↓	(Chen et al., 2013); (Wang et al., 2014)

IO curve – input-output curve; ppf – paired-pulse facilitation; PTP – post-tetanic potentiation; STP – short-term potentiation; LTP – long-term potentiation; PS1 - presenilin 1; APP mutations: Swe - Swedish, Flo - Florida, Lon - London, Ind – Indiana; mo – age in months; n.a. - not analyzed; ↓ - decreased; ↑ - increased

The findings of neurophysiological alterations led to extended studies analyzing how Aβ targets neurons and synapses. It was suggested that Aβ directly binds to one or more receptors impairing several signaling pathways (Pozueta et al., 2013). This also includes interaction of Aβ oligomers with the low-affinity nerve growth factor (NGF) or the Frizzled (Fz) receptor ultimately causing cellular dysfunction or cell death. Moreover, Aβ oligomers can induce the loss of insulin receptors, impair LTP-associated kinase activity, bind to prion protein or interact with cell-surface APP. They are also capable of interacting with synaptic proteins or channels impairing calcium currents at glutamatergic and GABA-ergic synapses. Furthermore, it was also shown that Aβ can form pores in the membrane leading to abnormal flow of Ca^{2+} into the synapse (Pozueta et al., 2013). Other studies reported that Aβ oligomers bind to NMDA receptors leading to abnormal calcium homeostasis, oxidative stress and synapse loss (Shankar et al., 2007, Koffie et al., 2011) or contribute to synaptic deficits by affecting NMDAR subunit NR2B, PSD95 and α-CamKII (Dewachter et al., 2009, Rönicke et al., 2011). Renner and coworkers reported that Aβ oligomers form clusters at the synaptic plasma membrane. The formation of these clusters was dependent on the presence of mGluR5 receptors whose diffusion properties were altered afterwards. Additionally, distribution of mGluR5 receptors within the plasma membrane was changed leading to increased intracellular calcium followed by loss of receptors (Renner et al., 2010). Moreover, several studies showed that Aβ oligomers interact (either functionally and/or structurally) with anchored receptors (e.g. α7 nicotinic acetylcholine receptors), RAGE and EphB2 (Mucke and Selkoe, 2012). Rowan and colleagues proposed a model where Aβ oligomers bind to a target on microglia that promotes a stress cascade leading to disruption of NMDAR function and subsequently to inhibition of neuronal kinases needed for LTP induction (Rowan et al., 2004). It was also suggested that tau is able to mediate Aβ toxicity by modulating tyrosine kinase Fyn which then interacts with NMDA receptors (Ittner et al., 2010, Roberson et al., 2011). However, the mechanism by which Aβ impairs synaptic plasticity still remains manifold and controversial (Small et al., 2001; Benilova et al., 2012). Since the Tg4-42 mouse model did not show any alterations in synaptic plasticity and additional mechanistical studies were not performed, further statements on $Aβ_{4-42}$-toxicity in Tg4-42 cannot be made.

In summary, electrophysiological recordings revealed an Aβ-induced hyperexcitability in young Tg4-42 mice that develops prior to phenotypic alterations. This corroborates the hypothesis that intraneuronal Aβ is able to alter neuronal excitability. However, effects of $Aβ_{4-42}$ on synaptic short-term or long-term potentiation were not verifiable.

4.7 Altered gene expression levels in Tg4-42 mice

It is known that levels of several synaptic markers are altered in AD patients, e.g. synaptophysin (Masliah et al., 1994) and PSD95 (Shinohara et al., 2014). Interestingly, Shimohama *et al.* demonstrated that synaptic components are differently involved in AD pathogenesis as the decrease of some synaptic proteins was more pronounced (Shimohama et al., 1997). Following the functional analysis of synaptic transmission and plasticity, relative gene expression levels of synaptic markers were analyzed using quantitative real-time PCR (qRT-PCR).

An alteration in synaptic function was only evident for basal synaptic transmission in three-month-old Tg4-42 mice. Hence, only hippocampal tissue of Tg4-42 mice at three months of age was used to analyze expression levels of some selected markers. Two presynaptic markers (synaptoporin, SNAP25) and two postsynaptic (neuroligin 1, PSD95) markers were examined for the purpose of a pilot study.

Synaptoporin is a synaptic vesicle membrane protein of 37 kDa. It is a member of the synaptophysin/connexin superfamily and closely related to synaptophysin as they share 58 % amino acid identity (Knaus et al., 1990). Like synaptophysin, synaptoporin has four transmembrane domains and the N- and C-terminals are exposed to the cytoplasmic side even though these terminals are divergent (Singec et al., 2002). In general, synaptic vesicles are “responsible for the uptake, storing, docking and regulating release of transmitter” (Dai et al., 2003). It was suggested that synaptophysin and synaptoporin are negative regulators of SNARE (soluble N-ethylmaleimide-sensitive fusion protein attachment protein receptor) assembly. They are able to interact with VAMP/synaptobrevin and can “prevent the *v*-SNARE from entering into SNARE complexes” (Gerst, 2003). Nevertheless, the specific biological function of synaptoporin is not fully understood.

Synaptosome-associated protein of 25 kDa (SNAP25) is a presynaptic plasma membrane protein. Two alternatively spliced isoforms of SNAP25 (SNAP25a and SNAP25b) were identified which differ by nine amino acids. Those isoforms have different quantitative and anatomical expression patterns and might have different functions in vesicular fusion events. As one of the t-SNAREs it forms a core complex with syntaxin, synaptobrevin and synaptotagmin and is essential for regulating exocytosis of presynaptic vesicles (Bark et al., 1995, Südhof, 1995) as well as for maintaining normal synaptic activity (Tafoya et al., 2008).

Neuroligin 1 is a postsynaptic cell-adhesion molecule of excitatory synapses (Song et al., 1999) and belongs to the neuroligin family (Varoqueaux et al., 2006). Neuroligins are

type 1 transmembrane proteins and comprise four to five different postsynaptic proteins (neuroligin 1 – 4/5). They can either “interact with presynaptic α– and β-neurexins via a large extracellular esterase-like domain” or intracellularly “bind to several PDZ domain-containing scaffolding proteins [e.g. PSD95], which in turn interact with postsynaptic transmitter receptors, ion channels, and signaling proteins” (Varoqueaux et al., 2006).

Postsynaptic density protein 95 (PSD95) is a neuronal PDZ protein and a member of the membrane-associated guanylate kinase (MAGUK) family. Besides PSD95, this family contains three other proteins, namely SAP97, PSD93 and SAP102. All those proteins contain three N-terminal PDZ domains, an SH3 domain and a guanylate kinase-like (GUK) domain. They act as scaffolds and bind different signal transduction components to the cell membrane (Larsson et al., 2003).

The present study revealed that two out of four synaptic markers showed altered expression levels. The relative expression levels of synaptoporin and neuroligin 1 were significantly down-regulated in hippocampal tissue of three-month-old Tg4-42 compared to wildtype mice. In contrast, expression levels of PSD95 and both isoforms of SNAP25 remained unchanged in Tg4-42 compared to the control group.

Although further detailed investigations are indispensable one can speculate that a reduction in synaptoporin and neuroligin expression levels might contribute to the observed hyperexcitability in young Tg4-42 mice. Given that synaptoporin negatively regulates formation of vesicles (Gerst, 2003), a reduction of synaptoporin levels might facilitate SNARE assembly and secretion of vesicles that eventually might lead to alterations in synaptic transmission. Previously, it was shown that during development as well as in the adult brain neuroligins and their synaptic binding partners play a key role in modulating the development of excitatory and inhibitory synapses as well as controlling the balance between excitation and inhibition, respectively (Levinson and El-Husseini, 2005, Craig and Kang, 2007). It was proposed that an increased PSD95/neuroligin ratio leads to an “enhancement of excitatory presynaptic terminals and a reduction in the number of inhibitory contacts, thus shifting the E/I synaptic ratio [excitatory vs. inhibitory synaptic input] toward higher overall excitation” (Levinson and El-Husseini, 2005). Since Tg4-42 mice demonstrated unaltered PSD95 level but decreased neuroligin 1 level, the PSD95/neuroligin ratio is increased. Potentially, this might contribute to the observed alterations in synaptic transmission. However, additional analyses are needed to confirm those hypotheses.

Levels of synaptophysin were most frequently investigated and found to be decreased e.g. in 5XFAD (Oakley et al., 2006), icv-STZ (Chen et al., 2013), Tg2576 (Calkins et al.,

2011), APP^{SL}PS1KI (Brasnjevic et al., 2013), PD-APP (Mucke et al., 2000) and APP E693Δ (Tomiyama et al., 2010) mice. Primary neurons from Tg2576 mouse model revealed a decrease in several other synaptic markers including PSD95, synapsin 1, synapsin 2, synaptobrevin 1, synaptobrevin 2 and GAP43 (Almeida et al., 2005, Calkins et al., 2011). The 5XFAD mouse model additionally showed a reduction in PSD95 and syntaxin levels (Oakley et al., 2006, Shao et al., 2011). Different from the Tg4-42 mouse model, levels of SNAP25 and PSD95 were reduced in APP^{SL}PS1KI (Breyhan et al., 2009). These mouse models did not only show altered levels of synaptic markers but also changes in synaptic transmission or plasticity as seen by functional analyses mentioned before. Moreover, data in the literature indicate that altered levels of synaptic markers are often found in the absence of Aβ plaques (cf. Duyckaerts et al., 2007) which is in good agreement with the findings in Tg4-42 mice.

In summary, expression levels of one presynaptic and one postsynaptic marker were decreased in Tg4-42 mice. This reduction appeared simultaneously with an increased basal synaptic transmission in young transgenic mice.

4.8 Contradicting results in the Tg4-42 mouse model

The objective of the present study was to characterize the new transgenic mouse model Tg4-42 which exclusively expresses the N-truncated $Aβ_{4-42}$ form. The analyses revealed a severe astro- and microgliosis, distinct neuron loss, deficits in spatial learning, spatial reference memory and associative (i.e. context) memory as well as an increased basal synaptic transmission and decreased expression levels of specific synaptic markers in the mice. In contrast, neither motor function or working memory impairments nor altered anxiety levels were evident. Additionally, synaptic plasticity was not affected in Tg4-42 mice. The intraneuronal accumulation of Aβ in the hippocampus was followed by a distinct neuron loss in the same brain region. Moreover, this Aβ immunoreactivity was associated with impairments in cognitive functions that are assumed to be hippocampus-dependent. Surprisingly, an intact synaptic plasticity was observed in the hippocampus raising the question if there is a causal relationship between Aβ accumulations, memory impairments, neuron loss and altered synaptic plasticity.

The Morris water maze is a widely accepted test to assess hippocampal-dependent spatial and non-spatial learning in rodents (Morris, 1984, Puzzo et al., 2014, Vorhees and Williams, 2006). Various studies confirmed that the hippocampus plays a key role in information processing that is associated with spatial and non-spatial memory (e.g. Wood et al., 1999). However, it is also known that a network of other brain regions including the parietal cortex, cingulate cortex, the medial frontal cortex, the prefrontal cortex, the

nucleus basalis magnocellularis, the caudate nucleus and the fimbria-fornix are involved in spatial learning and memory (Olsen et al., 1994). Hence, it cannot be excluded that those brain regions also contribute to the observed deficits in spatial learning and memory in Tg4-42 mice. Accumulation of Aβ in the mentioned brain regions might be undetected so far due to the antibodies used in the present study. Nevertheless, a causal relation between hippocampal Aβ accumulation and spatial memory deficits seems to be very likely. Several lesion studies revealed that spatial memory performance requires hippocampal formation (e.g. Moser et al., 1995, Olsen et al., 1994, Broadbent et al., 2004). The groups of Moser and Broadbent were able to show that neuron loss can be compensated up to a certain level until it causes severe memory impairments (Moser et al., 1995, Broadbent et al., 2004). This could be corroborated by findings in the Tg4-42 mouse model. Hemizygous Tg4-42 mice at eight months of age demonstrated a neuron loss of 38 % while showing an intact spatial reference memory. In contrast, 12-month-old Tg4-42 mice displayed severe deficits in spatial memory performance and a 49 % loss of neuronal cells (Bouter et al., 2013). Thus, it seems that spatial memory impairments and neuron loss are causally related, although hippocampal damage needs to reach a certain degree.

Performance in MWM was often linked to LTP and the function of certain receptor types (e.g. Moser et al., 1998, Morris et al., 1986, Tsien et al., 1996). Even in transgenic (e.g. Tomiyama et al., 2010) and non-transgenic (e.g. Ardiles et al., 2012) models of AD memory impairments often appeared together with altered synaptic plasticity. The question if LTP and LTD are cellular mechanisms that underlie memory was and is still controversially discussed (Stevens, 1998, Martin et al., 2000, Lynch, 2004). Martin *et al.* establish a “synaptic plasticity and memory (SPM) hypothesis” which claims that “activity-dependent synaptic plasticity is induced at appropriate synapses during memory formation, and is both necessary and sufficient for the information storage underlying the type of memory mediated by the brain area in which that plasticity is observed” (Martin et al., 2000). Additionally, they outlined four criteria for assessing this hypothesis: detectability, mimicry, anterograde alteration and retrograde alteration. However, they had to concede that at least for the hippocampus it remained difficult to apply these criteria to verify the SPM hypothesis (Martin et al., 2000). The difficulty of proving a causal relationship between memory impairments and altered synaptic plasticity was evident in several studies including one of Moser and colleagues. They reported a learning deficit due to lesions in the hippocampus while electrophysiological responses stayed normal (Moser et al., 1995). This was similar to the Tg4-42 mouse model where synaptic plasticity was unaffected albeit a severe neuron loss and memory deficits. Likewise, two other

mouse models, Tg2576 and APP23, showed normal synaptic plasticity even in the presence of Aβ deposits and/or neuron loss (Fitzjohn et al., 2001, Roder et al., 2003).

Taken together, it must be stated that causal dependencies between Aβ accumulations, memory impairments, neuron loss and altered synaptic plasticity cannot be easily made, although these pathologies were all observed or measured in the same brain region. $A\beta_{4-42}$ seems to be able to induce neuron loss and memory deficits, however, it does not affect synaptic plasticity suggesting that even in the presence of $A\beta_{4-42}$ the surviving neurons of the hippocampal circuitry are able to compensate and maintain normal synaptic functionality.

5 Summary & Conclusion

Research of the past years revealed a large heterogeneity of C- and N-truncated Aβ variants. In particular, N-terminally truncated Aβ species displayed specific characteristics including a high aggregation propensity and a distinct toxicity. However, a profound analysis of specific N-truncated Aβ variants except for $Aβ_{pE3-42}$ was lacking.

In the present study the novel transgenic mouse model Tg4-42 was characterized to investigate the potential neurotoxic effects of $Aβ_{4-42}$ *in vivo* and *in vitro*. This mouse model expresses exclusively N-truncated $Aβ_{4-42}$ without an overexpression of mutated APP or PS1. Since the vast majority of AD patients do not possess mutations, research on sporadic AD is of great importance. Tg4-42 is one of the few mouse models which do not reflect familial AD but rather a sporadic-like pathology. In this mouse model overexpression of $Aβ_{4-42}$ led to early, region-specific intraneuronal Aβ accumulations most notably in the hippocampus. Simultaneously, Tg4-42 mice revealed a pronounced astro- and microgliosis in the same brain region. Additionally, these mice developed an age-dependent severe neuron loss in the hippocampal CA1 region. The absence of motor impairments facilitated the analysis of deficits in learning and memory. Using the Morris water maze and fear conditioning tasks, Tg4-42 mice demonstrated age-dependent deficits in spatial learning, spatial reference memory and forms of associative memory. Functional analyses in acute hippocampal tissue slices revealed an increased basal synaptic transmission at Schaffer collateral/CA1 synapses. In contrast, short-term and long-term plasticity were not affected. Analysis of gene expression levels demonstrated a down-regulation of synaptoporin and neuroligin 1 levels in hippocampal tissue of three-month-old transgenic mice which might be linked to the detected hyperexcitability.

Based on the results of the current work the following conclusions can be drawn: Since this mouse model did not develop amyloid plaques even at late ages the observed $Aβ_{4-42}$-induced pathology further supports the intraneuronal Aβ hypothesis. The abundance and intracellular localization of $Aβ_{4-42}$ prompts early pathological alterations that might trigger further upstream and downstream processes. This mouse model is suitable for the analysis of physiological and pathological roles of one specific Aβ variant in the absence of confounding effects of APP overexpression. Similar to other mouse models, Tg4-42 does not recapitulate the entirety of AD in humans and thus caution must be applied when extrapolating from findings in animal models to complex human diseases. However, the observed cognitive deficits as well as the neuron loss may relate to soluble forms of $Aβ_{4-42}$ and are comparable to AD-related changes. Thus, a pathological role for $Aβ_{4-42}$ in AD etiology was identified and further studies including evaluation of treatment strategies are feasible.

6 Bibliography

Abraham, J.-D., Promé, S., Salvetat, N., Rubrecht, L., and Cobo, S., et al. (2013). Cerebrospinal Aβ11-x and 17-x levels as indicators of mild cognitive impairment and patients' stratification in Alzheimer's disease. Transl Psychiatry *3*, e281.

Abramov, E., Dolev, I., Fogel, H., Ciccotosto, G.D., and Ruff, E., et al. (2009). Amyloid-beta as a positive endogenous regulator of release probability at hippocampal synapses. Nat. Neurosci. *12*, 1567-1576.

Abramowski, D., Rabe, S., Upadhaya, A.R., Reichwald, J., and Danner, S., et al. (2012). Transgenic expression of intraneuronal Aβ42 but not Aβ40 leads to cellular Aβ lesions, degeneration, and functional impairment without typical Alzheimer's disease pathology. J. Neurosci. *32*, 1273-1283.

Akiyama, H., Barger, S., Barnum, S., Bradt, B., and Bauer, J., et al. (2000). Inflammation and Alzheimer's disease. Neurobiol Aging *21*, 383-421.

Albert, M.S., DeKosky, S.T., Dickson, D., Dubois, B., and Feldman, H.H., et al. (2011). The diagnosis of mild cognitive impairment due to Alzheimer's disease: recommendations from the National Institute on Aging-Alzheimer's Association workgroups on diagnostic guidelines for Alzheimer's disease. Alzheimers Dement *7*, 270-279.

Alexandru, A., Jagla, W., Graubner, S., Becker, A., and Bauscher, C., et al. (2011). Selective Hippocampal Neurodegeneration in Transgenic Mice Expressing Small Amounts of Truncated Aβ Is Induced by Pyroglutamate-Aβ Formation. J Neurosci *31*, 12790-12801.

Almeida, C.G., Tampellini, D., Takahashi, R.H., Greengard, P., and Lin, M.T., et al. (2005). Beta-amyloid accumulation in APP mutant neurons reduces PSD-95 and GluR1 in synapses. Neurobiol. Dis. *20*, 187-198.

Alzheimer's Association (2014). 2014 Alzheimer's Disease Facts and Figures. Alzheimers Dement *10*.

Alzheimer's Society (2014). Drug treatments for Alzheimer's disease. Factsheet 407LP. alzheimers.org.uk.

Amaral, D.G., Scharfman, H.E., and Lavenex, P. (2007). The dentate gyrus: fundamental neuroanatomical organization (dentate gyrus for dummies). In The Dentate Gyrus: A Comprehensive Guide to Structure, Function, and Clinical Implications (Elsevier), pp. 3–790.

Amaral, D.G., and Witter, M.P. (1989). The three-dimensional organization of the hippocampal formation: a review of anatomical data. Neuroscience *31*, 571-591.

Antonios, G., Saiepour, N., Bouter, Y., Richard, B.C., and Paetau, A., et al. (2013). N-truncated Abeta starting with position four: early intraneuronal accumulation and rescue of toxicity using NT4X-167, a novel monoclonal antibody. Acta Neuropathol Commun *1*, 56.

Ardiles, A.O., Tapia-Rojas, C.C., Mandal, M., Alexandre, F., and Kirkwood, A., et al. (2012). Postsynaptic dysfunction is associated with spatial and object recognition memory loss in a natural model of Alzheimer's disease. Proc. Natl. Acad. Sci. U.S.A. *109*, 13835-13840.

Arendash, G.W., King, D.L., Gordon, M.N., Morgan, D., and Hatcher, J.M., et al. (2001). Progressive, age-related behavioral impairments in transgenic mice carrying both mutant amyloid precursor protein and presenilin-1 transgenes. Brain Res. *891*, 42-53.

Arendash, G.W., Lewis, J., Leighty, R.E., McGowan, E., and Cracchiolo, J.R., et al. (2004). Multi-metric behavioral comparison of APPsw and P301L models for Alzheimer's disease: linkage of poorer cognitive performance to tau pathology in forebrain. Brain Res. *1012*, 29-41.

Ashe, K.H., and Zahs, K.R. (2010). Probing the biology of Alzheimer's disease in mice. Neuron *66*, 631-645.

Bagley, E.E., and Westbrook, G.L. (2012). Short-term field stimulation mimics synaptic maturation of hippocampal synapses. J. Physiol. *590*, 1641-1654.

Bahr, B.A., Hoffman, K.B., Yang, A.J., Hess, U.S., and Glabe, C.G., et al. (1998). Amyloid beta protein is internalized selectively by hippocampal field CA1 and causes neurons to accumulate amyloidogenic carboxyterminal fragments of the amyloid precursor protein. J. Comp. Neurol. *397*, 139-147.

Bark, I.C., Hahn, K.M., Ryabinin, A.E., and Wilson, M.C. (1995). Differential expression of SNAP-25 protein isoforms during divergent vesicle fusion events of neural development. Proc. Natl. Acad. Sci. U.S.A. *92*, 1510-1514.

Bast, T., Zhang, W.-N., and Feldon, J. (2003). Dorsal hippocampus and classical fear conditioning to tone and context in rats: effects of local NMDA-receptor blockade and stimulation. Hippocampus *13*, 657-675.

Bayer, T.A., Jawhar, S., Wittnam, J.L., and Wirths, O. (2013). Problems During Aging (Alzheimer's and Others). In Neuroscience in the 21st Century, D.W. Pfaff, ed. (New York, NY: Springer New York), pp. 2953–2969.

Bayer, T.A., and Wirths, O. (2010). Intracellular accumulation of amyloid-Beta - a predictor for synaptic dysfunction and neuron loss in Alzheimer's disease. Front Aging Neurosci *2*, 8.

Bayer, T.A., and Wirths, O. (2014). Focusing the amyloid cascade hypothesis on N-truncated Abeta peptides as drug targets against Alzheimer's disease. Acta Neuropathol *127*, 787-801.

Becker, A., Kohlmann, S., Alexandru, A., Jagla, W., and Canneva, F., et al. (2013). Glutaminyl cyclase-mediated toxicity of pyroglutamate-beta amyloid induces striatal neurodegeneration. BMC Neurosci *14*, 108.

Benilova, I., Karran, E., and De Strooper, B. (2012). The toxic Aβ oligomer and Alzheimer's disease: an emperor in need of clothes. Nat Neurosci *15*, 349-357.

Bickel, H. (2014). Das Wichtigste 1: Die Häufigkeit von Demenzerkrankungen. Deutsche Alzheimer Gesellschaft e.V., www.deutsche-alzheimer.de.

Bien, J., Jefferson, T., Causevic, M., Jumpertz, T., and Munter, L., et al. (2012). The Metalloprotease Meprin Generates Amino Terminal-truncated Amyloid Peptide Species. J Biol. Chem. *287*, 33304-33313.

Billings, L.M., Oddo, S., Green, K.N., McGaugh, J.L., and LaFerla, F.M. (2005). Intraneuronal Aβ Causes the Onset of Early Alzheimer's Disease-Related Cognitive Deficits in Transgenic Mice. Neuron *45*, 675-688.

Blennow, K., Leon, M.J. de, and Zetterberg, H. (2006). Alzheimer's disease. Lancet *368*, 387-403.

Bliss, T.V.P., and Collingridge, G.L. (1993). A synaptic model of memory: long-term potentiation in the hippocampus. Nature *361*, 31-39.

Bliss, T.V.P., and Collingridge, G.L. (2013). Expression of NMDA receptor-dependent LTP in the hippocampus: bridging the divide. Mol Brain *6*, 5.

Bouter, Y., Dietrich, K., Wittnam, J.L., Rezaei-Ghaleh, N., and Pillot, T., et al. (2013). N-truncated amyloid β (Aβ) 4-42 forms stable aggregates and induces acute and long-lasting behavioral deficits. Acta Neuropathol *126*, 189-205.

Bouter, Y., Kacprowski, T., Weissmann, R., Dietrich, K., and Borgers, H., et al. (2014). Deciphering the Molecular Profile of Plaques, Memory Decline and Neuron Loss in Two Mouse Models for Alzheimer's Disease by Deep Sequencing. Front. Aging Neurosci. *6*, 75.

Brasnjevic, I., Lardenoije, R., Schmitz, C., van der Kolk, N., and Dickstein, D.L., et al. (2013). Region-specific neuron and synapse loss in the hippocampus of APPSL/PS1 knock-in mice. Transl. Neurosci. *4*, 8-19.

Breyhan, H., Wirths, O., Duan, K., Marcello, A., and Rettig, J., et al. (2009). APP/PS1KI bigenic mice develop early synaptic deficits and hippocampus atrophy. Acta Neuropathol *117*, 677-685.

Broadbent, N.J., Squire L. R., and Clark R. E. (2004). Spatial memory, recognition memory, and the hippocampus. Proc. Natl. Acad. Sci. U.S.A. *101*, 14515-14520.

Busche, M.A., Chen, X., Henning, H.A., Reichwald, J., and Staufenbiel, M., et al. (2012). Critical role of soluble amyloid-β for early hippocampal hyperactivity in a mouse model of Alzheimer's disease. Proc. Natl. Acad. Sci. U.S.A. *109*, 8740-8745.

Buxbaum, J.D., Liu, K.N., Luo, Y., Slack, J.L., and Stocking, K.L., et al. (1998). Evidence that tumor necrosis factor alpha converting enzyme is involved in regulated alpha-secretase cleavage of the Alzheimer amyloid protein precursor. J. Biol. Chem. *273*, 27765-27767.

Caillé, I., Allinquant, B., Dupont, E., Bouillot, C., and Langer, A., et al. (2004). Soluble form of amyloid precursor protein regulates proliferation of progenitors in the adult subventricular zone. Development *131*, 2173-2181.

Calhoun, M.E., Wiederhold, K.H., Abramowski, D., Phinney, A.L., and Probst, A., et al. (1998). Neuron loss in APP transgenic mice. Nature *395*, 755-756.

Calkins, M.J., Manczak, M., Mao, P., Shirendeb, U., and Reddy, P.H. (2011). Impaired mitochondrial biogenesis, defective axonal transport of mitochondria, abnormal mitochondrial dynamics and synaptic degeneration in a mouse model of Alzheimer's disease. Hum. Mol. Genet. *20*, 4515-4529.

Caroni, P. (1997). Overexpression of growth-associated proteins in the neurons of adult transgenic mice. J. Neurosci. Methods *71*, 3-9.

Carrillo-Mora, P., Luna, R., and Colín-Barenque, L. (2014). Amyloid Beta: Multiple Mechanisms of Toxicity and Only Some Protective Effects? Oxid Med Cell Longev *2014*, 1-15.

Casas, C., Sergeant, N., Itier, J.-M., Blanchard, V., and Wirths, O., et al. (2004). Massive CA1/2 neuronal loss with intraneuronal and N-terminal truncated Abeta42 accumulation in a novel Alzheimer transgenic model. Am. J. Pathol. *165*, 1289-1300.

Chapman, P.F., White, G.L., Jones, M.W., Cooper-Blacketer, D., and Marshall, V.J., et al. (1999). Impaired synaptic plasticity and learning in aged amyloid precursor protein transgenic mice. Nat. Neurosci. *2*, 271-276.

Chen, G., Chen, K.S., Knox, J., Inglis, J., and Bernard, A., et al. (2000). A learning deficit related to age and beta-amyloid plaques in a mouse model of Alzheimer's disease. Nature *408*, 975-979.

Cheng, I.H., Scearce-Levie, K., Legleiter, J., Palop, J.J., and Gerstein, H., et al. (2007). Accelerating Amyloid-beta Fibrillization Reduces Oligomer Levels and Functional Deficits in Alzheimer Disease Mouse Models. J Biol. Chem. *282*, 23818-23828.

Chen, Y., Liang, Z., Blanchard, J., Dai, C.-L., and Sun, S., et al. (2013). A non-transgenic mouse model (icv-STZ mouse) of Alzheimer's disease: similarities to and differences from the transgenic model (3xTg-AD mouse). Mol. Neurobiol. *47*, 711-725.

Chishti, M.A., Yang, D.S., Janus, C., Phinney, A.L., and Horne, P., et al. (2001). Early-onset amyloid deposition and cognitive deficits in transgenic mice expressing a double mutant form of amyloid precursor protein 695. J. Biol. Chem. *276*, 21562-21570.

Christensen, D.Z., Bayer, T.A., and Wirths, O. (2008a). Intracellular Aβ triggers neuron loss in the cholinergic system of the APP/PS1KI mouse model of Alzheimer's disease. Neurobiol Aging *31*, 1153-1163.

Christensen, D.Z., Kraus, S.L., Flohr, A., Cotel, M.-C., and Wirths, O., et al. (2008b). Transient intraneuronal Aβ rather than extracellular plaque pathology correlates with neuron loss in the frontal cortex of APP/PS1KI mice. Acta Neuropathol *116*, 647-655.

Cleary, J.P., Walsh, D.M., Hofmeister, J.J., Shankar, G.M., and Kuskowski, M.A., et al. (2004). Natural oligomers of the amyloid-β protein specifically disrupt cognitive function. Nat Neurosci *8*, 79-84.

Collingridge, G.L., Isaac, J.T.R., and Wang, Y.T. (2004). Receptor trafficking and synaptic plasticity. Nat Rev Neurosci *5*, 952-962.

Combs, C.K. (2009). Inflammation and microglia actions in Alzheimer's disease. J Neuroimmune Pharmacol *4*, 380-388.

Cooke, S.F., and Bliss, T.V.P. (2006). Plasticity in the human central nervous system. Brain *129*, 1659-1673.

Corder, E.H., Saunders, A.M., Risch, N.J., Strittmatter, W.J., and Schmechel, D.E., et al. (1994). Protective effect of apolipoprotein E type 2 allele for late onset Alzheimer disease. Nat. Genet. *7*, 180-184.

Corder, E.H., Saunders, A.M., Strittmatter, W.J., Schmechel, D.E., and Gaskell, P.C., et al. (1993). Gene dose of apolipoprotein E type 4 allele and the risk of Alzheimer's disease in late onset families. Science *261*, 921-923.

Craig, A.M., and Kang, Y. (2007). Neurexin-neuroligin signaling in synapse development. Curr. Opin. Neurobiol. *17*, 43-52.

Crouzin, N., Baranger, K., Cavalier, M., Marchalant, Y., and Cohen-Solal, C., et al. (2013). Area-specific alterations of synaptic plasticity in the 5XFAD mouse model of Alzheimer's disease: dissociation between somatosensory cortex and hippocampus. PLoS ONE *8*, e74667.

Curzon, P., Rustay, N.R., and Browman, K.E. (2009). Cued and Contextual Fear Conditioning for Rodents. In Methods of behavioral analysis in neuroscience, J.J. Buccafusco, ed. (Boca Raton: CRC Press), pp. Chapter 2.

Cynis, H., Schilling, S., Bodnár, M., Hoffmann, T., and Heiser, U., et al. (2006). Inhibition of glutaminyl cyclase alters pyroglutamate formation in mammalian cells. BBA-Proteins Proteom. *1764*, 1618-1625.

Dai, J., Ji, C., Gu, S., Wu, Q., and Wang, L., et al. (2003). Cloning and sequence analysis of the human cDNA encoding the synaptoporin (Δ), a highly conservative synaptic vesicle protein. Mol. Biol. Rep. *30*, 185-191.

D'Amelio, M., Cavallucci, V., Middei, S., Marchetti, C., and Pacioni, S., et al. (2011). Caspase-3 triggers early synaptic dysfunction in a mouse model of Alzheimer's disease. Nat. Neurosci. *14*, 69-76.

David, A., and Pierre, L. (2006). Hippocampal Neuroanatomy. In The Hippocampus Book, P. Andersen, R. Morris, D. Amaral, T. Bliss and J. O'Keefe, eds. (Oxford University Press), pp. 37–114.

De Strooper, B. (2010). Proteases and proteolysis in Alzheimer disease: a multifactorial view on the disease process. Physiol. Rev. *90*, 465-494.

De Strooper, B., and Annaert, W. (2010). Novel research horizons for presenilins and γ-secretases in cell biology and disease. Annu. Rev. Cell Dev. Biol. *26*, 235-260.

DeKosky, S.T., and Scheff, S.W. (1990). Synapse loss in frontal cortex biopsies in Alzheimer's disease: Correlation with cognitive severity. Ann Neurol. *27*, 457-464.

Deng, W., Aimone, J.B., and Gage, F.H. (2010). New neurons and new memories: how does adult hippocampal neurogenesis affect learning and memory? Nat Rev Neurosci *11*, 339-350.

Dewachter, I., Filipkowski, R.K., Priller, C., Ris, L., and Neyton, J., et al. (2009). Deregulation of NMDA-receptor function and down-stream signaling in APP[V717I] transgenic mice. Neurobiol. Aging *30*, 241-256.

Dudchenko, P.A. (2004). An overview of the tasks used to test working memory in rodents. Neurosci Biobehav Rev *28*, 699-709.

Duyckaerts, C., Delatour, B., and Potier, M.-C. (2009). Classification and basic pathology of Alzheimer disease. Acta Neuropathol. *118*, 5-36.

Duyckaerts, C., Potier, M.-C., and Delatour, B. (2007). Alzheimer disease models and human neuropathology: similarities and differences. Acta Neuropathol *115*, 5-38.

España, J., Giménez-Llort, L., Valero, J., Miñano, A., and Rábano, A., et al. (2010). Intraneuronal beta-amyloid accumulation in the amygdala enhances fear and anxiety in Alzheimer's disease transgenic mice. Biol. Psychiatry *67*, 513-521.

Fanselow, M.S. (2000). Contextual fear, gestalt memories, and the hippocampus. Behav. Brain Res. *110*, 73-81.

Faure, A., Verret, L., Bozon, B., El Tannir El Tayara, N., and Ly, M., et al. (2011). Impaired neurogenesis, neuronal loss, and brain functional deficits in the APPxPS1-Ki mouse model of Alzheimer's disease. Neurobiol. Aging *32*, 407-418.

Fernández-Vizarra, P., Fernández, A.P., Castro-Blanco, S., Serrano, J., and Bentura, M.L., et al. (2004). Intra- and extracellular Abeta and PHF in clinically evaluated cases of Alzheimer's disease. Histol. Histopathol. *19*, 823-844.

Fischer, M., Reuter, J., Gerich, F.J., Hildebrandt, B., and Hägele, S., et al. (2009). Enhanced Hypoxia Susceptibility in Hippocampal Slices From a Mouse Model of Rett Syndrome. J Neurophysiol *101*, 1016-1032.

Fitzjohn, S.M., Morton, R.A., Kuenzi, F., Rosahl, T.W., and Shearman, M., et al. (2001). Age-related impairment of synaptic transmission but normal long-term potentiation in transgenic mice that overexpress the human APP695SWE mutant form of amyloid precursor protein. J. Neurosci. *21*, 4691-4698.

Frautschy, S.A., Yang, F., Irrizarry, M., Hyman, B., and Saido, T.C., et al. (1998). Microglial response to amyloid plaques in APPsw transgenic mice. Am. J. Pathol. *152*, 307-317.

Games, D., Adams, D., Alessandrini, R., Barbour, R., and Berthelette, P., et al. (1995). Alzheimer-type neuropathology in transgenic mice overexpressing V717F beta-amyloid precursor protein. Nature *373*, 523-527.

Gerst, J.E. (2003). SNARE regulators: matchmakers and matchbreakers. Biochim. Biophys. Acta *1641*, 99-110.

Giannakopoulos, P., Herrmann, F.R., Bussière, T., Bouras, C., and Kövari, E., et al. (2003). Tangle and neuron numbers, but not amyloid load, predict cognitive status in Alzheimer's disease. Neurology *60*, 1495-1500.

Giménez-Llort, L., Blázquez, G., Cañete, T., Johansson, B., and Oddo, S., et al. (2007). Modeling behavioral and neuronal symptoms of Alzheimer's disease in mice: A role for intraneuronal amyloid. Neurosci Biobehav Rev *31*, 125-147.

Glabe, C.G. (2008). Structural classification of toxic amyloid oligomers. J. Biol. Chem. *283*, 29639-29643.

Gómez-Isla, T., Hollister, R., West, H., Mui, S., and Growdon, J.H., et al. (1997). Neuronal loss correlates with but exceeds neurofibrillary tangles in Alzheimer's disease. Ann. Neurol. *41*, 17-24.

Gouras, G.K., Tsai, J., Naslund, J., Vincent, B., and Edgar, M., et al. (2000). Intraneuronal Abeta42 accumulation in human brain. Am. J. Pathol. *156*, 15-20.

Graeber, M.B., and Streit, W.J. (2010). Microglia: biology and pathology. Acta Neuropathol. *119*, 89-105.

Greenfield, J.P., Tsai, J., Gouras, G.K., Hai, B., and Thinakaran, G., et al. (1999). Endoplasmic reticulum and trans-Golgi network generate distinct populations of Alzheimer beta-amyloid peptides. Proc. Natl. Acad. Sci. U.S.A. *96*, 742-747.

Grundke-Iqbal, I., Iqbal, K., George, L., Tung, Y.C., and Kim, K.S., et al. (1989). Amyloid protein and neurofibrillary tangles coexist in the same neuron in Alzheimer disease. Proc. Natl. Acad. Sci. U.S.A. *86*, 2853-2857.

Guzmán, E., Bouter, Y., Richard, B.C., Lannfelt, L., and Ingelsson, M., et al. (2014). Abundance of Aβ5-x like immunoreactivity in transgenic 5XFAD, APP/PS1KI and 3xTG mice, sporadic and familial Alzheimer's disease. Mol Neurodegener. *9*, 13.

Haass, C. (2004). Take five--BACE and the gamma-secretase quartet conduct Alzheimer's amyloid beta-peptide generation. EMBO J. *23*, 483-488.

Haass, C., Schlossmacher, M.G., Hung, A.Y., Vigo-Pelfrey, C., and Mellon, A., et al. (1992). Amyloid β-peptide is produced by cultured cells during normal metabolism. Nature *359*, 322-325.

Haass, C., and Selkoe, D.J. (2007). Soluble protein oligomers in neurodegeneration: lessons from the Alzheimer's amyloid β-peptide. Nat Rev Mol Cell Biol *8*, 101-112.

Hall, A.M., and Roberson, E.D. (2012). Mouse models of Alzheimer's disease. Brain Res Bull *88*, 3-12.

Halliday, G. (2003). Identifying severely atrophic cortical subregions in Alzheimer's disease. Neurobiol. Aging *24*, 797-806.

Hardy, J., and Allsop, D. (1991). Amyloid deposition as the central event in the aetiology of Alzheimer's disease. Trends Pharmacol. Sci. *12*, 383-388.

Hardy, J., and Selkoe, D.J. (2002). The Amyloid Hypothesis of Alzheimer's Disease: Progress and Problems on the Road to Therapeutics. Science *297*, 353-356.

Holmes, C., Boche, D., Wilkinson, D., Yadegarfar, G., and Hopkins, V., et al. (2008). Long-term effects of Aβ42 immunisation in Alzheimer's disease: follow-up of a randomised, placebo-controlled phase I trial. Lancet *372*, 216-223.

Holtzman, D.M., Morris, J.C., and Goate, A.M. (2011). Alzheimer's Disease: The Challenge of the Second Century. Sci Transl Med *3*, 77sr1.

Howell, S., Nalbantoglu, J., and Crine, P. (1995). Neutral endopeptidase can hydrolyze β-amyloid(1–40) but shows no effect on β-amyloid precursor protein metabolism. Peptides *16*, 647-652.

Hsia, A.Y., Masliah, E., McConlogue, L., Yu, G.Q., and Tatsuno, G., et al. (1999). Plaque-independent disruption of neural circuits in Alzheimer's disease mouse models. Proc. Natl. Acad. Sci. U.S.A. *96*, 3228-3233.

Hsiao, K., Chapman, P., Nilsen, S., Eckman, C., and Harigaya, Y., et al. (1996). Correlative memory deficits, Abeta elevation, and amyloid plaques in transgenic mice. Science *274*, 99-102.

Hsieh, H., Boehm, J., Sato, C., Iwatsubo, T., and Tomita, T., et al. (2006). AMPAR removal underlies Abeta-induced synaptic depression and dendritic spine loss. Neuron *52*, 831-843.

Hu, J., Igarashi, A., Kamata, M., and Nakagawa, H. (2001). Angiotensin-converting enzyme degrades Alzheimer amyloid beta-peptide (A beta); retards Abeta aggregation, deposition, fibril formation; and inhibits cytotoxicity. J. Biol. Chem. *276*, 47863-47868.

Hyman, B.T., van Hoesen, G.W., Damasio, A.R., and Barnes, C.L. (1984). Alzheimer's disease: cell-specific pathology isolates the hippocampal formation. Science *225*, 1168-1170.

Irizarry, M.C., McNamara, M., Fedorchak, K., Hsiao, K., and Hyman, B.T. (1997a). APPSw transgenic mice develop age-related A beta deposits and neuropil abnormalities, but no neuronal loss in CA1. J. Neuropathol. Exp. Neurol. *56*, 965-973.

Irizarry, M.C., Soriano, F., McNamara, M., Page, K.J., and Schenk, D., et al. (1997b). Abeta deposition is associated with neuropil changes, but not with overt neuronal loss in the human amyloid precursor protein V717F (PDAPP) transgenic mouse. J. Neurosci. *17*, 7053-7059.

Ittner, L.M., Ke, Y.D., Delerue, F., Bi, M., and Gladbach, A., et al. (2010). Dendritic function of tau mediates amyloid-beta toxicity in Alzheimer's disease mouse models. Cell *142*, 387-397.

Iwatsubo, T., Odaka, A., Suzuki, N., Mizusawa, H., and Nukina, N., et al. (1994). Visualization of A beta 42(43) and A beta 40 in senile plaques with end-specific A beta monoclonals: evidence that an initially deposited species is A beta 42(43). Neuron *13*, 45-53.

Jacobsen, J.S., Wu, C.-C., Redwine, J.M., Comery, T.A., and Arias, R., et al. (2006). Early-onset behavioral and synaptic deficits in a mouse model of Alzheimer's disease. Proc. Natl. Acad. Sci. U.S.A. *103*, 5161-5166.

Janc, O.A., and Müller, M. (2014). The free radical scavenger Trolox dampens neuronal hyperexcitability, reinstates synaptic plasticity, and improves hypoxia tolerance in a mouse model of Rett syndrome. Front. Cell. Neurosci. *8*, 56.

Jang, H., Teran Arce, F., Ramachandran, S., Kagan, B.L., and Lal, R., et al. (2014). Disordered amyloidogenic peptides may insert into the membrane and assemble into common cyclic structural motifs. Chem Soc Rev *43*, 6750-6764.

Jawhar, S., Trawicka, A., Jenneckens, C., Bayer, T.A., and Wirths, O. (2010). Motor deficits, neuron loss, and reduced anxiety coinciding with axonal degeneration and intraneuronal Aβ aggregation in the 5XFAD mouse model of Alzheimer's disease. Neurobiol Aging *33*, 196.e29–196.e40.

Jawhar, S., Wirths, O., and Bayer, T.A. (2011a). Pyroglutamate Amyloid-β (Aβ): A Hatchet Man in Alzheimer Disease. J Biol. Chem. *286*, 38825-38832.

Jawhar, S., Wirths, O., Schilling, S., Graubner, S., and Demuth, H.-U., et al. (2011b). Overexpression of Glutaminyl Cyclase, the Enzyme Responsible for Pyroglutamate Aβ Formation, Induces Behavioral Deficits, and Glutaminyl Cyclase Knock-out Rescues the Behavioral Phenotype in 5XFAD Mice. J Biol. Chem. *286*, 4454-4460.

Jolas, T., Zhang, X.-S., Zhang, Q., Wong, G., and Del Vecchio, R., et al. (2002). Long-term potentiation is increased in the CA1 area of the hippocampus of APP(swe/ind) CRND8 mice. Neurobiol. Dis. *11*, 394-409.

Kamenetz, F., Tomita, T., Hsieh, H., Seabrook, G., and Borchelt, D., et al. (2003). APP processing and synaptic function. Neuron *37*, 925-937.

Kandalepas, P.C., and Vassar, R. (2012). Identification and biology of β-secretase. J. Neurochem. *120 (Suppl 1)*, 55-61.

Karch, C.M., Cruchaga, C., and Goate, A.M. (2014). Alzheimer's disease genetics: from the bench to the clinic. Neuron *83*, 11-26.

Karl, T., Bhatia, S., Cheng, D., Kim, W.S., and Garner, B. (2012). Cognitive phenotyping of amyloid precursor protein transgenic J20 mice. Behav. Brain Res. *228*, 392-397.

Karl, T., Pabst, R., and Hörsten, S. von (2003). Behavioral phenotyping of mice in pharmacological and toxicological research. Exp. Toxicol. Pathol. *55*, 69-83.

Kauer, J.A., and Malenka, R.C. (2007). Synaptic plasticity and addiction. Nat Rev Neurosci *8*, 844-858.

Kessels, H.W., Nabavi, S., and Malinow, R. (2013). Metabotropic NMDA receptor function is required for β-amyloid-induced synaptic depression. Proc. Natl. Acad. Sci. U.S.A. *110*, 4033-4038.

Kimura, R., and Ohno, M. (2009). Impairments in remote memory stabilization precede hippocampal synaptic and cognitive failures in 5XFAD Alzheimer mouse model. Neurobiol. Dis. *33*, 229-235.

King, D.L., and Arendash, G.W. (2002). Behavioral characterization of the Tg2576 transgenic model of Alzheimer's disease through 19 months. Physiol. Behav. *75*, 627-642.

Kinoshita, A., Fukumoto, H., Shah, T., Whelan, C.M., and Irizarry, M.C., et al. (2003). Demonstration by FRET of BACE interaction with the amyloid precursor protein at the cell surface and in early endosomes. J. Cell. Sci. *116*, 3339-3346.

Klein, W.L. (2002). Aβ toxicity in Alzheimer’s disease: globular oligomers (ADDLs) as new vaccine and drug targets. Neurochem Int, 345-352.

Klyubin, I., Cullen, W.K., Hu, N.-W., and Rowan, M.J. (2012). Alzheimer's disease Aβ assemblies mediating rapid disruption of synaptic plasticity and memory. Mol Brain *5*, 25.

Knaus, P., Marquèze-Pouey, B., Scherer, H., and Betz, H. (1990). Synaptoporin, a novel putative channel protein of synaptic vesicles. Neuron *5*, 453-462.

Knobloch, M., Farinelli, M., Konietzko, U., Nitsch, R.M., and Mansuy, I.M. (2007). Abeta oligomer-mediated long-term potentiation impairment involves protein phosphatase 1-dependent mechanisms. J. Neurosci. *27*, 7648-7653.

Koffie, R.M., Hyman, B.T., and Spires-Jones, T.L. (2011). Alzheimer's disease: synapses gone cold. Mol Neurodegener. *6*, 63.

Koike, H., Tomioka, S., Sorimachi, H., Saido, T.C., and Maruyama, K., et al. (1999). Membrane-anchored metalloprotease MDC9 has an alpha-secretase activity responsible for processing the amyloid precursor protein. Biochem. J. *343*, 371-375.

Koss, D.J., Drever, B.D., Stoppelkamp, S., Riedel, G., and Platt, B. (2013). Age-dependent changes in hippocampal synaptic transmission and plasticity in the PLB1Triple Alzheimer mouse. Cell. Mol. Life Sci. *70*, 2585-2601.

Kril, J.J., Hodges, J., and Halliday, G. (2004). Relationship between hippocampal volume and CA1 neuron loss in brains of humans with and without Alzheimer's disease. Neuroscience Letters *361*, 9-12.

Kuhnt, U., and Voronin, L. (1994). Interaction between paired-pulse facilitation and long-term potentiation in area CA1 of guinea-pig hippocampal slices: Application of quantal analysis. Neuroscience *62*, 391-397.

Kumar, S., Rezaei-Ghaleh, N., Terwel, D., Thal, D.R., and Richard, M., et al. (2011). Extracellular phosphorylation of the amyloid β-peptide promotes formation of toxic aggregates during the pathogenesis of Alzheimer's disease. EMBO J. *30*, 2255-2265.

Kummer, M.P., and Heneka, M.T. (2014). Truncated and modified amyloid-beta species. Alzheimers Res Ther *6*, 28.

Kuo, Y.M., Beach, T.G., Sue, L.I., Scott, S., and Layne, K.J., et al. (2001). The evolution of Abeta peptide burden in the APP23 transgenic mice: implications for Abeta deposition in Alzheimer disease. Mol. Med. *7*, 609-618.

LaFerla, F.M., Tinkle, B.T., Bieberich, C.J., Haudenschild, C.C., and Jay, G. (1995). The Alzheimer's Abeta peptide induces neurodegeneration and apoptotic cell death in transgenic mice. Nat. Genet. *9*, 21-30.

Lalonde, R. (2002b). The neurobiological basis of spontaneous alternation. Neurosci Biobehav Rev *26*, 91-104.

Lalonde, R., Dumont, M., Staufenbiel, M., Sturchler-Pierrat, C., and Strazielle, C. (2002a). Spatial learning, exploration, anxiety, and motor coordination in female APP23 transgenic mice with the Swedish mutation. Brain Res. *956*, 36-44.

Lalonde, R., Fukuchi, K.-I., and Strazielle, C. (2012). Neurologic and motor dysfunctions in APP transgenic mice. Rev Neurosci *23*, 363-379.

Lammich, S., Kojro, E., Postina, R., Gilbert, S., and Pfeiffer, R., et al. (1999). Constitutive and regulated alpha-secretase cleavage of Alzheimer's amyloid precursor protein by a disintegrin metalloprotease. Proc. Natl. Acad. Sci. U.S.A. *96*, 3922-3927.

Larson, J., Lynch, G., Games, D., and Seubert, P. (1999). Alterations in synaptic transmission and long-term potentiation in hippocampal slices from young and aged PDAPP mice. Brain Res. *840*, 23-35.

Larsson, M., Hjälm, G., Sakwe, A.M., Engström, A., and Höglund, A.-S., et al. (2003). Selective interaction of megalin with postsynaptic density-95 (PSD-95)-like membrane-associated guanylate kinase (MAGUK) proteins. Biochem. J. *373*, 381-391.

Lavenex, P., and Amaral, D.G. (2000). Hippocampal-neocortical interaction: a hierarchy of associativity. Hippocampus *10*, 420-430.

Leissring, M.A. (2014). Aβ degradation - the inside story. Front. Aging Neurosci. *6*, 229.

Leissring, M.A., Lu, A., Condron, M.M., Teplow, D.B., and Stein, R.L., et al. (2003). Kinetics of Amyloid β-Protein Degradation Determined by Novel Fluorescence- and Fluorescence Polarization-based Assays. J Biol. Chem. *278*, 37314-37320.

Lesné, S., Koh, M.T., Kotilinek, L., Kayed, R., and Glabe, C.G., et al. (2006). A specific amyloid-β protein assembly in the brain impairs memory. Nature *440*, 352-357.

Levinson, J.N., and El-Husseini, A. (2005). Building excitatory and inhibitory synapses: balancing neuroligin partnerships. Neuron *48*, 171-174.

Lewis, H., Beher, D., Cookson, N., Oakley, A., and Piggott, M., et al. (2006). Quantification of Alzheimer pathology in ageing and dementia: age-related accumulation of amyloid-beta(42) peptide in vascular dementia. Neuropathol Appl Neurobiol *32*, 103-118.

Liao, M.-C., Ahmed, M., Smith, S.O., and van Nostrand, W.E. (2009). Degradation of amyloid beta protein by purified myelin basic protein. J. Biol. Chem. *284*, 28917-28925.

Li, H.L., Roch, J.M., Sundsmo, M., Otero, D., and Sisodia, S., et al. (1997). Defective neurite extension is caused by a mutation in amyloid beta/A4 (Abeta) protein precursor found in familial Alzheimer's disease. J. Neurobiol. *32*, 469-480.

Lin, N., Pan, X.-d., Chen, A.-q., Zhu, Y.-g., and Wu, M., et al. (2014). Tripchlorolide improves age-associated cognitive deficits by reversing hippocampal synaptic plasticity impairment and NMDA receptor dysfunction in SAMP8 mice. Behav. Brain Res. *258*, 8-18.

Lyketsos, C.G., Lopez, O., Jones, B., Fitzpatrick, A.L., and Breitner, J., et al. (2002). Prevalence of neuropsychiatric symptoms in dementia and mild cognitive impairment: results from the cardiovascular health study. JAMA *288*, 1475-1483.

Lynch, M.A. (2004). Long-Term Potentiation and Memory. Physiol Rev *84*, 87-136.

Malenka, R.C., and Bear, M.F. (2004). LTP and LTD: An Embarrassment of Riches. Neuron *44*, 5-21.

Malenka, R.C., and Nicoll, R.A. (1999). Long-Term Potentiation--A Decade of Progress? Science *285*, 1870-1874.

Mandrekar-Colucci, S., and Landreth, G.E. (2010). Microglia and inflammation in Alzheimer's disease. CNS Neurol Disord Drug Targets *9*, 156-167.

Mann, D.M. (1988). Alzheimer's disease and Down's syndrome. Histopathology *13*, 125-137.

Marcello, E., Epis, R., Saraceno, C., and Luca, M. (2012). Synaptic Dysfunction in Alzheimer's Disease. In Synaptic Plasticity, M.R. Kreutz and C. Sala, eds. (Vienna: Springer Vienna), pp. 573–601.

Marr, R.A., and Hafez, D.M. (2014). Amyloid-beta and Alzheimer's disease: the role of neprilysin-2 in amyloid-beta clearance. Front. Aging Neurosci. *6*, 187.

Martin, S.J., Grimwood, P.D., and Morris, R.G. (2000). Synaptic plasticity and memory: an evaluation of the hypothesis. Annu. Rev. Neurosci. *23*, 649-711.

Maruszak, A., and Thuret, S. (2014). Why looking at the whole hippocampus is not enough - a critical role for anteroposterior axis, subfield and activation analyses to enhance predictive value of hippocampal changes for Alzheimer's disease diagnosis. Front. Cell. Neurosci. *8*, 95.

Masliah, E., Mallory, M., Hansen, L., Richard, D., and Alford, M., et al. (1994). Synaptic and neuritic alterations during the progression of Alzheimer's disease. Neurosci Lett *174*, 67-72.

Masters, C.L., Gail Simms, N., Weinman, A., Multhaupt, G., and MCDonald, B.L., et al. (1985a). Amyloid plaque core protein in Alzheimer disease and Down syndrome. Proc. Natl. Acad. Sci. U.S.A., 4245-4249.

Masters, C.L., Multhaup, G., Simms, G., Pottgiesser, J., and Martins, R.N., et al. (1985b). Neuronal origin of a cerebral amyloid: neurofibrillary tangles of Alzheimer's disease contain the same protein as the amyloid of plaque cores and blood vessels. EMBO J. *4*, 2757-2763.

Maurer, K., Volk, S., and Gerbaldo, H. (1997). Auguste D and Alzheimer's disease. The Lancet *349*, 1546-1549.

McGowan, E., Pickford, F., Kim, J., Onstead, L., and Eriksen, J., et al. (2005). Abeta42 is essential for parenchymal and vascular amyloid deposition in mice. Neuron *47*, 191-199.

McKhann, G.M., Knopman, D.S., Chertkow, H., Hyman, B.T., and Jack, C.R., et al. (2011). The diagnosis of dementia due to Alzheimer's disease: recommendations from the National Institute on Aging-Alzheimer's Association workgroups on diagnostic guidelines for Alzheimer's disease. Alzheimers Dement *7*, 263-269.

Medway, C., and Morgan, K. (2014). Review: The genetics of Alzheimer's disease; putting flesh on the bones. Neuropathol. Appl. Neurobiol. *40*, 97-105.

Miller, D., Papayannopoulos, I., Styles, J., Bobin, S., and Lin, Y., et al. (1993). Peptide Compositions of the Cerebrovascular and Senile Plaque Core Amyloid Deposits of Alzheimer's Disease. Arch. Biochem. Biophys. *301*, 41-52.

Miravalle, L., Calero, M., Takao, M., Roher, A.E., and Ghetti, B., et al. (2005). Amino-Terminally Truncated Aβ Peptide Species Are the Main Component of Cotton Wool Plaques. Biochemistry *44*, 10810-10821.

Moechars, D., Dewachter, I., Lorent, K., Reversé, D., and Baekelandt, V., et al. (1999). Early phenotypic changes in transgenic mice that overexpress different mutants of amyloid precursor protein in brain. J. Biol. Chem. *274*, 6483-6492.

Morris, R. (1984). Developments of a water-maze procedure for studying spatial learning in the rat. J Neurosci Meth *11*, 47-60.

Morris, R.G.M., Anderson, E., Lynch, G.S., and Baudry, M. (1986). Selective impairment of learning and blockade of long-term potentiation by an N-methyl-D-aspartate receptor antagonist, AP5. Nature *319*, 774-776.

Moser, E.I., Krobert, K.A., Moser, M.-B., and Morris, R.G.M. (1998). Impaired spatial learning after saturation of long-term potentiation. Science *281*, 2038-2042.

Moser, M.-B., Moser, E.I., Forrest, E., Andersen, P., and Morris, R.G.M. (1995). Spatial Learning with a Minislab in the Dorsal Hippocampus. Proc. Natl. Acad. Sci. U.S.A. *92*, 9697-9701.

Mucke, L., Masliah, E., Yu, G.Q., Mallory, M., and Rockenstein, E.M., et al. (2000). High-level neuronal expression of Abeta 1-42 in wild-type human amyloid protein precursor transgenic mice: synaptotoxicity without plaque formation. J. Neurosci. *20*, 4050-4058.

Mucke, L., and Selkoe, D.J. (2012). Neurotoxicity of Amyloid β-Protein: Synaptic and Network Dysfunction. Cold Spring Harb Perspect Med. *2*, a006338.

Nakazawa, K., McHugh, T.J., Wilson, M.A., and Tonegawa, S. (2004). NMDA receptors, place cells and hippocampal spatial memory. Nat. Rev. Neurosci. *5*, 361-372.

Näslund, J., Schierhorn, A., Hellman, U., Lannfelt, L., and Roses, A.D., et al. (1994). Relative abundance of Alzheimer Abeta amyloid peptide variants in Alzheimer disease and normal aging. Proc. Natl. Acad. Sci. U.S.A. *91*, 8378-8382.

Neves, G., Cooke, S.F., and Bliss, T.V.P. (2008). Synaptic plasticity, memory and the hippocampus: a neural network approach to causality. Nat. Rev. Neurosci. *9*, 65-75.

Nicoll, R.A., and Malenka, R.C. (1999). Expression mechanisms underlying NMDA receptor-dependent long-term potentiation. Ann. N. Y. Acad. Sci. *868*, 515-525.

Nussbaum, J.M., Schilling, S., Cynis, H., Silva, A., and Swanson, E., et al. (2012). Prion-like behaviour and tau-dependent cytotoxicity of pyroglutamylated amyloid-β. Nature *485*, 651-655.

Oakley, H., Cole, S.L., Logan, S., Maus, E., and Shao, P., et al. (2006). Intraneuronal beta-Amyloid Aggregates, Neurodegeneration, and Neuron Loss in Transgenic Mice with Five Familial Alzheimer's Disease Mutations: Potential Factors in Amyloid Plaque Formation. J Neurosci *26*, 10129-10140.

Oddo, S., Caccamo, A., Shepherd, J.D., Murphy, M., and Golde, T.E., et al. (2003). Triple-Transgenic Model of Alzheimer's Disease with Plaques and Tangles: Intracellular Abeta and Synaptic Dysfunction. Neuron *39*, 409-421.

Ohno, M. (2009). Failures to reconsolidate memory in a mouse model of Alzheimer's disease. Neurobiol Learn Mem *92*, 455-459.

Olsen, G.M.S.-K.J.M.R.J.L., Olsen, G.M., Scheel-Krüger, J., Moller, A., and Jensen, L.H. (1994). Relation of Spatial Learning of Rats in the Morris Water Maze Task to the Number of Viable CA1 Neurons Following Four-Vessel Occlusion. Behav Neurosci *108*, 681-690.

Ondrejcak, T., Klyubin, I., Hu, N.-W., Barry, A.E., and Cullen, W.K., et al. (2010). Alzheimer's Disease Amyloid β-Protein and Synaptic Function. Neuromol Med *12*, 13-26.

Palop, J.J., Chin, J., Roberson, E.D., Wang, J., and Thwin, M.T., et al. (2007). Aberrant Excitatory Neuronal Activity and Compensatory Remodeling of Inhibitory Hippocampal Circuits in Mouse Models of Alzheimer's Disease. Neuron *55*, 697-711.

Palop, J.J., Jones, B., Kekonius, L., Chin, J., and Yu, G.-Q., et al. (2003). Neuronal depletion of calcium-dependent proteins in the dentate gyrus is tightly linked to Alzheimer's disease-related cognitive deficits. Proc. Natl. Acad. Sci. U.S.A. *100*, 9572-9577.

Panegyres, P.K., and Atkins, E.R. (2011). The Functions of the Amyloid Precursor Protein Gene and Its Derivative Peptides: I Molecular Biology and Metabolic Processing. NM *02*, 120-131.

Park, P., Volianskis, A., Sanderson, T.M., Bortolotto, Z.A., and Jane, D.E., et al. (2014). NMDA receptor-dependent long-term potentiation comprises a family of temporally overlapping forms of synaptic plasticity that are induced by different patterns of stimulation. Philos. Trans. R. Soc. Lond., B, Biol. Sci. *369*, 20130131.

Perez, R.G., Soriano, S., Hayes, J.D., Ostaszewski, B., and Xia, W., et al. (1999). Mutagenesis identifies new signals for beta-amyloid precursor protein endocytosis, turnover, and the generation of secreted fragments, including Abeta42. J. Biol. Chem. *274*, 18851-18856.

Pfaffl, M.W., Horgan, G.W., and Dempfle, L. (2002). Relative expression software tool (REST) for group-wise comparison and statistical analysis of relative expression results in real-time PCR. Nucleic Acids Res. *30*, e36.

Philipson, O., Lord, A., Gumucio, A., O'Callaghan, P., and Lannfelt, L., et al. (2010). Animal models of amyloid-beta-related pathologies in Alzheimer's disease. FEBS J. *277*, 1389-1409.

Phillips, R.G., and LeDoux, J.E. (1992). Differential contribution of amygdala and hippocampus to cued and contextual fear conditioning. Behav. Neurosci. *106*, 274-285.

Pike, C.J., Overman, M.J., and Cotman Carl W. (1995b). Amino-terminal Deletions Enhance Aggregation of beta-Amyloid Peptides in Vitro. J Biol. Chem. *270*, 23895-23898.

Pimplikar, S.W. (2009). Reassessing the amyloid cascade hypothesis of Alzheimer's disease. Int. J. Biochem. Cell Biol. *41*, 1261-1268.

Platt, T.L., Reeves, V.L., and Murphy, M.P. (2013). Transgenic models of Alzheimer's disease: better utilization of existing models through viral transgenesis. Biochim. Biophys. Acta *1832*, 1437-1448.

Portelius, E., Bogdanovic, N., Gustavsson, M.K., Volkmann, I., and Brinkmalm, G., et al. (2010). Mass spectrometric characterization of brain amyloid beta isoform signatures in familial and sporadic Alzheimer's disease. Acta Neuropathol *120*, 185-193.

Pozueta, J., Lefort, R., and Shelanski, M.L. (2013). Synaptic changes in Alzheimer's disease and its models. Neuroscience *251*, 51-65.

Prelli, F., Castaño, E., Glenner, G.G., and Frangione, B. (1988). Differences between vascular and plaque core amyloid in Alzheimer's disease. J. Neurochem. *51*, 648-651.

Puzzo, D., Lee, L., Palmeri, A., Calabrese, G., and Arancio, O. (2014). Behavioral assays with mouse models of Alzheimer's disease: practical considerations and guidelines. Biochem. Pharmacol. *88*, 450-467.

Puzzo, D., Privitera, L., Leznik, E., Fà, M., and Staniszewski, A., et al. (2008). Picomolar amyloid-beta positively modulates synaptic plasticity and memory in hippocampus. J. Neurosci. *28*, 14537-14545.

Qi, Y., Morishima-Kawashima, M., Sato, T., Mitsumori, R., and Ihara, Y. (2003). Distinct mechanisms by mutant presenilin 1 and 2 leading to increased intracellular levels of amyloid beta-protein 42 in Chinese hamster ovary cells. Biochemistry *42*, 1042-1052.

Querfurth, H.W., and LaFerla, F.M. (2010). Alzheimer's Disease. N Engl J Med *362*, 329-344.

Raber, J., Huang, Y., and Ashford, J.W. (2004). ApoE genotype accounts for the vast majority of AD risk and AD pathology. Neurobiol. Aging *25*, 641-650.

Renner, M., Lacor, P.N., Velasco, P.T., Xu, J., and Contractor, A., et al. (2010). Deleterious Effects of Amyloid β Oligomers Acting as an Extracellular Scaffold for mGluR5. Neuron *66*, 739-754.

Richards, J.G., Higgins, G.A., Ouagazzal, A.-M., Ozmen, L., and Kew, J.N.C., et al. (2003). PS2APP transgenic mice, coexpressing hPS2mut and hAPPswe, show age-related cognitive deficits associated with discrete brain amyloid deposition and inflammation. J. Neurosci. *23*, 8989-9003.

Roberson, E.D., Halabisky, B., Yoo, J.W., Yao, J., and Chin, J., et al. (2011). Amyloid-β/Fyn-Induced Synaptic, Network, and Cognitive Impairments Depend on Tau Levels in Multiple Mouse Models of Alzheimer's Disease. Journal of Neuroscience *31*, 700-711.

Roder, S., Danober, L., Pozza, M.F., Lingenhoehl, K., and Wiederhold, K.-H., et al. (2003). Electrophysiological studies on the hippocampus and prefrontal cortex assessing the effects of amyloidosis in amyloid precursor protein 23 transgenic mice. Neuroscience *120*, 705-720.

Roher, A.E., Lowenson, J.D., Clarke, S., Wolkow, C., and Wang, R., et al. (1993). Structural alterations in the peptide backbone of beta-amyloid core protein may account for its deposition and stability in Alzheimer's disease. J. Biol. Chem. *268*, 3072-3083.

Rönicke, R., Mikhaylova, M., Rönicke, S., Meinhardt, J., and Schröder, U.H., et al. (2011). Early neuronal dysfunction by amyloid β oligomers depends on activation of NR2B-containing NMDA receptors. Neurobiol Aging *32*, 2219-2228.

Rosenzweig, E.S., and Barnes, C.A. (2003). Impact of aging on hippocampal function: plasticity, network dynamics, and cognition. Prog. Neurobiol. *69*, 143-179.

Rossjohn, J., Cappai, R., Feil, S.C., Henry, A., and McKinstry, W.J., et al. (1999). Crystal structure of the N-terminal, growth factor-like domain of Alzheimer amyloid precursor protein. Nat. Struct. Biol. *6*, 327-331.

Rovelet-Lecrux, A., Hannequin, D., Raux, G., Le Meur, N., and Laquerrière, A., et al. (2006). APP locus duplication causes autosomal dominant early-onset Alzheimer disease with cerebral amyloid angiopathy. Nat. Genet. *38*, 24-26.

Rowan, M.J., Klyubin, I., Wang, Q., and Anwyl, R. (2004). Mechanisms of the inhibitory effects of amyloid β-protein on synaptic plasticity. Exp. Gerontol. *39*, 1661-1667.

Russo, C., Violani, E., Salis, S., Venezia, V., and Dolcini, V., et al. (2002). Pyroglutamate-modified amyloid beta-peptides--AbetaN3(pE)--strongly affect cultured neuron and astrocyte survival. J. Neurochem. *82*, 1480-1489.

Saganich, M.J., Schroeder, B.E., Galvan, V., Bredesen, D.E., and Koo, E.H., et al. (2006). Deficits in synaptic transmission and learning in amyloid precursor protein (APP) transgenic mice require C-terminal cleavage of APP. J. Neurosci. *26*, 13428-13436.

Saido, T.C., Iwatsubo, T., Mann, D.M., Shimada, H., and Ihara, Y., et al. (1995). Dominant and differential deposition of distinct beta-amyloid peptide species, Abeta N3(pE), in senile plaques. Neuron *14*, 457-466.

Sanes, J.R., and Lichtman, J.W. (2001). Induction, assembly, maturation and maintenance of a postsynaptic apparatus. Nat Rev Neurosci *2*, 791-805.

Savonenko, A.V., Xu, G.M., Price, D.L., Borchelt, D.R., and Markowska, A.L. (2003). Normal cognitive behavior in two distinct congenic lines of transgenic mice hyperexpressing mutant APP SWE. Neurobiol. Dis. *12*, 194-211.

Scarmeas, N., Hadjigeorgiou, G.M., Papadimitriou, A., Dubois, B., and Sarazin, M., et al. (2004). Motor signs during the course of Alzheimer disease. Neurology *63*, 975-982.

Scheff, S.W., Price, D.A., Schmitt, F.A., DeKosky, S.T., and Mufson, E.J. (2007). Synaptic alterations in CA1 in mild Alzheimer disease and mild cognitive impairment. Neurology *68*, 1501-1508.

Schilling, S., Lauber, T., Schaupp, M., Manhart, S., and Scheel, E., et al. (2006). On the seeding and oligomerization of pGlu-amyloid peptides (in vitro). Biochemistry *45*, 12393-12399.

Schlenzig, D., Manhart, S., Cinar, Y., Kleinschmidt, M., and Hause, G., et al. (2009). Pyroglutamate Formation Influences Solubility and Amyloidogenicity of Amyloid Peptides. Biochemistry *48*, 7072-7078.

Schlenzig, D., Rönicke, R., Cynis, H., Ludwig, H.-H., and Scheel, E., et al. (2012). N-Terminal pyroglutamate formation of Aβ38 and Aβ40 enforces oligomer formation and potency to disrupt hippocampal long-term potentiation. Journal of Neurochemistry *121*, 774-784.

Schmitz, C., Rutten, B.P.F., Pielen, A., Schäfer, S., and Wirths, O., et al. (2004). Hippocampal neuron loss exceeds amyloid plaque load in a transgenic mouse model of Alzheimer's disease. Am. J. Pathol. *164*, 1495-1502.

Selkoe, D.J. (1998). The cell biology of β-amyloid precursor protein and presenilin in Alzheimer's disease. Trends Cell Biol, 447-453.

Selkoe, D.J. (2001). Alzheimer's Disease: Genes, Proteins, and Therapy. Physiol Rev *81*, 741-766.

Selkoe, D.J. (2002). Alzheimer's disease is a synaptic failure. Science *298*, 789-791.

Selkoe, D.J. (2008). Soluble oligomers of the amyloid β-protein impair synaptic plasticity and behavior. Behav. Brain Res. *192*, 106-113.

Sergeant, N., Bombois, S., Ghestem, A., Drobecq, H., and Kostanjevecki, V., et al. (2003). Truncated beta-amyloid peptide species in pre-clinical Alzheimer's disease as new targets for the vaccination approach. J Neurochem *85*, 1581-1591.

Seubert, P., Vigo-Pelfrey, C., Esch, F., Lee, M., and Dovey, H., et al. (1992). Isolation and quantification of soluble Alzheimer's beta-peptide from biological fluids. Nature *359*, 325-327.

Sevalle, J., Amoyel, A., Robert, P., Fournié-Zaluski, M.-C., and Roques, B., et al. (2009). Aminopeptidase A contributes to the N-terminal truncation of amyloid β-peptide. J Neurochem *109*, 248-256.

Shankar, G.M., Bloodgood, B.L., Townsend, M., Walsh, D.M., and Selkoe, D.J., et al. (2007). Natural Oligomers of the Alzheimer Amyloid-β Protein Induce Reversible Synapse Loss by Modulating an NMDA-Type Glutamate Receptor-Dependent Signaling Pathway. J Neurosci *27*, 2866-2875.

Shankar, G.M., Li, S., Mehta, T.H., Garcia-Munoz, A., and Shepardson, N.E., et al. (2008). Amyloid-β protein dimers isolated directly from Alzheimer's brains impair synaptic plasticity and memory. Nat Med *14*, 837-842.

Shao, C.Y., Mirra, S.S., Sait, H.B.R., Sacktor, T.C., and Sigurdsson, E.M. (2011). Postsynaptic degeneration as revealed by PSD-95 reduction occurs after advanced Aβ and tau pathology in transgenic mouse models of Alzheimer's disease. Acta Neuropathol *122*, 285-292.

Shimohama, S., Kamiya, S., Taniguchi, T., Akagawa, K., and Kimura, J. (1997). Differential Involvement of Synaptic Vesicle and Presynaptic Plasma Membrane Proteins in Alzheimer's Disease. Biochem Biophys Res Commun *236*, 239-242.

Shinohara, M., Fujioka, S., Murray, M.E., Wojtas, A., and Baker, M., et al. (2014). Regional distribution of synaptic markers and APP correlate with distinct clinicopathological features in sporadic and familial Alzheimer's disease. Brain *137*, 1533-1549.

Siegelbaum, S.A., and Kandel, E.R. (2012). Chapter 67 Prefrontal Cortex, Hippocampus, and the Biology of Explicit Memory Storage. In Principles of neural science, E.R. Kandel, J.H. Schwartz, T.M. Jessel, S.A. Siegelbaum and A. Hudspeth, eds. (New York: McGraw-Hill Medical).

Singec, I., Knoth, R., Ditter, M., Hagemeyer, C.E., and Rosenbrock, H., et al. (2002). Synaptic vesicle protein synaptoporin is differently expressed by subpopulations of mouse hippocampal neurons. J. Comp. Neurol. *452*, 139-153.

Small, D.H., Mok, S.S., and Bornstein, J.C. (2001). Alzheimer's disease and Abeta toxicity: from top to bottom. Nat. Rev. Neurosci. *2*, 595-598.

Snowdon, D.A. (1997). Aging and Alzheimer's disease: lessons from the Nun Study. Gerontologist *37*, 150-156.

Sofroniew, M.V., and Vinters, H.V. (2010). Astrocytes: biology and pathology. Acta Neuropathol. *119*, 7-35.

Song, J.Y., Ichtchenko, K., Südhof, T.C., and Brose, N. (1999). Neuroligin 1 is a postsynaptic cell-adhesion molecule of excitatory synapses. Proc. Natl. Acad. Sci. U.S.A. *96*, 1100-1105.

Spencer, B., and Masliah, E. (2014). Immunotherapy for Alzheimer's disease: past, present and future. Front. Aging Neurosci. *6*, 114.

Sperling, R.A., Aisen, P.S., Beckett, L.A., Bennett, D.A., and Craft, S., et al. (2011). Toward defining the preclinical stages of Alzheimer's disease: recommendations from the National Institute on Aging-Alzheimer's Association workgroups on diagnostic guidelines for Alzheimer's disease. Alzheimers Dement *7*, 280-292.

Stalder, M., Phinney, A., Probst, A., Sommer, B., and Staufenbiel, M., et al. (1999). Association of microglia with amyloid plaques in brains of APP23 transgenic mice. Am. J. Pathol. *154*, 1673-1684.

Stevens, C.F. (1998). A million dollar question: does LTP = memory? Neuron *20*, 1-2.

Sturchler-Pierrat, C., Abramowski, D., Duke, M., Wiederhold, K.H., and Mistl, C., et al. (1997). Two amyloid precursor protein transgenic mouse models with Alzheimer disease-like pathology. Proc. Natl. Acad. Sci. U.S.A. *94*, 13287-13292.

Südhof, T.C. (1995). The synaptic vesicle cycle: a cascade of protein-protein interactions. Nature *375*, 645-653.

Sutherland, R.J., and McDonald, R.J. (1990). Hippocampus, amygdala, and memory deficits in rats. Behav. Brain Res. *37*, 57-79.

Szilágyi, T., Orbán-Kis, K., Horváth, E., Metz, J., and Pap, Z., et al. (2011). Morphological identification of neuron types in the rat hippocampus. Rom J Morphol Embryol *52*, 15-20.

Tafoya, L.C.R., Shuttleworth, C.W., Yanagawa, Y., Obata, K., and Wilson, M.C. (2008). The role of the t-SNARE SNAP-25 in action potential-dependent calcium signaling and expression in GABAergic and glutamatergic neurons. BMC Neurosci *9*, 105.

Takahashi, R.H., Almeida, C.G., Kearney, P.F., Yu, F., and Lin, M.T., et al. (2004). Oligomerization of Alzheimer's beta-amyloid within processes and synapses of cultured neurons and brain. J. Neurosci. *24*, 3592-3599.

Takahashi, R.H., Capetillo-Zarate, E., Lin, M.T., Milner, T.A., and Gouras, G.K. (2013). Accumulation of intraneuronal β-amyloid 42 peptides is associated with early changes in microtubule-associated protein 2 in neurites and synapses. PLoS ONE *8*, e51965.

Takeda, K., Araki, W., Akiyama, H., and Tabira, T. (2004). Amino-truncated amyloid -peptide (Aβ 5-40/42) produced from caspase-cleaved amyloid precursor protein is deposited in Alzheimer's disease brain. FASEB J *18*, 1755-1757.

Taylor, C.J., Ireland, D.R., Ballagh, I., Bourne, K., and Marechal, N.M., et al. (2008). Endogenous secreted amyloid precursor protein-alpha regulates hippocampal NMDA receptor function, long-term potentiation and spatial memory. Neurobiol. Dis. *31*, 250-260.

Thal, D.R., Rüb, U., Orantes, M., and Braak, H. (2002). Phases of Abeta-deposition in the human brain and its relevance for the development of AD. Neurology *58*, 1791-1800.

Thal, D.R., Schultz, C., Dehghani, F., Yamaguchi, H., and Braak, H., et al. (2000). Amyloid beta-protein (Abeta)-containing astrocytes are located preferentially near N-terminal-truncated Abeta deposits in the human entorhinal cortex. Acta Neuropathol. *100*, 608-617.

Thinakaran, G., and Koo, E.H. (2008). Amyloid precursor protein trafficking, processing, and function. J. Biol. Chem. *283*, 29615-29619.

Tomiyama, T., Matsuyama, S., Iso, H., Umeda, T., and Takuma, H., et al. (2010). A Mouse Model of Amyloid-β Oligomers: Their Contribution to Synaptic Alteration, Abnormal Tau Phosphorylation, Glial Activation, and Neuronal Loss In Vivo. J Neurosci *30*, 4845-4856.

Townsend, M., Shankar, G.M., Mehta, T.H., Walsh, D.M., and Selkoe, D.J. (2006). Effects of secreted oligomers of amyloid β-protein on hippocampal synaptic plasticity: a potent role for trimers. J. Physiol. *572*, 477-492.

Tsien, J.Z., Huerta, P.T., and Tonegawa, S. (1996). The essential role of hippocampal CA1 NMDA receptor-dependent synaptic plasticity in spatial memory. Cell *87*, 1327-1338.

van Dam, D., D'Hooge, R., Staufenbiel, M., van Ginneken, C., and van Meir, F., et al. (2003). Age-dependent cognitive decline in the APP23 model precedes amyloid deposition. Eur. J. Neurosci. *17*, 388-396.

van Nostrand, W.E., and Porter, M. (1999). Plasmin cleavage of the amyloid beta-protein: alteration of secondary structure and stimulation of tissue plasminogen activator activity. Biochemistry *38*, 11570-11576.

Varoqueaux, F., Aramuni, G., Rawson, R.L., Mohrmann, R., and Missler, M., et al. (2006). Neuroligins Determine Synapse Maturation and Function. Neuron *51*, 741-754.

Vassar, R., Bennett, B.D., Babu-Khan, S., Kahn, S., and Mendiaz, E.A., et al. (1999). Beta-secretase cleavage of Alzheimer's amyloid precursor protein by the transmembrane aspartic protease BACE. Science *286*, 735-741.

Venneti, S., Lopresti, B.J., Wang, G., Hamilton, R.L., and Mathis, C.A., et al. (2009). PK11195 labels activated microglia in Alzheimer's disease and in vivo in a mouse model using PET. Neurobiol Aging *30*, 1217-1226.

Volianskis, A., Collingridge, G.L., and Jensen, M.S. (2013). The roles of STP and LTP in synaptic encoding. PeerJ *1*, e3.

Vorhees, C.V., and Williams, M.T. (2006). Morris water maze: procedures for assessing spatial and related forms of learning and memory. Nat Protoc *1*, 848-858.

Walsh, D.M., Klyubin, I., Fadeeva, J.V., Cullen, W.K., and Anwyl, R., et al. (2002). Naturally secreted oligomers of amyloid β protein potently inhibit hippocampal long-term potentiation in vivo. Nature *416*, 535-539.

Walsh, D.M., Klyubin, I., Shankar, G.M., Townsend, M., and Fadeeva, J.V., et al. (2005). The role of cell-derived oligomers of Abeta in Alzheimer's disease and avenues for therapeutic intervention. Biochem. Soc. Trans. *33*, 1087-1090.

Walsh, D.M., Tseng, B.P., Rydel, R.E., Podlisny, M.B., and Selkoe, D.J. (2000). The oligomerization of amyloid beta-protein begins intracellularly in cells derived from human brain. Biochemistry *39*, 10831-10839.

Wang, L., Larson, E.B., Bowen, J.D., and van Belle, G. (2006). Performance-based physical function and future dementia in older people. Arch. Intern. Med. *166*, 1115-1120.

Wang, Y., Wu, L., Du Fang, Zhong, C., and Chen, J.X., et al. (2014). Synergistic Exacerbation of Mitochondrial and Synaptic Dysfunction and Resultant Learning and Memory Deficit in a Mouse Model of Diabetic Alzheimer's Disease. J. Alzheimers Dis.

Webster, S.J., Bachstetter, A.D., Nelson, P.T., Schmitt, F.A., and van Eldik, L.J. (2014). Using mice to model Alzheimer's dementia: an overview of the clinical disease and the preclinical behavioral changes in 10 mouse models. Front. Genet. *5*, 88.

Wilson, I.A., Ikonen, S., Gallagher, M., Eichenbaum, H., and Tanila, H. (2005). Age-associated alterations of hippocampal place cells are subregion specific. J. Neurosci. *25*, 6877-6886.

Wiltfang, J., Esselmann, H., Cupers, P., Neumann, M., and Kretzschmar, H., et al. (2001). Elevation of beta-amyloid peptide 2-42 in sporadic and familial Alzheimer's disease and its generation in PS1 knockout cells. J. Biol. Chem. *276*, 42645-42657.

Wirths, O., and Bayer, T.A. (2010). Neuron loss in transgenic mouse models of Alzheimer's disease. Int J Alzheimers Dis *2010*, 723782.

Wirths, O., Breyhan, H., Cynis, H., Schilling, S., and Demuth, H.-U., et al. (2009). Intraneuronal pyroglutamate-Abeta 3–42 triggers neurodegeneration and lethal neurological deficits in a transgenic mouse model. Acta Neuropathol *118*, 487-496.

Wirths, O., Breyhan, H., Schäfer, S., Roth, C., and Bayer, T.A. (2006). Deficits in working memory and motor performance in the APP/PS1ki mouse model for Alzheimer's disease. Neurobiol Aging *29*, 891-901.

Wirths, O., Multhaup, G., and Bayer, T.A. (2004). A modified beta-amyloid hypothesis: intraneuronal accumulation of the beta-amyloid peptide - the first step of a fatal cascade. J Neurochem *91*, 513-520.

Wirths, O., Multhaup, G., Czech, C., Blanchard, V., and Moussaoui, S., et al. (2001). Intraneuronal Aβ accumulation precedes plaque formation in β-amyloid precursor protein and presenilin-1 double-transgenic mice. Neurosci Lett *306*, 116-120.

Wirths, O., Multhaup, G., Czech, C., Feldmann, N., and Blanchard, V., et al. (2002). Intraneuronal APP/Abeta trafficking and plaque formation in beta-amyloid precursor protein and presenilin-1 transgenic mice. Brain Pathol. *12*, 275-286.

Wittnam, J.L. (2012). The contribution of N-terminally modified amyloid beta to the etiology of Alzheimer's disease. Dissertation. https://ediss.uni-goettingen.de/handle/11858/00-1735-0000-000D-F0BC-7. 06.08.2014.

Wittnam, J.L., Portelius, E., Zetterberg, H., Gustavsson, M.K., and Schilling, S., et al. (2012). Pyroglutamate Amyloid β (Aβ) Aggravates Behavioral Deficits in Transgenic Amyloid Mouse Model for Alzheimer Disease. J Biol. Chem. *287*, 8154-8162.

Wood, E.R., Dudchenko, P.A., and Eichenbaum, H. (1999). The global record of memory in hippocampal neuronal activity. Nature *397*, 613-616.

Wright, A.L., Zinn, R., Hohensinn, B., Konen, L.M., and Beynon, S.B., et al. (2013). Neuroinflammation and neuronal loss precede Aβ plaque deposition in the hAPP-J20 mouse model of Alzheimer's disease. PLoS ONE *8*, e59586.

Wyss-Coray, T., and Rogers, J. (2012). Inflammation in Alzheimer disease - a brief review of the basic science and clinical literature. Cold Spring Harb Perspect Med *2*, a006346.

Youssef, I., Florent-Béchard, S., Malaplate-Armand, C., Koziel, V., and Bihain, B., et al. (2008). N-truncated amyloid-β oligomers induce learning impairment and neuronal apoptosis. Neurobiol Aging *29*, 1319-1333.

Zolezzi, J.M., Bastí-as-Candia, S., Santos, M.J., and Inestrosa, N.C. (2014). Alzheimer's disease: relevant molecular and physiopathological events affecting amyloid-β brain balance and the putative role of PPARs. Front. Aging Neurosci. *6*, 176.

Zucker, R.S. (1989). Short-Term Synaptic Plasticity. Annu. Rev. Neurosci. *12*, 13-31.

Zucker, R.S., and Regehr, W.G. (2002). Short-term synaptic plasticity. Annu. Rev. Physiol. *64*, 355-405.